NASA TECHNICAL NOTE

NASA TN D-2263

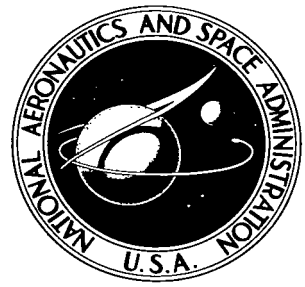

NASA TN D-2263

C.1

DYNAMIC PRESSURE AND THRUST CHARACTERISTICS OF COLD JETS DISCHARGING FROM SEVERAL EXHAUST NOZZLES DESIGNED FOR VTOL DOWNWASH SUPPRESSION

by C. C. Higgins and T. W. Wainwright

Prepared under Contract No. NASw-461 *by*
THE BOEING COMPANY
Renton, Washington
for

NATIONAL AERONAUTICS AND SPACE ADMINISTRATION • WASHINGTON, D. C. • APRIL 1964

DYNAMIC PRESSURE AND THRUST CHARACTERISTICS OF COLD JETS DISCHARGING FROM SEVERAL EXHAUST NOZZLES DESIGNED FOR VTOL DOWNWASH SUPPRESSION

By C. C. Higgins and T. W. Wainwright

Prepared under Contract No. NASw-461 by
THE BOEING COMPANY
Renton, Washington

NATIONAL AERONAUTICS AND SPACE ADMINISTRATION

For sale by the Office of Technical Services, Department of Commerce,
Washington, D. C. 20230 -- Price $2.00

DYNAMIC PRESSURE AND THRUST CHARACTERISTICS OF COLD JETS DISCHARGING FROM SEVERAL EXHAUST NOZZLES DESIGNED FOR VTOL DOWNWASH SUPPRESSION

By C. C. Higgins and T. W. Wainwright

SUMMARY

Several exhaust nozzle models were tested on a static rig using cold air flow to find the effect of exit design on thrust and jet wake dynamic pressure for use in VTOL downwash suppression. Data from both free jet and ground plane tests are presented to define dynamic pressure along the jet wake centerline and along the ground surface. Results show that three basic nozzle design factors can be very effective in causing rapid dynamic pressure decay in the jet wake with small effect on nozzle velocity coefficient. Dynamic pressure profiles are compared throughout the mixing region for each nozzle and are shown to be similar.

INTRODUCTION

Ground impingement of the downwash from any VTOL aircraft can produce operational problems of varying degree, depending on the type of landing site being used and disc-loading of the lift system. Since the severity of the downwash problem is a function of the maximum dynamic pressure in the jet wake at the ground surface, a general trend of designing for low-disc-loading lift devices on many current VTOL aircraft has resulted. However, high-speed airplane mission requirements have resulted in aircraft designs incorporating separate lift jet engines or combined lift and cruise turbo-fan engines. On jet VTOL aircraft currently in use, operations have been restricted in some manner to minimize ground damage. Such restrictions have included using hardened sites or reduction of exposure time by means of short ground roll or lift nozzle rotation at take-off.

A significant amount of research has been accomplished by several investigators in attempts to understand the action of a jet impinging on the ground and in finding the limits of erosion resistance that various surfaces have to jet

impingement, as described in references 1 to 3. Also, there have been efforts to develop various coverings, coatings, and structures that improve the erosion characteristics of ground surfaces. Many of the surface treatments have been shown to be effective, but, in most cases, logistic problems and installation requirements make it desirable to minimize or eliminate the need for ground preparation. This can be done only by reduction of the ground impingement dynamic pressures. The apparently conflicting requirements for jet engines in VTOL aircraft and low ground dynamic pressures have led to this study of exhaust nozzle design factors which, by increasing the rate of mixing with ambient air, will alleviate the ground impingement problem.

This investigation involved the testing of twelve nozzle configurations, including: circular designs which attempted to vary upstream turbulence; rectangular slot designs for a study of exit perimeter/area ratio and exit wall angle; and sectored configurations for the effect of exit area subdivision. These nozzles were tested on a static, cold air flow rig at the Airplane Division of The Boeing Company, Renton, Washington. Measurements of thrust and jet wake dynamic pressure were made for each nozzle at pressure ratios ranging from 1.4 to 2.4. Free jet wake surveys were made by traversing the jet at several downstream locations, and a ground plane was used to obtain dynamic pressures radially along the surface after jet impingement.

The similarity of the nozzles used in this program to those used in previous sound suppression work is apparent, and the objective is basically the same, namely, to increase the rate of jet mixing, although the effectiveness of a sound suppressor nozzle is primarily due to changes in the directivity and frequency of the noise, references 4 and 5. Thus sound suppression characteristics of a nozzle may or may not be related to the reduction of dynamic pressure in the jet wake, which is the goal of a VTOL downwash suppression nozzle.

This research was sponsored by the National Aeronautics and Space Administration through the Office of Grants and Research Contracts under contract NASw-461.

SYMBOLS

AR	aspect ratio, D^2/Area or length/width
C_F	mass flow coefficient, actual mass flow/ideal mass flow
C_{v_e}	effective velocity coefficient, effective exit velocity/ideal exit velocity. Effective velocity = $(\text{thrust/mass flow})_{\text{actual}}$
D_a	diameter of nozzle exit, inches

D_e	diameter of a circular nozzle with exit area equal to that of a non-circular nozzle, inches
L	length of rectangular exit planform, inches
W	width of rectangular exit planform, inches
R	radial distance from center of ground plane, inches
X, Y, Z	axes of a right hand coordinate system with the Z axis in the direction of flow. Also designates distances along each respective axis from center of nozzle exit, inches
I	designation of an axis intermediate between segments of nozzles No. 11 and No. 12
X	distance from core or "apparent core" to any point in the mixing region, measured parallel to the X axis, inches (ref.: figure 12)
$X_{.25q_{z_{max}}}$	distance from core or "apparent core" to reference contour at twenty-five per cent dynamic pressure, inches (ref.: figure 12)
Y	distance from core or "apparent core" to any point in the mixing region, measured parallel to the Y axis, inches (ref.: figure 12)
$Y_{.25q_{z_{max}}}$	distance from core or "apparent core" to reference contour at twenty-five per cent dynamic pressure, inches (ref.: figure 12)
h	height above the ground plane, inches
n	number of exit segments
p_o	atmospheric pressure, lbs/sq ft
p_t	total or stagnation pressure, lbs/sq ft
p_{t_n}	total or stagnation pressure at the nozzle exit, lbs/sq ft
p_{t_z}	total or stagnation pressure at any specified point in the jet wake, lbs/sq ft
p_{t_g}	total or stagnation pressure at any specified point on, or adjacent to the ground plane, lbs/sq ft

q	compressible dynamic pressure, $p_t - p_o$, lbs/sq ft
q_n	compressible dynamic pressure at the nozzle exit, $p_{t_n} - p_o$, lbs/sq ft
q_z	compressible dynamic pressure at any specified point in the jet wake, $p_{t_z} - p_o$, lbs/sq ft
$q_{z_{max}}$	maximum dynamic pressure measured at any specified transverse plane perpendicular to the Z axis, $p_{t_{z_{max}}} - p_o$, lbs/sq ft
q_g	compressible dynamic pressure at any specified point on, or adjacent to, the ground plane, $p_{t_g} - p_o$, lbs/sq ft
$q_{g_{max}}$	maximum compressible dynamic pressure measured on, or adjacent to, the ground plane at specified distances of the ground plane from the nozzle, $p_{t_{g_{max}}} - p_o$, lbs/sq ft
t_t	total or stagnation temperature, °F
t_{t_n}	total or stagnation temperature at nozzle exit, °F
β	nozzle wall divergence angle, referred to the longitudinal axis of the nozzle, degrees
θ	angle subtended by a nozzle sector, degrees

APPARATUS AND PROCEDURE

Models

The nozzle models used in this program are described in figures 1 to 3. Nine basic convergent nozzle designs were tested including a circular, five rectangular-slot, and three multiple-segment nozzles. The circular nozzle had provisions for incorporating turbulence-generating inserts consisting of a sandpaper lining, vortex generators, and concentric rings. The rectangular slot nozzles provided variations in exit aspect ratio and wall angle. The multiple-segment nozzles had the exit area divided equally into 2, 4, or 12 sectors.

All nozzles were designed to have the same physical exit area as that of the three inch diameter circular nozzle. In addition, the nozzles were designed to approximately the same cross-sectional area distribution from entrance to exit. This is shown in figure 4. The circular nozzles varied somewhat from the non-circular nozzles because a straight throat section was required for the turbulence inserts. Because the resulting profile of nozzles No. 7, 8, and 9 when viewed from the side resembles that of the Greek letter Δ, these nozzles have been termed "delta nozzles."

The models were fabricated from mild steel and fiberglass to be consistent with the cold air test requirement.

Nozzle Air Rig

The arrangement of the test facility which was used for this program is shown schematically in figure 5, with further details shown photographically in figure 6. Additional details of the instrumentation are shown in figure 7.

The nozzle models were installed on a bellmouth adapter at the end of the 24 inch inside-diameter plenum chamber. Acoustical lining installed on the interior of the plenum chamber reduced the effective plenum size to 20 inches inside diameter. Internal baffles and a fine mesh screen in the plenum chamber insured uniform distribution of the flow at the entrance of the bellmouth section. The plenum was hung from a super-structure by means of four flexures which minimized resistance to fore and aft motion. Air was introduced into the plenun by way of a flexible bellows joint arrangement. Nozzle thrust was measured by a strain gaged thrust ring installed between the plenum assembly and the rigidly supported air supply pipe.

Airflow was measured with an ASME long radius flow nozzle upstream of the load cell and flow rate was controlled by two valves, one upstream and one downstream of the flow nozzle. The dual valve arrangement maintained a constant Mach number through the flow nozzle for all data points and nozzle sizes. Filtered air for the nozzle tests was obtained from a laboratory supply system at approximately 70°F with a dew point of -40°F or less.

Pressure measurements in the jet wake were obtained with a traversing probe mounted downstream of the plenum. Operation of this probe was remotely controlled to vertical, lateral, or longitudinal positions with respect to the nozzles. Pressure readings were transmitted through transducers to the recording equipment.

A 56 inch diameter ground plane was installed on rails downstream of the plenum. A five-tube total pressure rake which measured pressures along a radial traverse above the surface was attached to the ground plane. The pressure tubes covered a height of .05 to 1.0 inches above the ground plane. The ground plane could be located at distances up to 20 feet from the nozzle.

All data obtained from nozzle testing was automatically recorded on IBM punch card equipment which made it possible to decrease data reduction time to approximately one day. In addition, a Moseley x-y plotter was used to record jet wake pressure for on-line evaluation of nozzle performance.

Data Accuracy

Calibrations of the static rig instrumentation showed that pressure measurements were accurate within ± 0.5 per cent in all axes, thrust scatter band width was 2.0 per cent, and air flow scatter band was 0.7 per cent. Although the test data scatter band appears large, repetition of the test runs six or more times provided a grouping of the data from which mean values of thrust and airflow were determined. It was found that these mean values were within ± 0.5 per cent of the values obtained on another extremely sensitive and precise nozzle calibration rig normally accepted as a standard within The Boeing Company.

The velocity profile of the air entering the nozzle models was closely checked with a rake incorporating ten total pressure probes located in the center of five equal areas. Distortion was found to be negligible for more than 90 per cent of the nozzle inlet diameter.

Plots of the jet wake traverses indicated that minor profile distortion occurred, with the amount of distortion dependent upon the dynamic pressure gradients and the level of pressures being measured. Attempts to eliminate this distortion were not successful. During the dynamic pressure traverses, it was apparent that intense, large scale turbulence was often encountered. No corrections were made in the measurements for the effects of turbulence, consequently the absolute value of dynamic pressure may be somewhat in doubt for specific points. On occasion, random variations of ± 0.05 nozzle exit dynamic pressure were noted; however, most data appeared to fall within a band ± 0.01 nozzle exit dynamic pressure.

Because of uncertainties associated with static pressure measurements in an intensely turbulent stream, all dynamic pressure measurements were obtained as a differential pressure between the indicated probe total pressure and atmospheric pressure. Presentation of the data in this form introduced effects of compressibility, but these were minimized by the low nozzle pressure ratio used for most of the tests.

RESULTS

Nozzle Performance Evaluation

Effective velocity and mass flow coefficients determined for all nozzles are presented in figure 8. Nozzle pressure ratio was varied from 1.4 to 2.4, and all tests were conducted with laboratory supply air of 60 to 80°F. The data shown were obtained by visually fairing results of six or more individual tests on each nozzle over the range of pressure ratios indicated.

Effective velocity coefficients were based on the ratio of effective jet velocity, determined from measured thrust and mass flow, to isentropic jet velocity resulting from the nozzle pressure ratio and temperature. Mass flow coefficients were based on the ratio of measured mass flow to theoretical mass flow determined by the nozzle area, pressure ratio, and temperature. When nozzle exit area is correctly selected to compensate for variation of mass flow coefficients, nozzle thrust efficiency is specified solely by effective velocity coefficient; consequently, effective velocity coefficient provides the best means of comparing the performance of various nozzle designs.

The two factors which were found to influence nozzle performance significantly included (1) internal roughness or flow obstructions near the nozzle throat section (nozzles no. 2 and 3), and (2) divergence of the nozzle walls (nozzles no. 7, 8, and 9). Both factors were found to be dependent upon nozzle pressure ratio, with the losses minimized at the higher nozzle pressure ratios. As may be seen from the results for nozzles no. 1, 2, 3, and 4, thrust losses were largest for obstructions placed in the high velocity regions of the nozzle. Despite the large amount of blockage introduced by the turbulence rings with configuration no. 4, thrust losses were nominal because of the low velocities at that location. The data clearly indicate that both effective velocity and mass flow coefficients decrease with increasing divergence angle for the delta nozzles, but the effect of increasing aspect ratio is less well defined.

Comparison of the effective velocity and mass flow coefficients for nozzles no. 1, 5, 6, 10, and 11 indicates that variation of nozzle exit planform had only small effect upon these coefficients. Consideration of the results of nozzle no. 12, however, suggests that the effective velocity coefficient may be adversely affected by changes of planform in which the nozzle exit perimeter is greatly increased over that of a circular nozzle. The data do not permit precise definition of this trend, nor will the data permit isolation of the effects of other design variables (such as the number and radii of internal corners, area progression changes, surface roughness, etc.). The variation of mass flow coefficient shows even less dependence on nozzle perimeter than does the effective velocity coefficient; consequently, it may be concluded from these data that friction losses associated with large nozzle wetted areas may be a secondary factor in determining nozzle performance.

Free Jet Wake Surveys

Surveys of the dynamic pressures in the free jet wake were completed for all nozzles operating at a pressure ratio of 1.5. The maximum values of dynamic pressure at each survey station are presented as a function of distance from the nozzle exit in figure 9. These data at a nozzle pressure ratio of 1.5 show that substantial reductions of dynamic pressure in the free jet wake may be achieved by each of three methods, namely:

1) distribution of the nozzle exit area in the shape of a long rectangular slot; i.e., increased aspect ratio of the nozzle exit planform. (nozzle no. 6)

2) introduction of lateral components into the flow prior to discharge from the nozzle, as is accomplished with the delta nozzles. (nozzles no. 7, 8, and 9)

3) subdivision of the nozzle into several elements (nozzles no. 10, 11, and 12).

The data of figure 9a indicate also that dynamic pressure degradation of the free jet wake is influenced only to a small degree by disturbances or turbulence introduced into the stream prior to discharge from the nozzle. Two possible explanations for these results may be considered:

1) the scale and intensity of the turbulence generated in the nozzle were of such a small magnitude and persisted for such a short time that the jet was essentially free of turbulence at the nozzle exit.

2) turbulence of the scale, intensity, and orientation that was generated in the nozzle does not play a significant part in the jet wake mixing process.

Of the two possible explanations offered, the latter appears to be more plausible.

Comparison of the results of nozzles no. 1 and no. 5, figures 9a and 9b, shows that changes of the nozzle exit planform from a circular to a square shape had a very minor effect upon the dynamic degradation characteristics of the wake. Increasing the nozzle exit aspect ratio from 1.0 to 6.0, nozzles no. 5 and 6, figure 9b, significantly changed the dynamic pressure degradation characteristics of the rectangular nozzles, but increasing the aspect ratio from 2.0 to 5.0, nozzles no. 7 and 9, figure 9c, for delta nozzles with a 30° divergence angle made a much smaller change in degradation characteristics. In this case, the effect of divergence angle dominates all other variables in determining dynamic pressure degradation.

An interesting effect associated with multiple element nozzles is shown in figure 9d. Comparison of the results of nozzles no. 10, 11, and 12 shows a crossing of the degradation curves at distances of ten equivalent nozzle diameters or more; these results are believed to be caused by a merging of the small jet segments into a very much larger jet wake. The resulting degradation rate of the large jet is much less than that of the smaller jets, consequently, the degradation curves exhibit a "plateau" in which very little reduction of maximum dynamic pressures occur. Note that this effect is much less pronounced

with nozzle no. 11 than with nozzle no. 12; this is a reflection of the fewer number of segments used in nozzle no. 11.

During free jet wake surveys of circular nozzle no. 1, it was noted that a distinct instability in the shape and degradation characteristics of the wake occurred at pressure ratios of approximately 2.1 or greater. At the higher nozzle pressure ratios, the jet wake appeared to divide into a two-lobe pattern which would rotate slowly around the longitudinal axis of the nozzle. This behavior was apparently associated with the appearance of shock wave formations at the nozzle exit, and it was noted that any obstruction immediately adjacent to the nozzle exit would change the occurrence and shape of the lobed jet wake pattern. (For example, placing a hand near the nozzle would alter the jet wake instability characteristics.) This instability, although completely reproducible with the circular nozzle no. 1, was never observed with any of the other nozzles.

Because of the instability noted above, jet wake surveys were completed for a range of nozzle pressure ratios from 1.1 to 2.4 with circular nozzle no. 1, as shown in figure 10a. In addition to the usual jet wake surveys at selected nozzle pressure ratios, a variable pressure survey was conducted with the probe located at the point in the jet wake where maximum values had been previously measured for the various survey stations; this data is shown also in figure 10a.

Because instabilities of the type noted above were not observed with the other nozzles, only limited jet wake surveys at nozzle pressure ratios other than 1.5 were taken. These results are presented in figure 10b through 10d.

Jet wake contour maps of equal dynamic pressure levels were constructed for various nozzles operating at a pressure ratio of 1.5 by cross-plotting data from traverses of the free jet wake at various stations downstream of the nozzle; these contour maps are shown in figure 11. In general, reduction of the length of the dynamic pressure contours appears to be associated with increased width or dispersion of the jet wake. The contour maps show that non-circular jet wakes apparently mix in such a manner that the jet wake approaches a circular cross-section at some point well downstream of the nozzle. This characteristic may be seen in the plot for the rectangular nozzle, AR = 6, figure 11c, and the delta nozzle, AR = 5, $\beta = 5°$, figure 11d. The strong influence of delta nozzle divergence angle is apparent in the plot for nozzle no. 9, AR = 5, $\beta = 30°$, figure 11e; the jet wake does not approach symmetry within the range for which data are available.

It should be noted here that the edge of the jet designated by the symbol $q_z/q_n \approx 0$ exists only as a threshold sensitivity for the equipment used in the wake surveys. Although the boundaries determined in this manner are somewhat fictitious, they provide a basis of comparison of jet spreading characteristics. While not determined precisely, the threshold sensitivity of the equipment appeared to be on the order of 0.0075 psi, which is 0.1% of dynamic

pressure at nozzle exit for the test condition shown. In considering the above profile maps, as well as the similitude plots which follow, it should be noted that individual measurements in turbulent flow may vary widely with time. Because of random variation of both instantaneous and mean values with time, some latitude in interpretation of the results obtained at specific points is possible. In general, all data were interpreted in a manner which would provide conservative values of dynamic pressure degradation.

The results obtained from the free jet wake surveys were analyzed in a manner similar to that of references 6 through 10 to determine the regions of the jet where similitude of the mixing processes existed. If similitude exists, velocity profiles at various distances from the nozzle can be made congruent by suitable choice of velocity and width scale factors, and the analysis of the mixing region will be considerably simplified. Previous investigators have shown by means of numerous experimental and theoretical studies during the past fifty years (references 6 through 10) that the wake of circular jets is characterized by velocity distributions which are approximately similar at large distances from the nozzle. As a result of this similitude, the development of a circular jet may be described by specifying the variation of velocity along the longitudinal axis of the jet, together with a typical lateral dimension related to the spreading of the jet. Previous investigators have successfully extended analyses of this type to the jet wake of two-dimensional slot nozzles, and it was believed that the results of the current tests presented an opportunity to investigate whether similitude exists for a variety of nozzle shapes with three-dimensional jet wakes. Although velocity ratios are normally used in similarity studies, the current analyses were conducted using the data as available in terms of dynamic pressure ratios.

Establishment of similitude in this manner requires knowledge of (1) the transverse distance from the jet axis to the initiation of the active mixing region; i.e., distance to the outer extremity of the core or "apparent core" region, and (2) location of a consistent reference point somewhere in the mixing region. The reference point commonly chosen is the point where the velocity is one-half that of the maximum velocity measured during each traverse; the corresponding reference point in the present tests was selected as the point where dynamic pressure was twenty-five percent of the maximum value measured during each probe traverse across the jet. Figure 12 illustrates the geometry used to specify each of the above quantities, together with a plot illustrating the variation of the core, or "apparent core," width for various non-circular nozzles.

The core is defined to be that region in the center of the jet wake in which the velocity or dynamic pressure is undiminished from that at the nozzle exit, i.e., that area in which no mixing has occurred. The "apparent core" is defined to be that region exclusive of the core in which the velocity or dynamic pressure is essentially constant and equal in value to the maximum value which may be measured at any given axial distance from the nozzle. The values of velocity or dynamic pressure in the "apparent core" are always less than those

in the core region. The "apparent core" provides a means of describing the progression of mixing along two or more coordinate axes toward the center of the jet.

The location of the twenty-five percent reference contours of dynamic pressure, together with the dynamic pressure similarity profiles, are shown for all nozzles in figure 13. From these plots, it is apparent that a high degree of two-dimensional similitude does exist in the mixing region of each of the nozzles. It is also apparent from the twenty-five percent reference contours that these contours were often quite non-linear with respect to distance from the nozzle exit. Greatest non-linearities were noted for the delta nozzles and the segmented nozzles, which is an indication that the high rates of dynamic pressure degradation were obtained from the three-dimensional aspects of these nozzle designs. It should be noted that similitude does not appear to be preserved in regions where merging of two or more jets occur; i.e., near the axis of the twelve-segment nozzle, figure 13j.

The results shown in figure 13 thus indicate that mixing processes in non-circular nozzles may be considered similar in the sense that the non-dimensionalized dynamic pressure distribution of the mixing regions for all nozzles may be approximated by a single curve. However, the utility of this finding is virtually negated by the non-linear characteristics of the "apparent core" region and the twenty-five percent dynamic pressure reference contours. Further study of methods to predict the boundary of the "apparent core" and the twenty-five percent dynamic pressure reference contour will be necessary in order to properly define three-dimensional jet wake characteristics.

Other information related to the mixing processes may also be derived from the twenty-five percent reference contours. The spread of the jet wake is directly related to the spread of these reference contours, and it is apparent that jet spreading does not occur uniformly along the various coordinate axes. This is shown in figure 13d, 13e, 13f, and 13g. It is readily apparent that the jet wakes of nozzle no. 6, figure 13d, and nozzle no. 8, figure 13f, approach symmetry at some point downstream of the nozzle, while the jet wakes of nozzle no. 7, figure 13e, and nozzle no. 9, figure 13g, do not approach symmetry within the distances downstream of the nozzle for which data are available. These results with nozzles no. 7 and no. 9 again demonstrate the strong influence of large nozzle divergence angles upon jet wake spreading and degradation characteristics.

The data shown for nozzle no. 10, figure 13h, nozzle no. 11, figure 13i, and nozzle no. 12, figure 13j, illustrate some of the variations of jet wake spreading and degradation which may be encountered with multiple element nozzles. In these plots, the jet wake from a single sector of the various nozzles is analyzed in the same manner as was done with the preceding nine nozzles. However, the unsymmetrical shape of the jet wake led to an analysis of the inner and outer portion of the jet separately (the terms "inner" and "outer" are related to the longitudinal axis of the nozzle, i.e., that part of the pie-shaped jet wake be-

tween the longitudinal axis of the nozzle and the point of maximum dynamic pressure was termed the "inner" region while the remaining truncated sector of the jet wake was termed the outer region of the wake). In particular, the inner region of the jet showed a distinctly non-linear mixing characteristic which is associated with the merging of the jets near the longitudinal axis of the nozzle. The disappearance of the twenty-five percent reference contour is an indication that the center of the wake for the complete nozzle had merged into one region with all dynamic pressures greater than twenty-five percent of the maximum dynamic pressure which existed at that distance from the nozzle. From figures 13h, 13i, and 13j, it may be seen that merging of the jets occurred more rapidly as the number of nozzle segments became larger. It is also significant that the spread of the twenty-five percent reference contours for the outer mixing region became less as the number of nozzle segments became larger. In this respect, the spreading characteristics of a nozzle with a large number of segments may approach the spreading characteristics of a circular nozzle.

Ground Plane Surveys

Surveys of the dynamic pressure over the ground plane were obtained with a traversing, five-element, total pressure rake. Static pressure taps were also positioned flush with the ground plane surface at five radial locations, figure 7. The maximum dynamic pressures measured adjacent to the ground plane are shown in figure 14, together with the stagnation pressures sensed by the pressure tap at the center of the ground plane.

Because of the limited number of radial stations, the location and magnitude of maximum dynamic pressure adjacent to the ground plane were not identified. However, stagnation pressure measured at the ground plane provides a direct measure of the maximum possible value of dynamic pressure which may exist over the ground plane.

Nozzle pressure ratio was found to have a very minor effect upon dynamic pressure degradation, figure 14a. The reduction in dynamic pressures previously observed in the free jet surveys was confirmed by a corresponding reduction in the stagnation or dynamic pressures measured on or above the ground plane, figures 14a to 14m. Data for the segmented nozzles indicate that the maximum dynamic pressure along the ground plane is represented by the centerline stagnation pressure only at Z/De greater than 10. At the closer ground plane locations maximum stagnation pressure occurs at some radial distance from the center.

The distribution of dynamic pressures above the ground is presented in figures 15 and 16. Figure 15 again illustrates the small effect of nozzle pressure ratio upon the dynamic pressures at the ground surface, while figure 16 shows the variation of dynamic pressure distribution above the ground plane for various nozzles at a pressure ratio of 1.5. It is apparent from these plots that dynamic pressure distributions above the ground plane for non-circular nozzles departed substantially from the profiles associated with conventional circular nozzles.

The plots of figure 16 show the development of dynamic pressure profiles for various axial and radial distances from the nozzle and ground plane. It is apparent that the combined effects of free stream mixing and boundary layer growth contribute to a rapid degradation of dynamic pressures in a radial direction from the point of jet wake impingement on the ground plane. For circular nozzles, highest dynamic pressures in the radial flow over the ground plane were found at heights of 0.05 nozzle diameter or less above the surface of the ground plane. However, for non-circular nozzles, the highest dynamic pressures in the radial flow over the ground were found at heights of 0.07 nozzle diameter or higher above the ground plane. The data for nozzle no. 12, figure 16m, when compared with that of nozzle no. 1, figure 12a, show particularly well changes of distribution of dynamic pressure over the ground plane that may be anticipated as the result of increased mixing prior to impingement with the ground surface. The profiles of dynamic pressure for non-circular nozzles may also exhibit differences of shape and maximum values, depending upon the coordinate axis surveyed. These characteristics are particularly evident in the plots for nozzle no. 6, figure 16f, nozzle no. 7, figure 16g, nozzle no. 8, figure 16h, nozzle no. 9, figure 16i, nozzle no. 10, figure 16j, and nozzle no. 11, figure 16k. The figures also indicate that coalescence of the jets prior to impingement with the ground surface will be reflected in a much thicker flow profile over the ground surface. A profile of this type may be desirable to minimize erosion of loosely held ground surfaces.

DISCUSSION

In order to present more concisely some of the results of these tests, five nozzles were selected for comparison of the thrust and free jet wake dynamic pressure degradation characteristics, figure 17. Effective thrust coefficient shows a small variation with nozzle pressure ratio, while dynamic pressure degradation varies principally as a function of axial distance from the nozzle exit to the plane of measurement. Both effective thrust coefficient and dynamic pressure degradation show large variation with nozzle configuration; however, the changes related to dynamic pressure degradation are much larger than are the changes in effective thrust coefficient. For example; at a nozzle pressure ratio of 1.5 and a distance of four diameters from the nozzle exit, the twelve segment nozzle was found to reduce dynamic pressures in the jet wake by more than eighty percent of that of the circular nozzle, while effective velocity coefficient was reduced by only three and one-half percent. In the case of the delta nozzle (β = 5°, AR = 5.0) at a nozzle pressure ratio of 1.5 and a distance of four diameters from the nozzle exit, the results show a fifty percent reduction in dynamic pressure with less than one percent reduction in effective velocity coefficient. It may be noted that the delta nozzle (β = 30°, AR = 5) was also very effective in achieving dynamic pressure degradation of more than 80%; however, the effective velocity coefficient was reduced by approximately seven percent with this nozzle design.

Further analyses of the interrelationship of dynamic pressure degradation and thrust are shown in figure 18. Using the difference between the free jet dynamic pressure of a circular nozzle and that of other nozzles as a criterion, it may be seen that maximum reductions of dynamic pressure relative to that of the circular nozzle are achieved in the range of four to eight nozzle diameters from the nozzle exit. Significantly, the greatest reductions are achieved at the correspondingly closer locations with respect to the nozzle exit. Figure 18 also indicates that a large reduction of dynamic pressures may be achieved with small thrust losses. For two nozzles tested, no. 6 and no. 11, no thrust losses were incurred despite the fact that dynamic pressures were greatly reduced from that of the circular nozzle. Within certain limits, it may be concluded that dynamic pressure degradation of the free jet wake is virtually independent of nozzle thrust performance. For the largest values of dynamic pressure degradation, a reduction of nozzle thrust is indicated by the data.

Correlation of free jet wake dynamic pressure degradation characteristics as a function of nozzle exit perimeter is shown in figure 19. Although dynamic pressure degradation appears to increase with increasing nozzle exit perimeter, it is clear that other factors also exert a very large influence upon dynamic pressure degradation. This effect is shown most clearly in the data for delta nozzles no. 8 and 9 of figure 19. Both nozzle no. 8 and no. 9 had essentially equal values of exit perimeter, but the nozzle divergence angle for nozzle no. 8 was 5°, compared with a corresponding divergence angle of 30° for nozzle no. 9. The curves were faired through data points of nozzles no. 7 and no. 9 because both nozzles had the same divergence angle of 30°.

During analysis of the data, it was found that the curves of figure 19a were not completely defined by the rectangular nozzles tested in the present program. Additional data, shown by the flagged symbols in figure 12a, were obtained from reference 4 by computing jet wake dynamic pressures, then extrapolating the results to a nozzle pressure ratio of 1.5 to be consistent with the other nozzle data.

Replotting the data of figure 19a, with aspect ratio of the nozzle exit as a primary variable, produced the results shown in figure 20. Extrapolated data from reference 4 were utilized again as shown by the flagged symbols in figure 20. It is clear from figure 20 that increasing aspect ratio results in lower dynamic pressures in the exhaust jet wake; however, the change of dynamic pressure as a function of aspect ratio becomes progressively less as aspect ratio is increased.

By combining data from figures 19 and 20, it was found that the effect of delta nozzle divergence angle could be represented by the curves shown in figure 21. It is apparent from these curves that increasing nozzle divergence angle provides corresponding lower dynamic pressures in the exhaust jet wake, with progressively smaller benefits obtained as nozzle divergence angle increases.

A comparison of maximum dynamic pressures in the free jet wake with the maximum dynamic pressures or stagnation pressures measured on or adjacent to the ground plane is shown in figure 22. From these results, it is apparent that the ground plane did not substantially change the free jet mixing characteristics. Although the effect of the ground plane was similar for all nozzles tested, those nozzles with very rapid jet wake degradation characteristics were least affected by the presence of the ground plane.

CONCLUDING REMARKS

Several small-scale exhaust nozzle models have been evaluated with respect to nozzle performance and jet wake degradation characteristics. Effective velocity and mass flow coefficients were found to be related primarily to internal passage details (i.e., roughness and wall divergence), while jet wake degradation characteristics were related to nozzle exit planform, divergence of the flow at the nozzle exit, and subdivision of the jet wake into smaller elements. The present results indicate that additional dynamic pressure degradation may be achieved by nozzle designs which combine all three of these factors, (i.e., nozzle exit planform, flow divergence, and subdivisions of the wake). Although thrust losses do not appear to be directly related to dynamic degradation characteristics, it appears that nozzle designs for maximum dynamic pressure degradation will be somewhat larger, will have more wetted surface area, and will be more susceptible to internal flow losses than circular nozzles. Nozzles which incorporate flow divergence (as exemplified by the delta nozzles) will be penalized also by the cosine law of vectored thrust components.

The present results indicate that a high degree of similarity exists throughout the free jet mixing region of each nozzle; however, strong three-dimensional effects make prediction of the boundaries and reference contours of the mixing region difficult.

The close correlation between free jet wake characteristics and the dynamic pressure imposed upon the ground plane has been demonstrated, and it is evident that any significant reduction of dynamic pressures in the free jet wake will produce a corresponding reduction of the dynamic pressures imposed upon the ground surface.

Airplane Division, The Boeing Company
Renton, Washington
October 25, 1963

REFERENCES

1. Kuhn, Richard E.: An Investigation to Determine Conditions Under Which Downwash from VTOL Aircraft Will Start Surface Erosion From Various Types of Terrain. NASA TN D-56, September 1959.

2. Morse, A.: VTOL Downwash Impingement Study, Summary Report. TREC Technical Report 61-37, Hiller Aircraft Corp., August 1960.

3. Grotz, C. A.: Simulated VTOL Exhaust Impingement on Ground Surfaces. D2-6791, The Boeing Company, June 1960.

4. Laurence, James C., and Benninghaff, Jean M.: Turbulence Measurements in Multiple Interfering Air Jets. NACA TN 4029, December 1957.

5. Coles, Willard D.: Jet Engine Exhaust Noise From Slot Nozzles. NASA TN D-60, September 1959.

6. Prandtl, L.: The Mechanics of Viscous Fluids. (Included in Durand's Aerodynamic Theory, Volume III, Division G, 1935, Julius Springer, Berlin.)

7. Schlichting, H.: Boundary Layer Theory, McGraw-Hill, New York, 1955.

8. Townsend, A. A.: The Structure of Turbulent Shear Flow. Cambridge University Press, London, 1956.

9. Johannesen, N. H.: Further Results on the Mixing of Free Axially Symmetrical Jets of Mach Number 1.40. A.R.C. 20, 281, F.M. 2817, N.88. University of Manchester, May 1959.

10. Kolpin, Marc A.: Flow in the Mixing Region of a Jet. ASRL TR 92-3, Massachusetts Institute of Technology, June 1962.

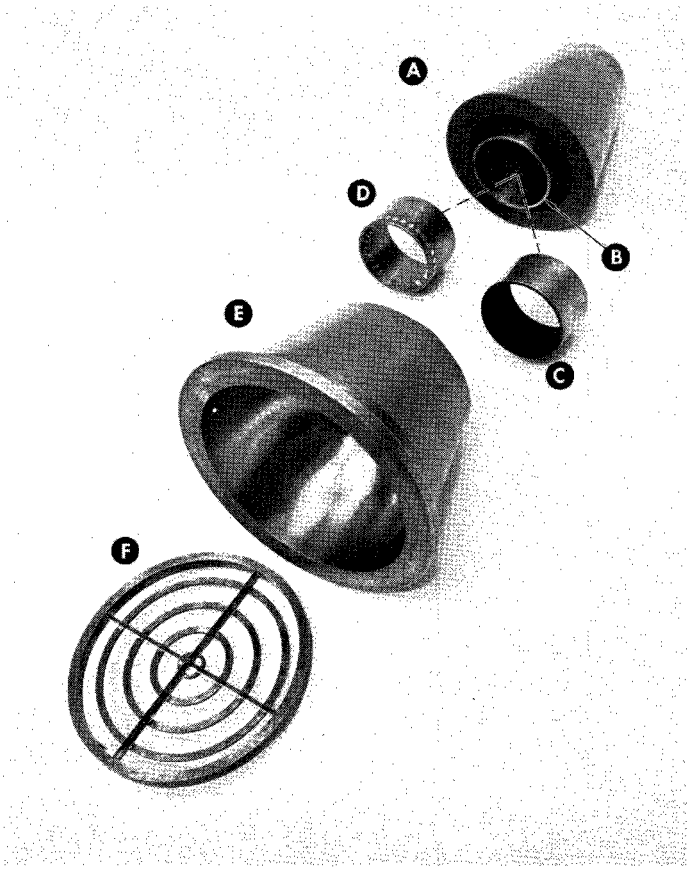

A. PARALLEL SECTION (ADAPTER FOR INSERTS)

B. SMOOTH INSERT (USED WITH NOZZLE CONFIGURATION NO. 1)

C. SANDPAPER INSERT (USED WITH NOZZLE CONFIGURATION NO. 2)

D. VORTEX GENERATOR INSERT (USED WITH NOZZLE CONFIGURATION NO. 3)

E. CONVERGENT SECTION (USED WITH NOZZLE CONFIGURATIONS NO. 1 THROUGH NO. 4)

F. TURBULENCE RINGS (USED WITH NOZZLE CONFIGURATION NO. 4)

NOTE:
CONFIGURATION NO. 4 CONSISTED OF NOZZLE CONFIGURATION NO. 1 WITH THE ADDITION OF THE TURBULENCE RINGS UPSTREAM OF THE CONVERGENT SECTION

Figure 1.- Circular nozzle configurations.

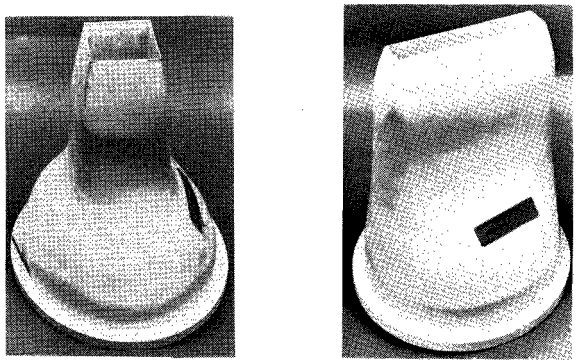

NO. 5 NO. 6

RECTANGULAR NOZZLES

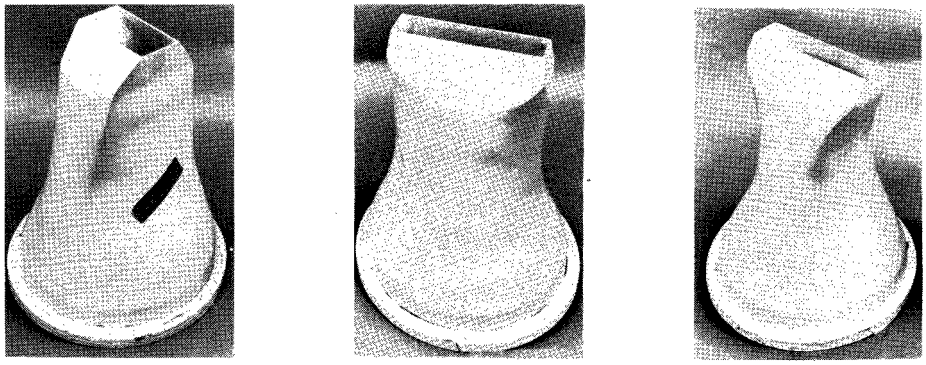

NO. 7 NO. 8 NO. 9

DELTA NOZZLES

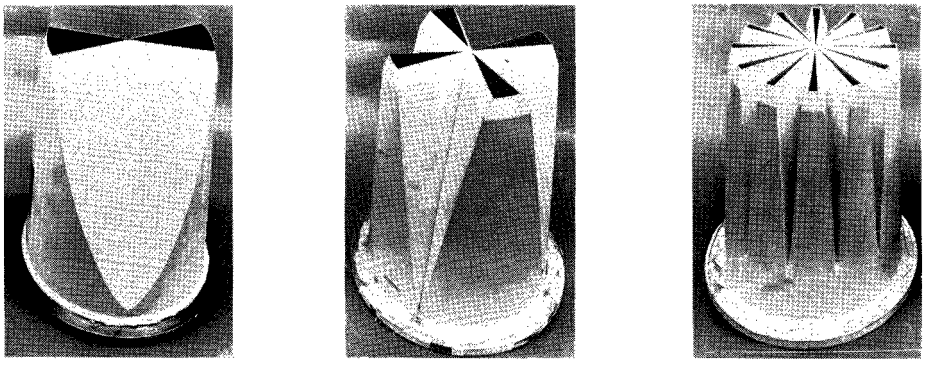

NO. 10 NO. 11 NO. 12

SEGMENTED NOZZLES

Figure 2.- Non-circular nozzle configurations.

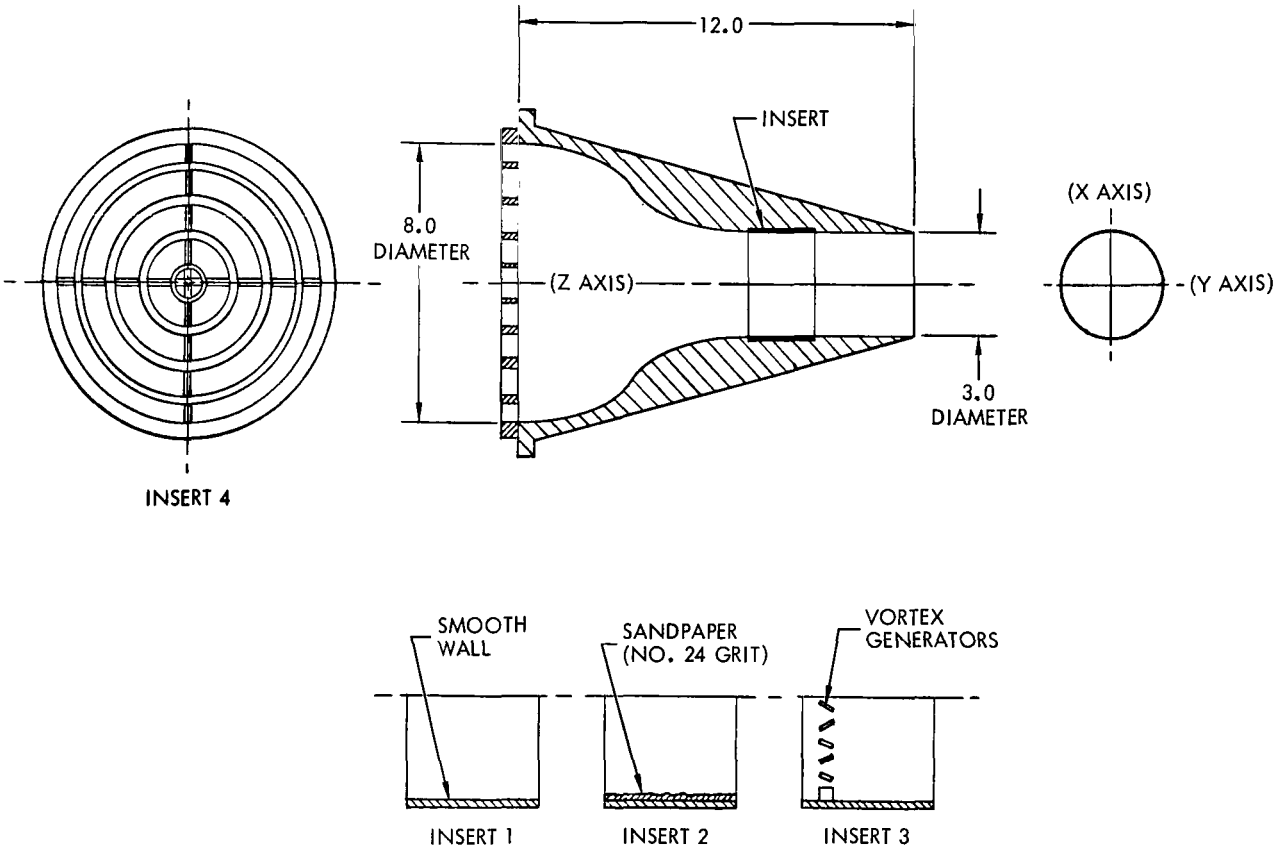

(a) CIRCULAR NOZZLE AND INSERTS

Figure 3. - Nozzle configurations.

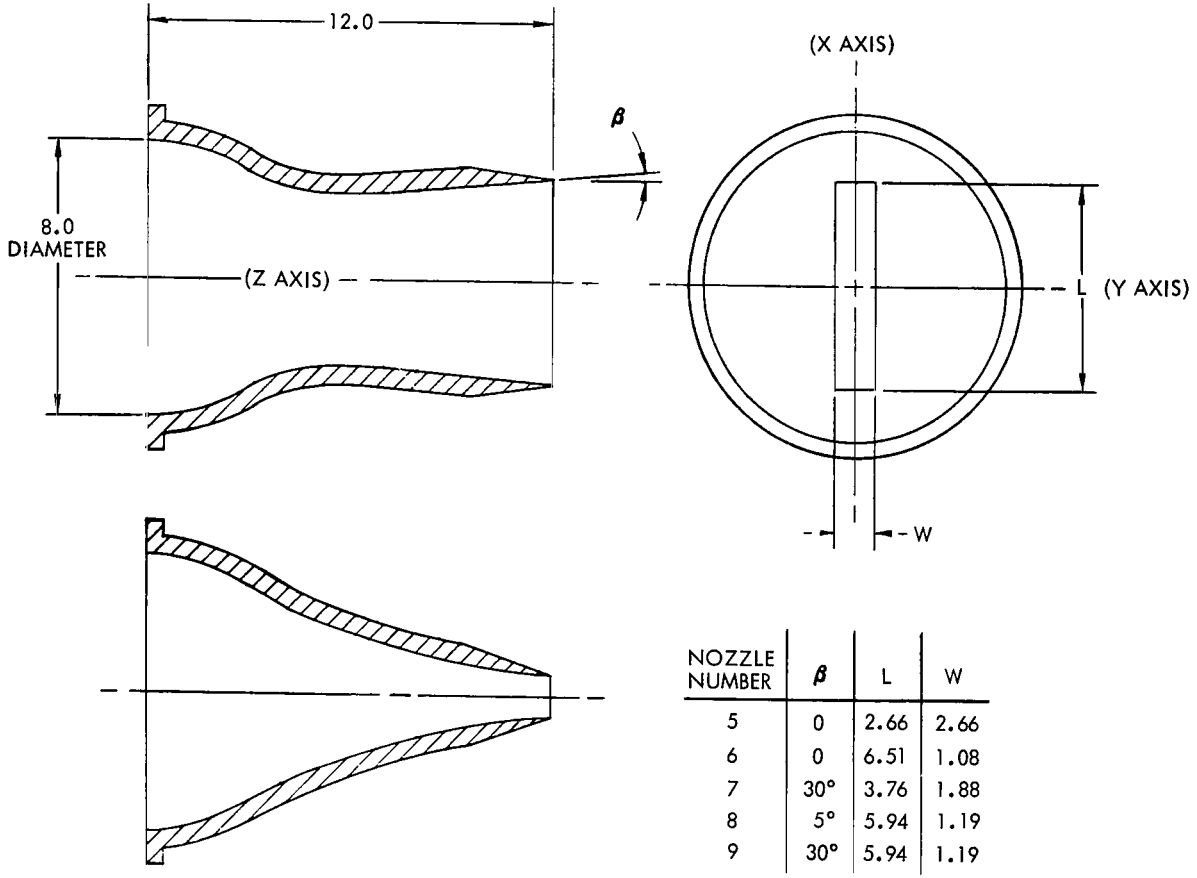

NOZZLE NUMBER	β	L	W
5	0	2.66	2.66
6	0	6.51	1.08
7	30°	3.76	1.88
8	5°	5.94	1.19
9	30°	5.94	1.19

(b) RECTANGULAR SLOT NOZZLES

Figure 3.- Continued.

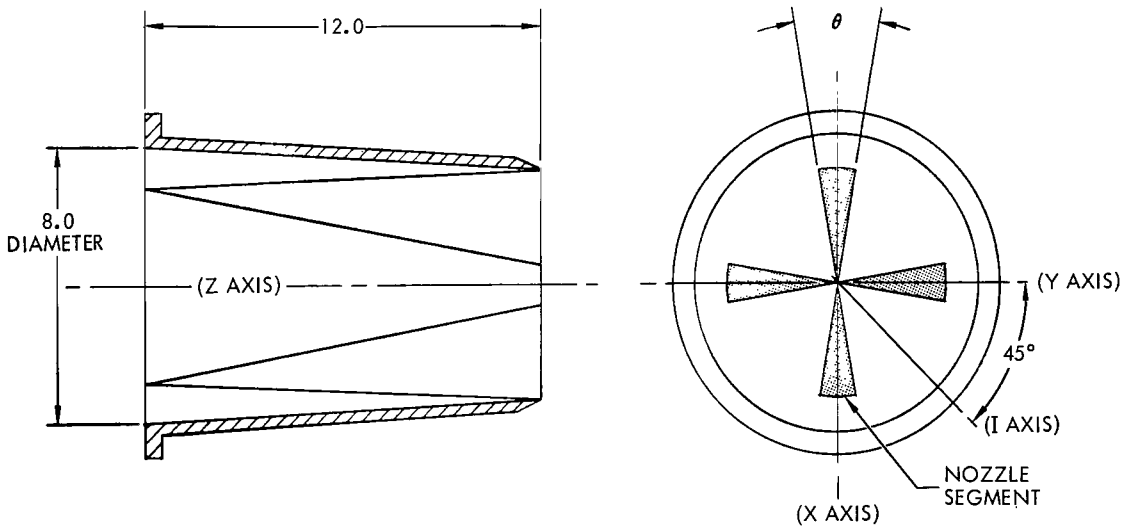

NOZZLE NUMBER	NUMBER OF SEGMENTS	θ
10	2	36°
11	4	18°
12	12	6°

(c) MULTIPLE SEGMENT NOZZLES

Figure 3.- Concluded.

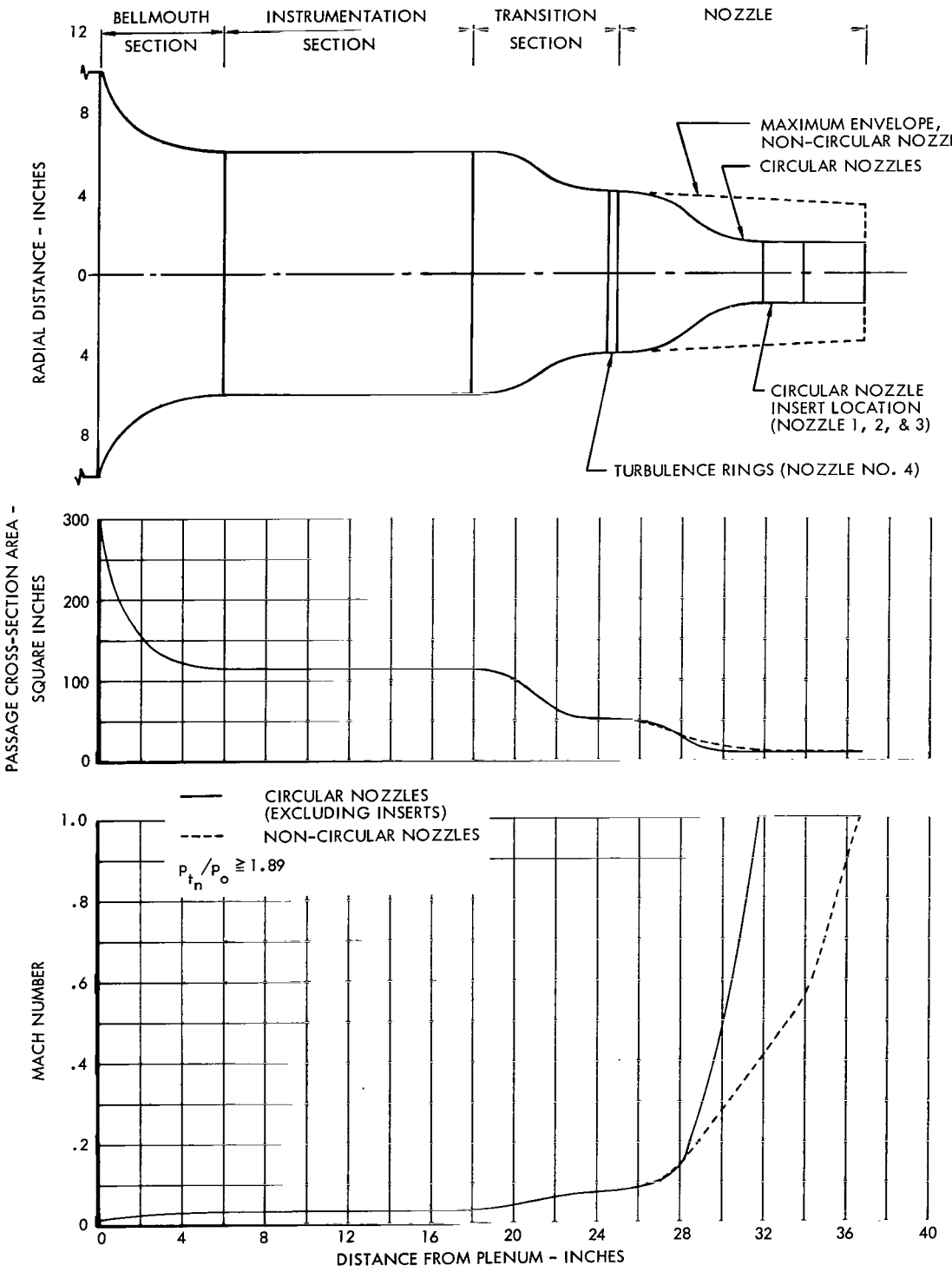

Figure 4. - Typical nozzle cross-sectional area and Mach number progression.

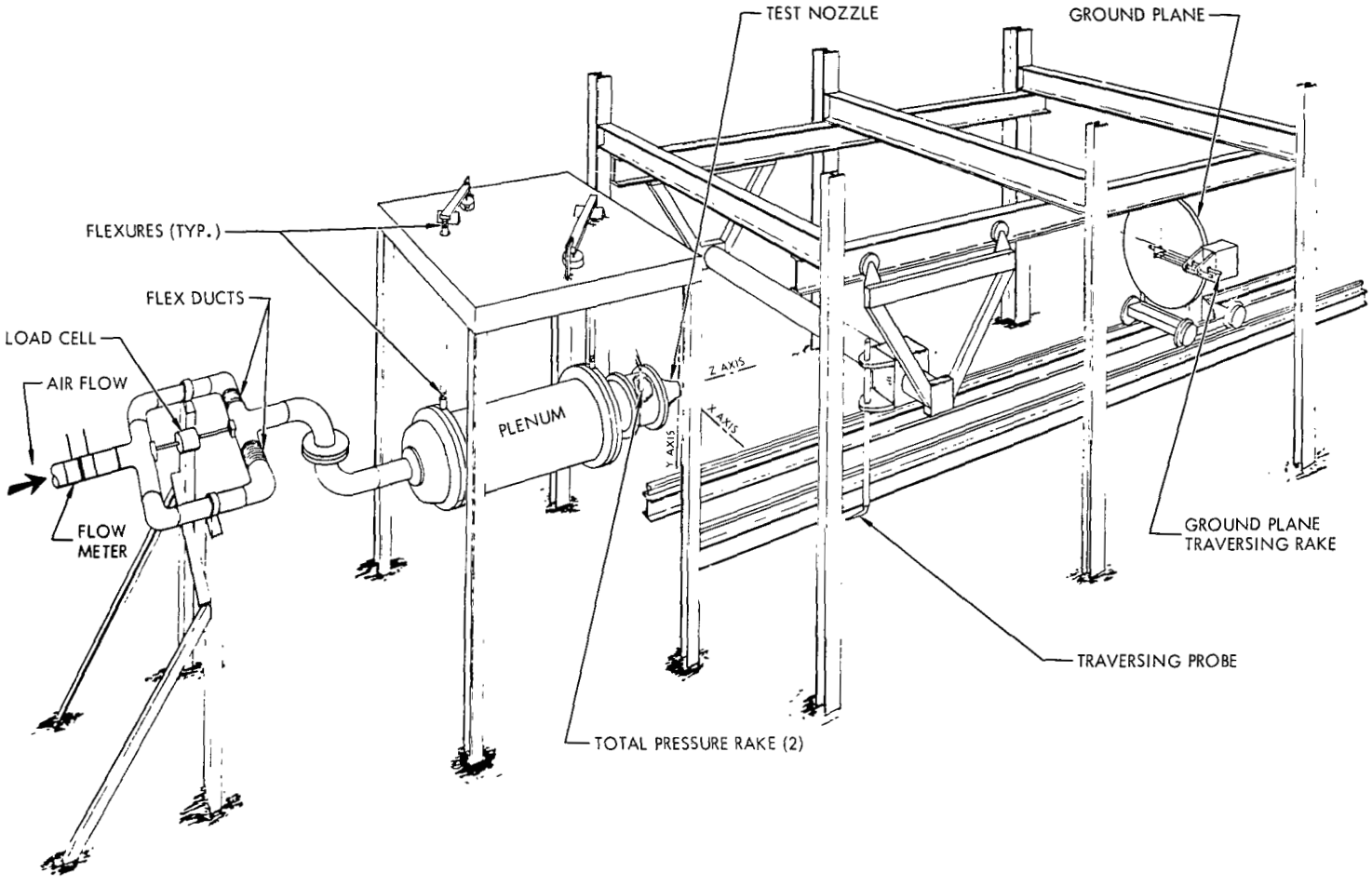

Figure 5. - Schematic of test rig and facilities.

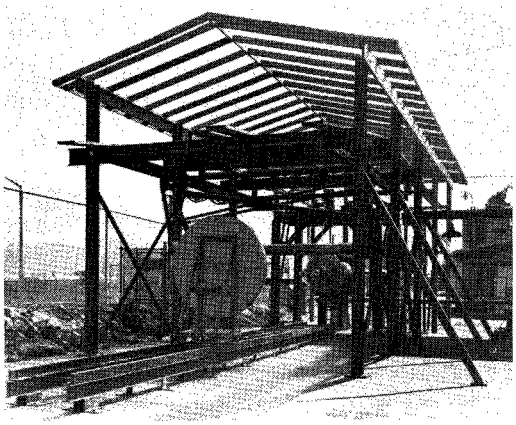

TEST RIG

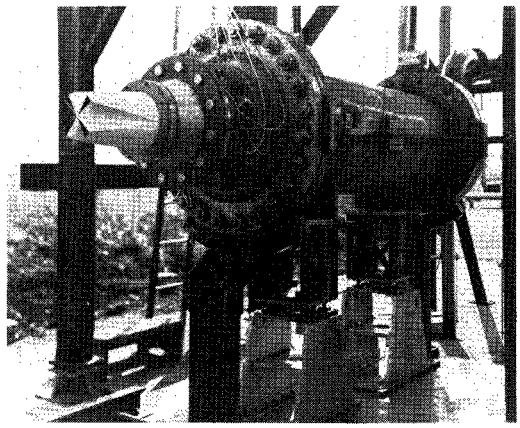

PLENUM CHAMBER

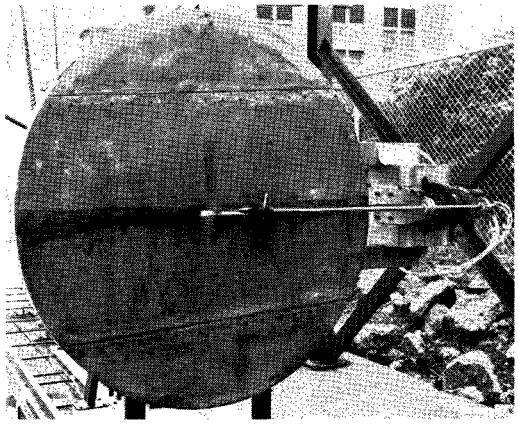

GROUND PLANE WITH
TOTAL PRESSURE RAKE

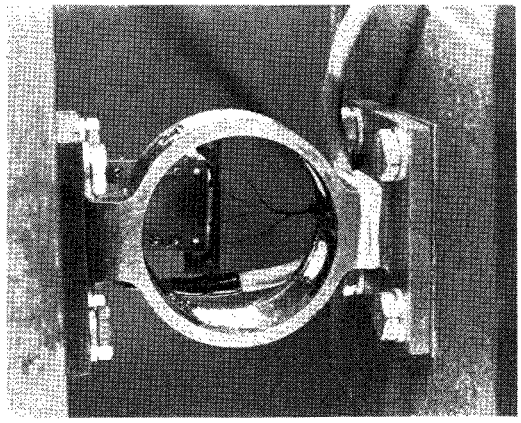

THRUST MEASURING RING
WITH STRAIN GAGES

Figure 6.- Photographs of test rig.

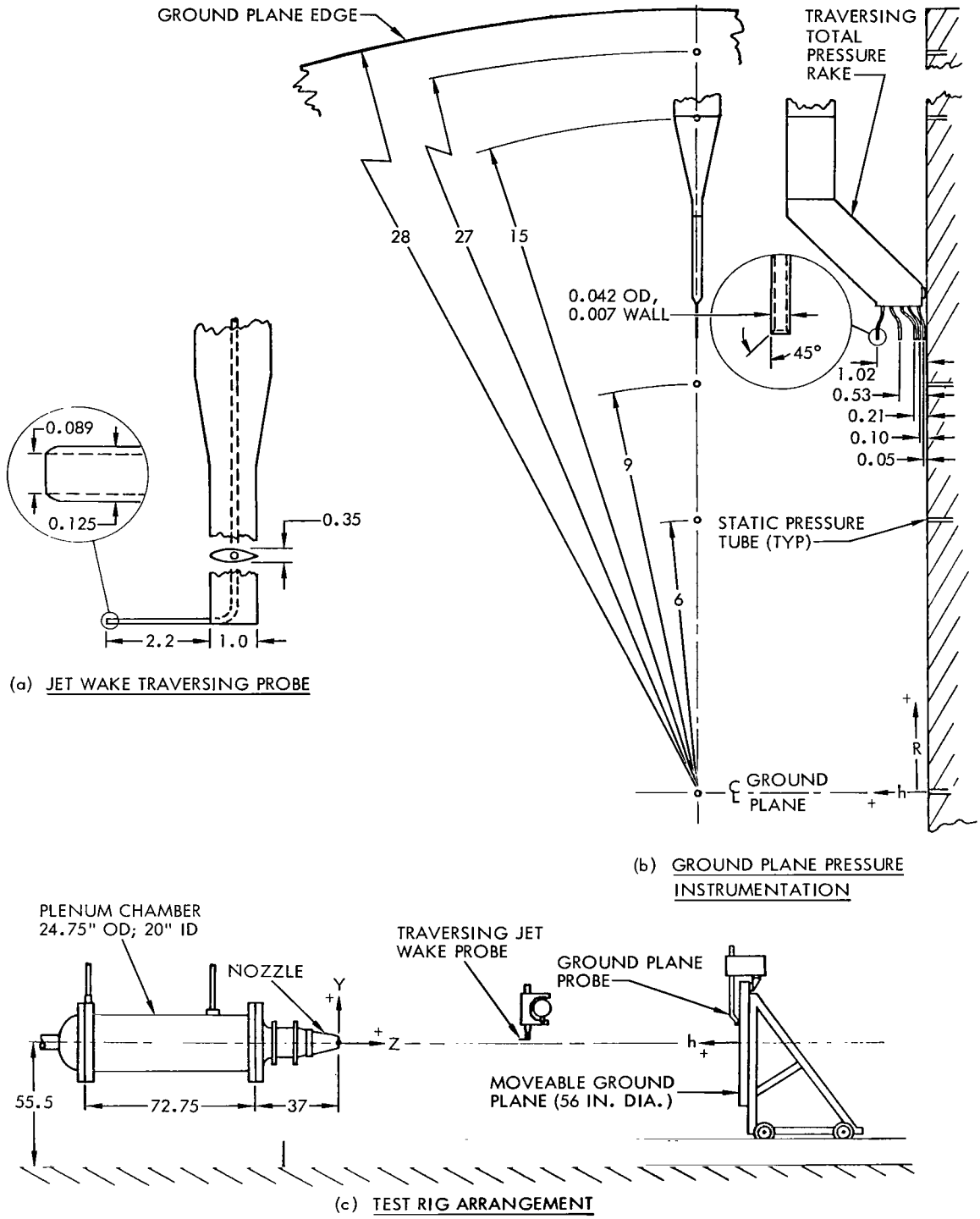

Figure 7.- Schematic of test rig and instrumentation.

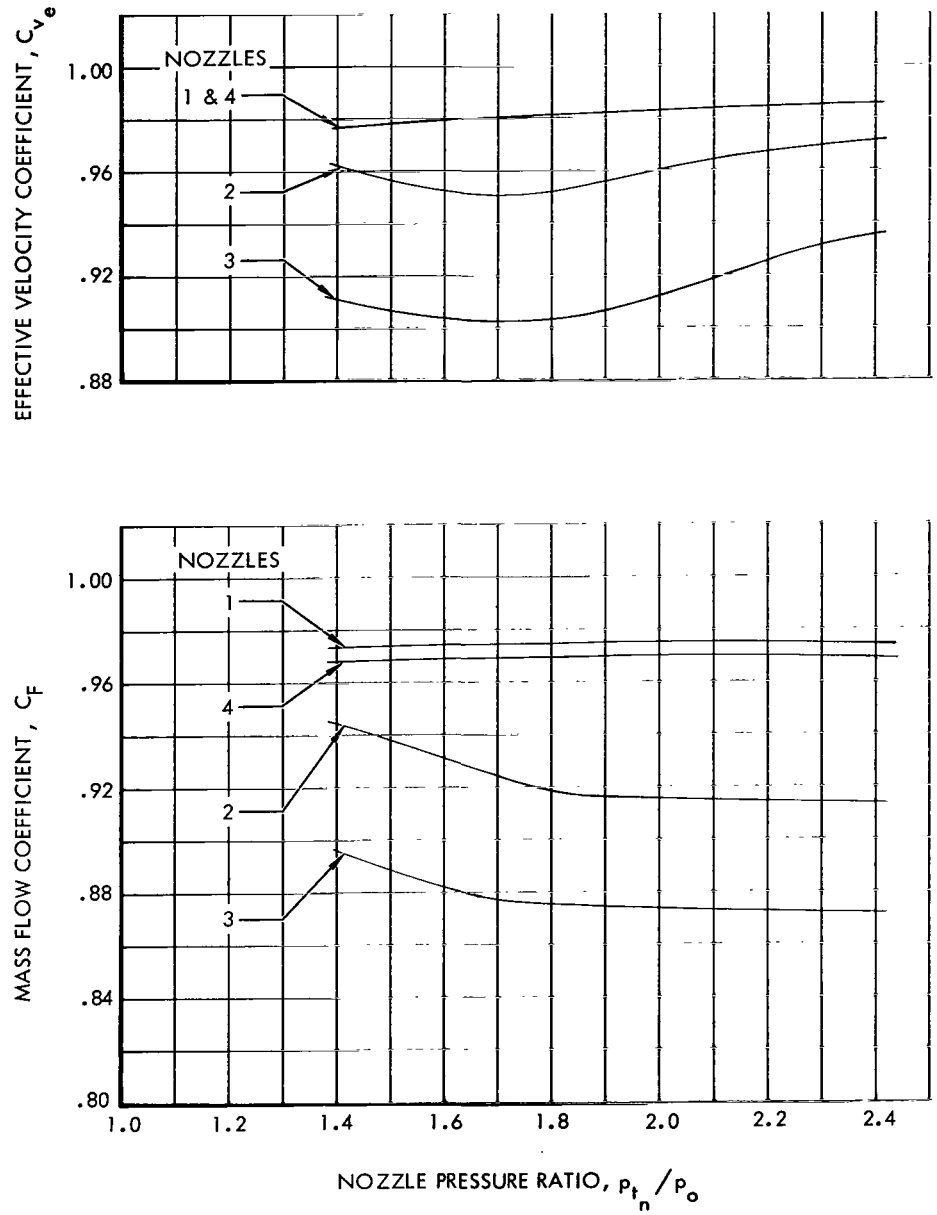

(a) CIRCULAR NOZZLES

Figure 8.- Variation of effective velocity and mass flow coefficients with nozzle pressure ratio.

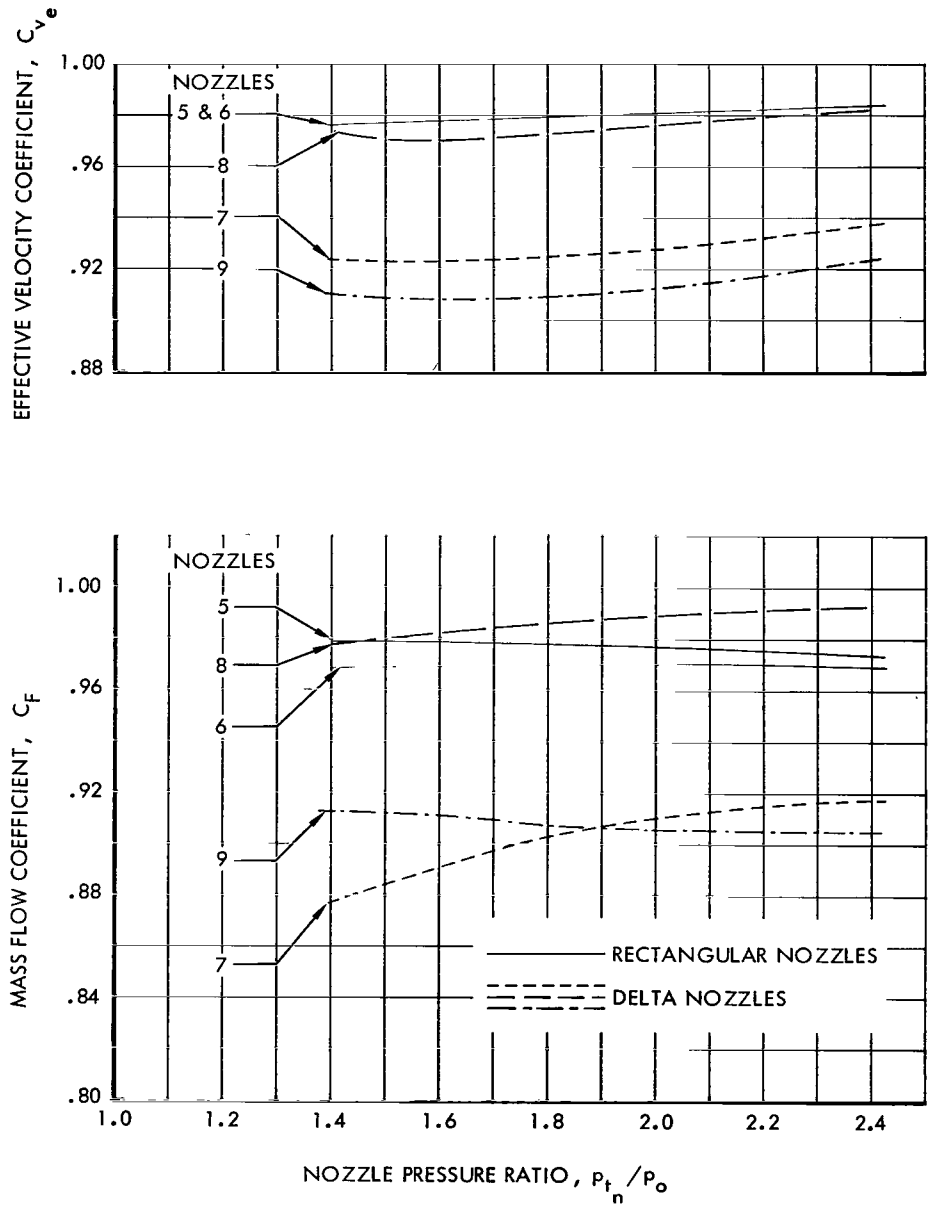

(b) RECTANGULAR AND DELTA NOZZLES

Figure 8.- Continued.

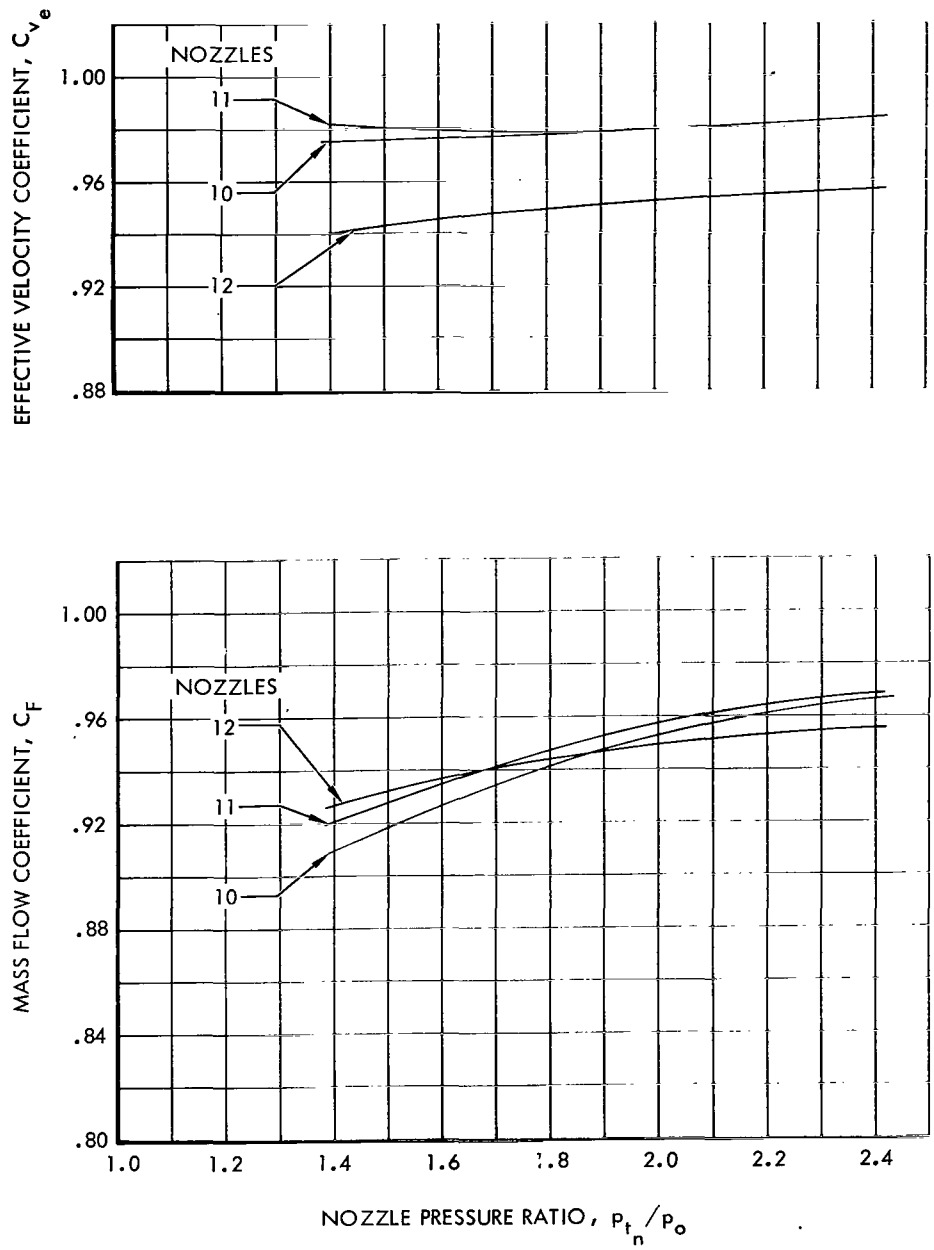

(c) SEGMENTED NOZZLES

Figure 8.- Concluded.

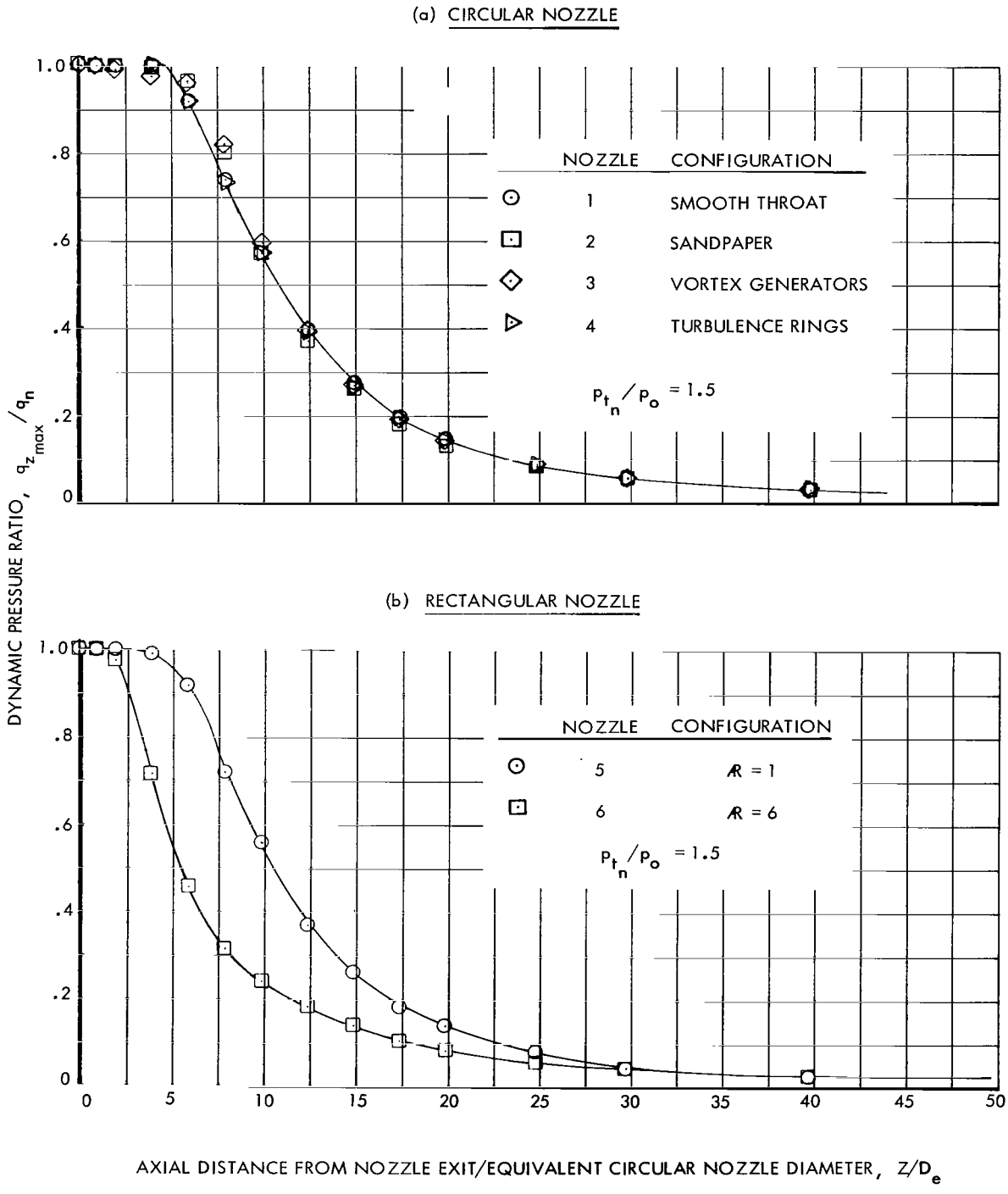

Figure 9.- Jet wake dynamic pressure degradation.

(c) DELTA NOZZLES

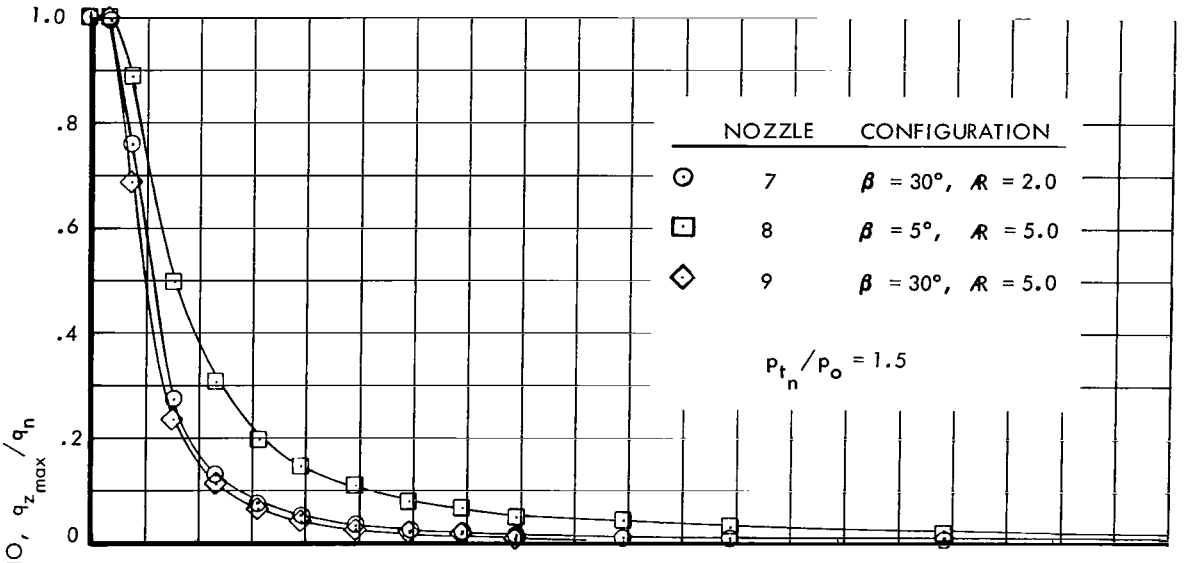

(d) SEGMENTED NOZZLES

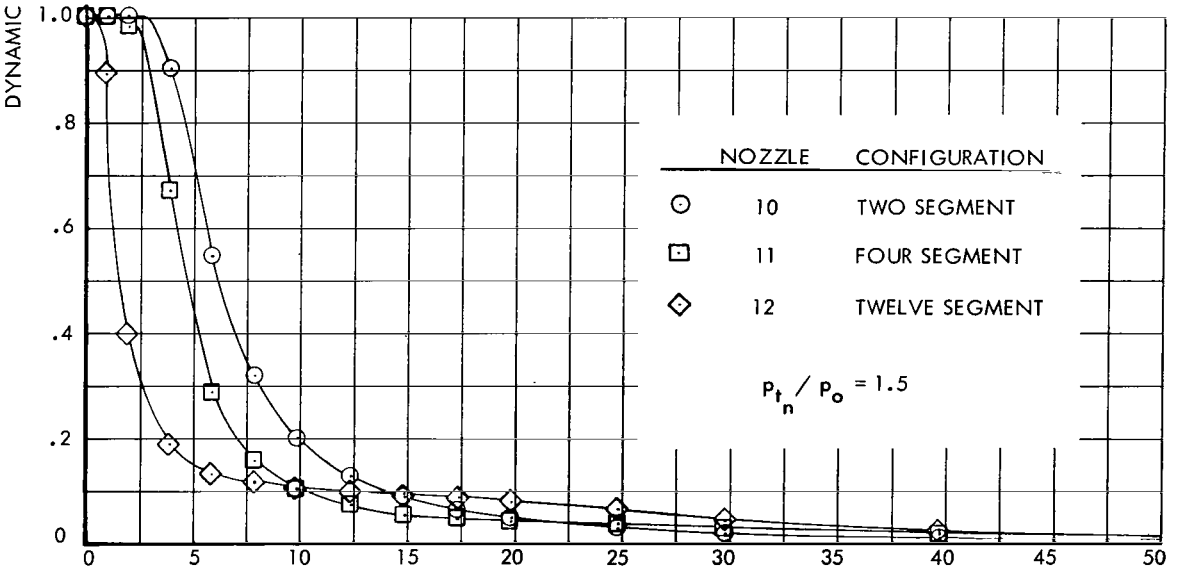

DYNAMIC PRESSURE RATIO, $q_{z_{max}}/q_n$

AXIAL DISTANCE FROM NOZZLE EXIT/EQUIVALENT CIRCULAR NOZZLE DIAMETER, Z/D_e

Figure 9.- Concluded.

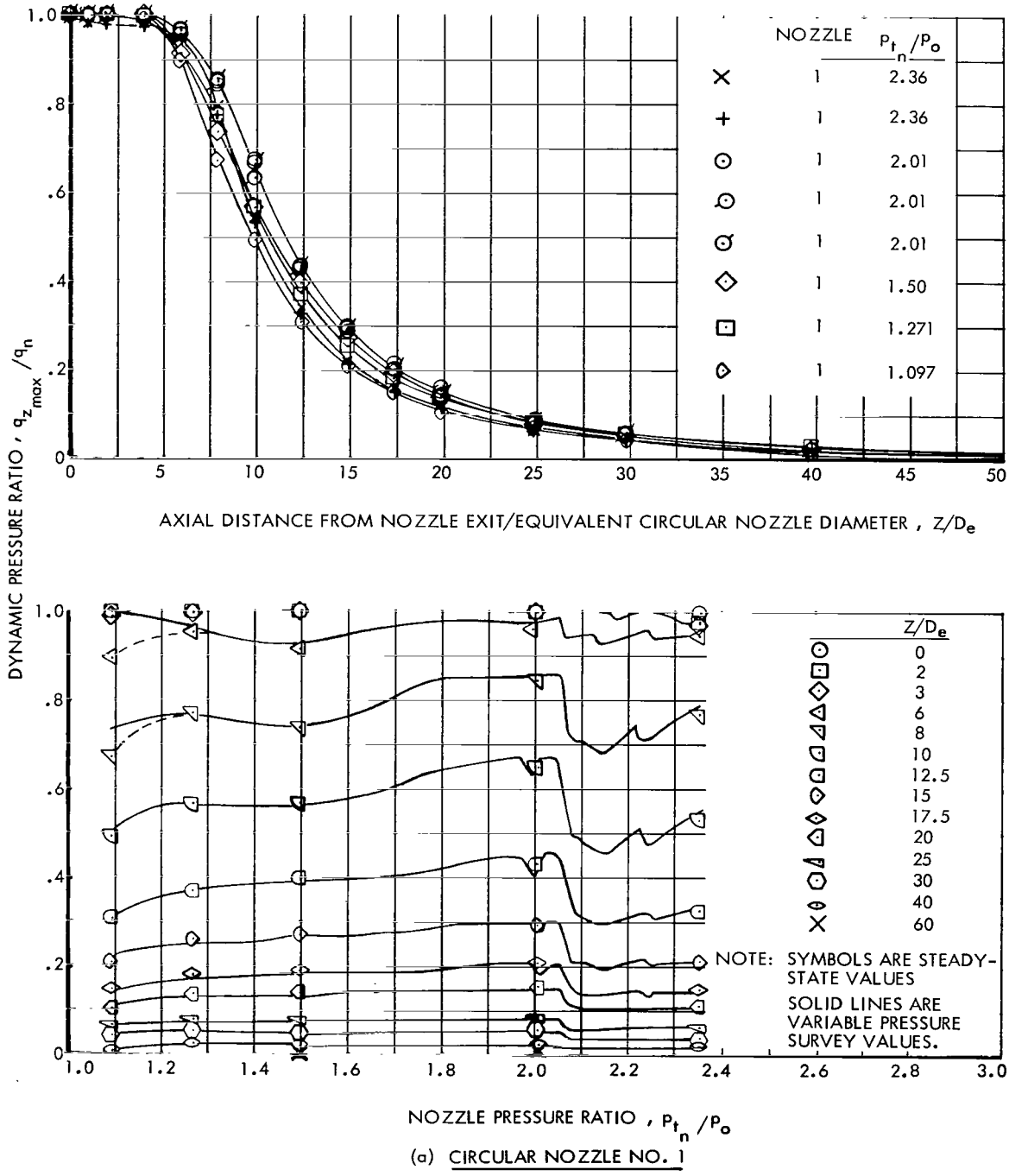

(a) CIRCULAR NOZZLE NO. 1

Figure 10.- Jet wake dynamic pressure degradation for various nozzle pressure ratios.

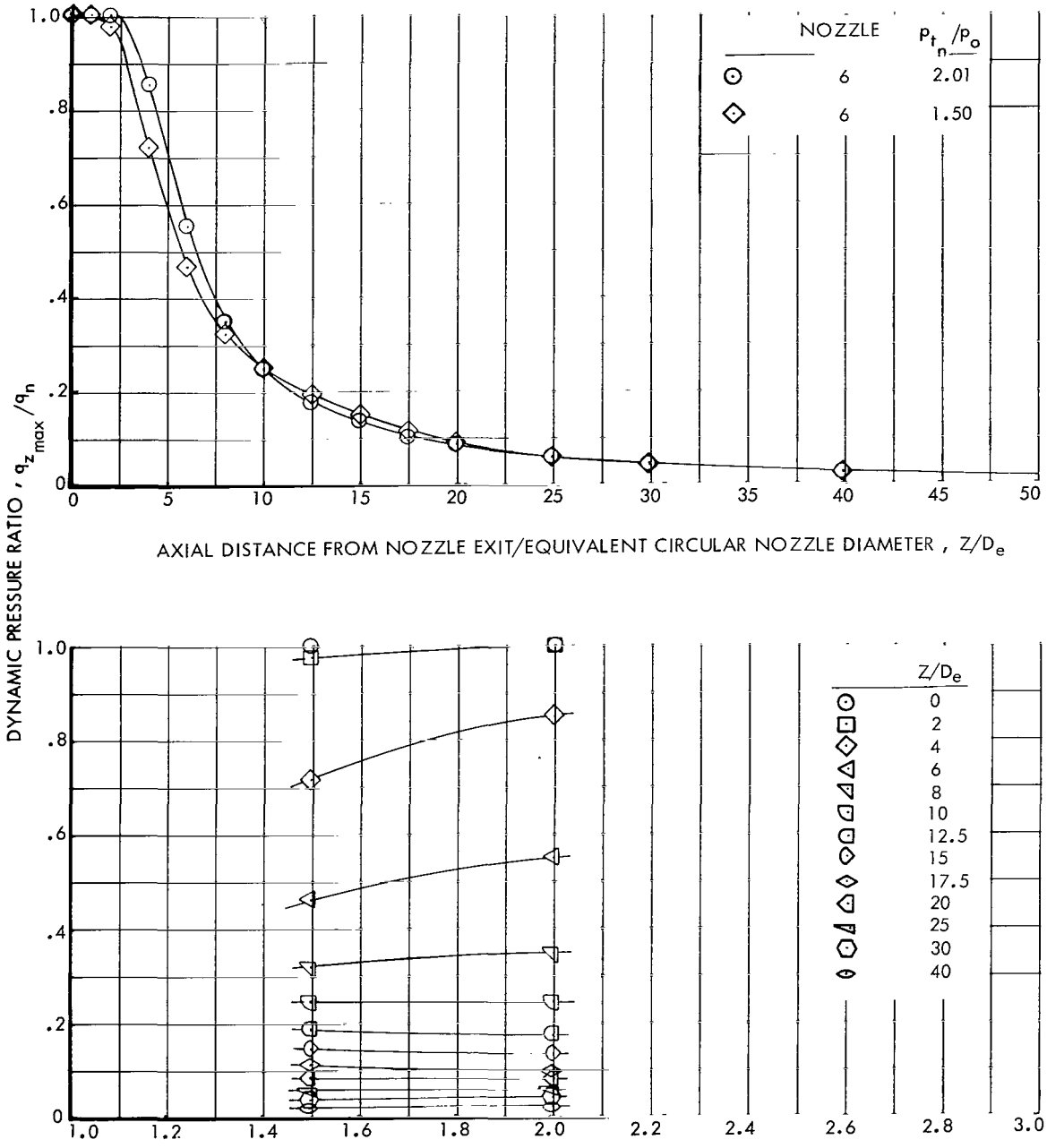

(b) RECTANGULAR NOZZLE NO. 6 ($AR = 6$)

Figure 10.- Continued.

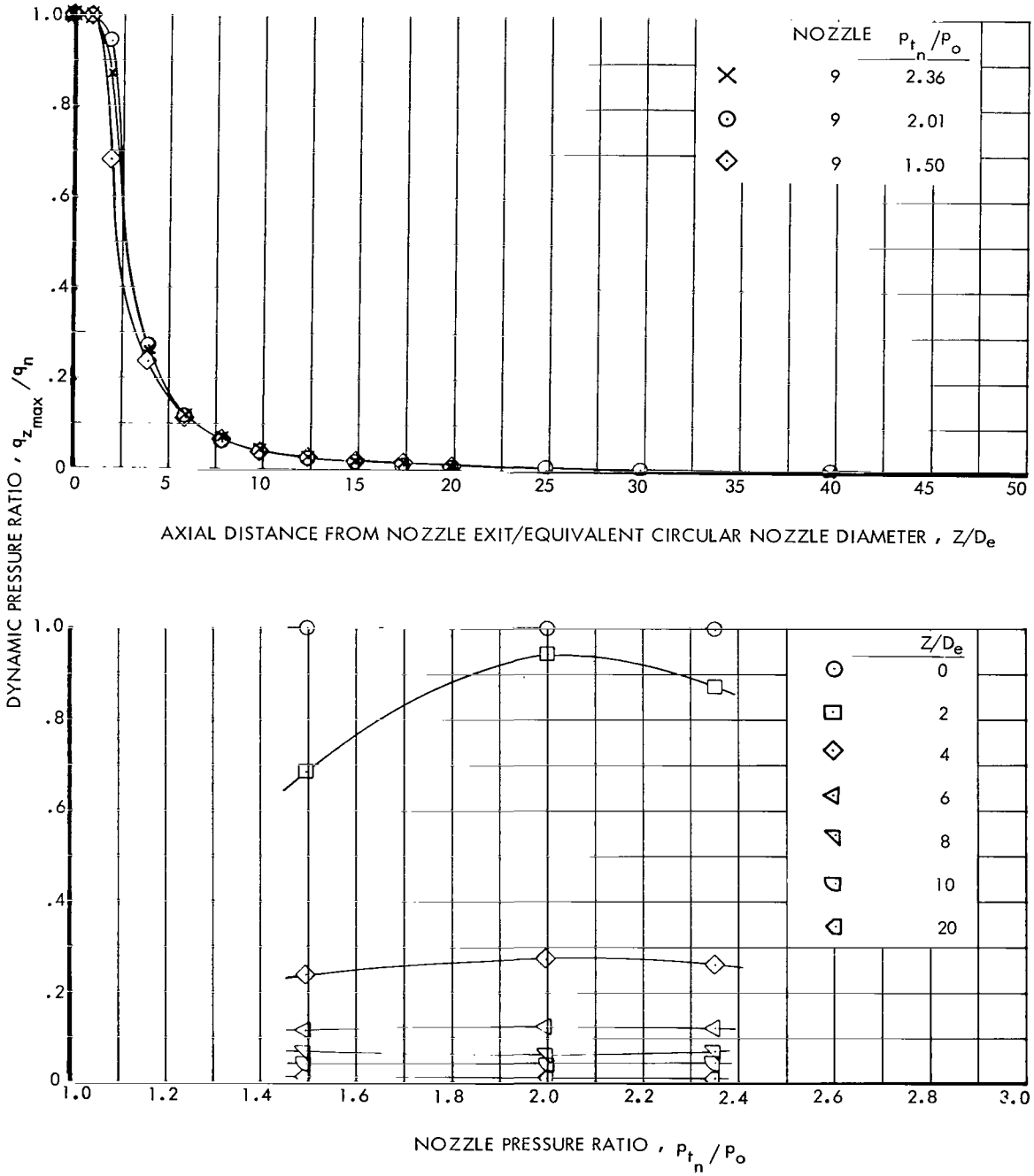

(c) DELTA NOZZLE NO. 9 ($A = 5, \beta = 30°$)

Figure 10.- Continued.

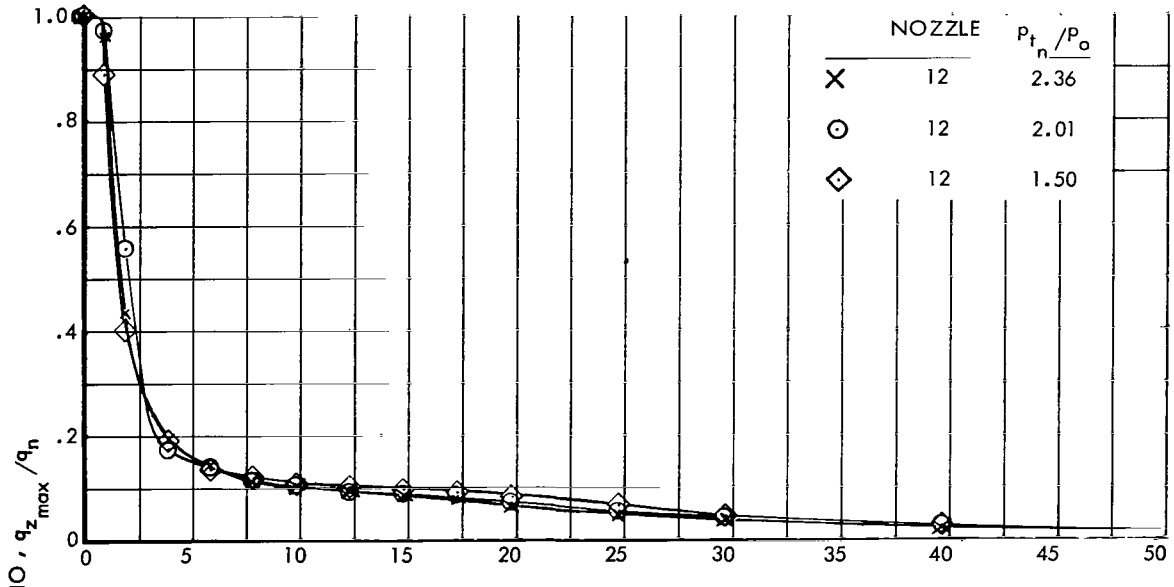

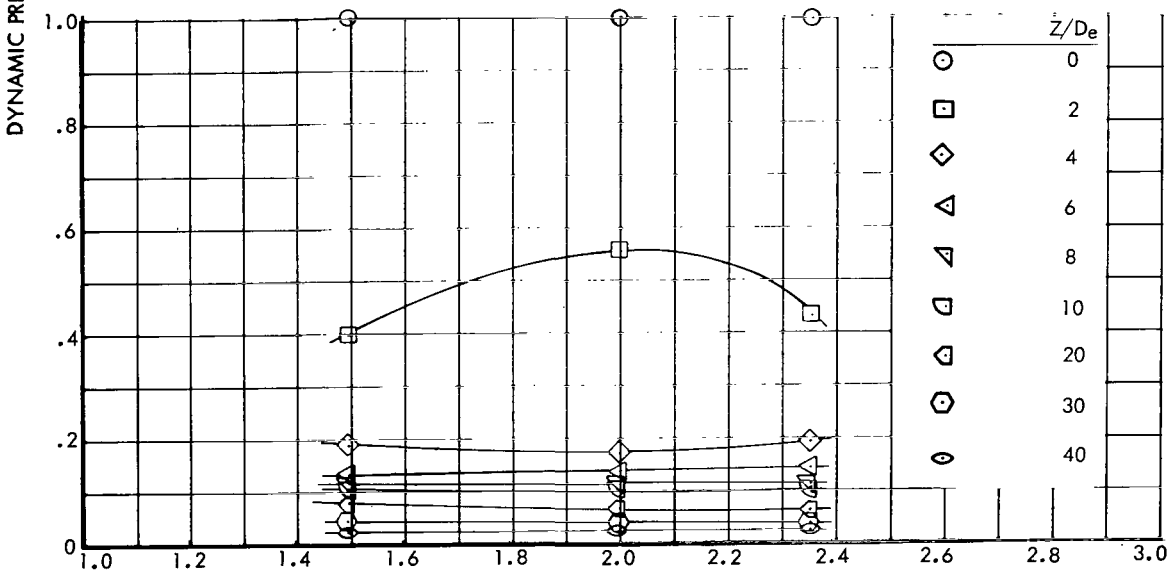

(d) TWELVE SEGMENT NOZZLE NO. 12

Figure 10.- Concluded.

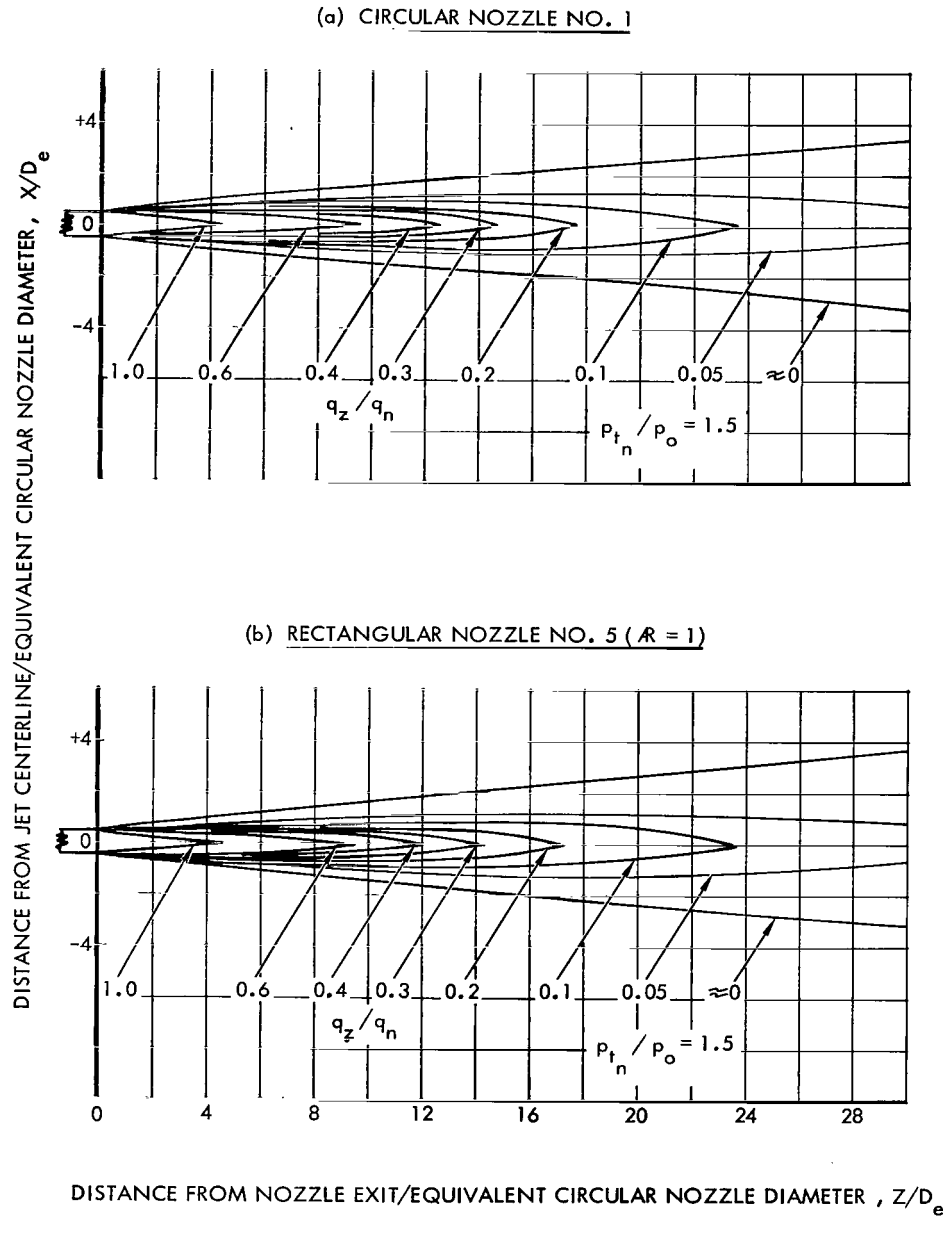

Figure 11.- Jet wake dynamic pressure maps.

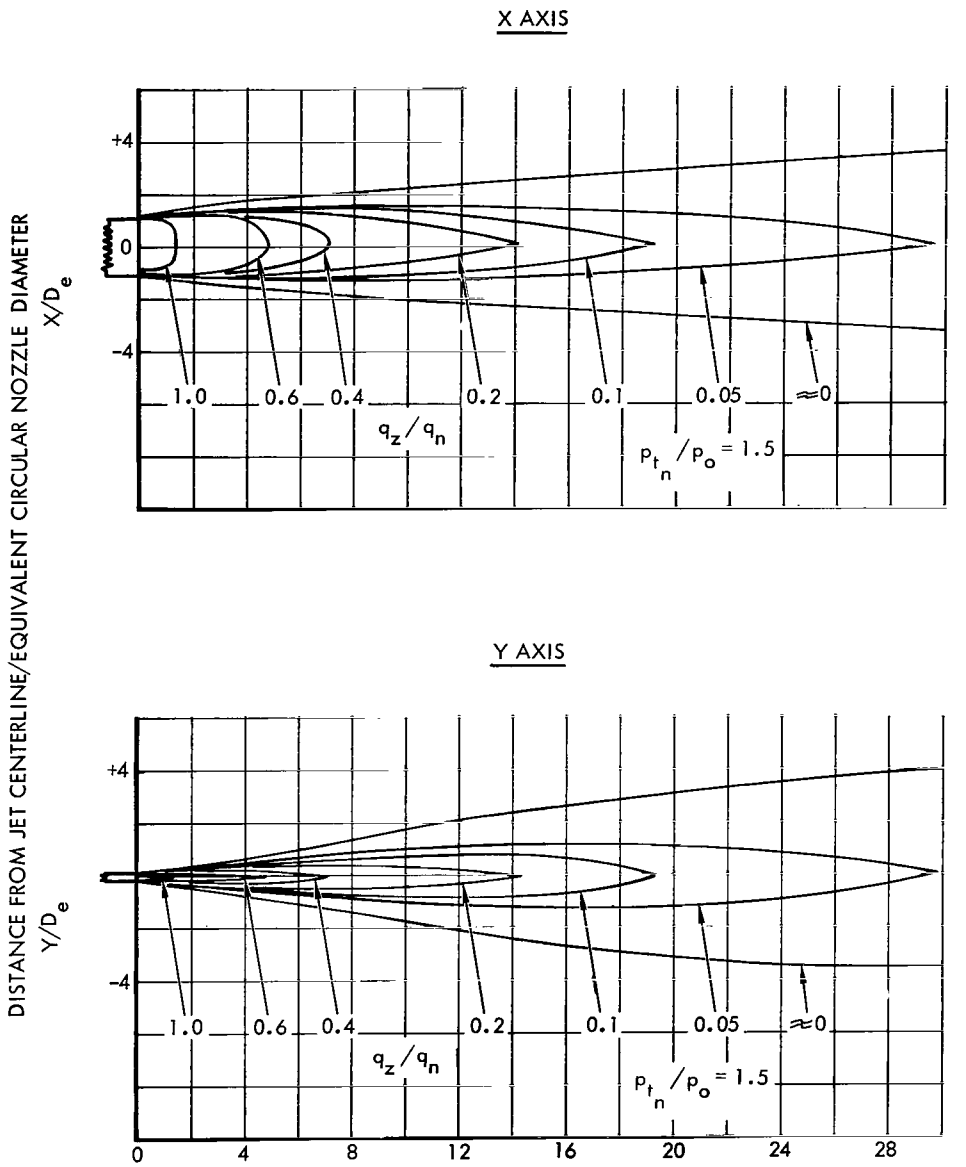

(c) RECTANGULAR NOZZLE NO. 6 ($\mathcal{AR}$ = 6)

Figure 11.- Continued.

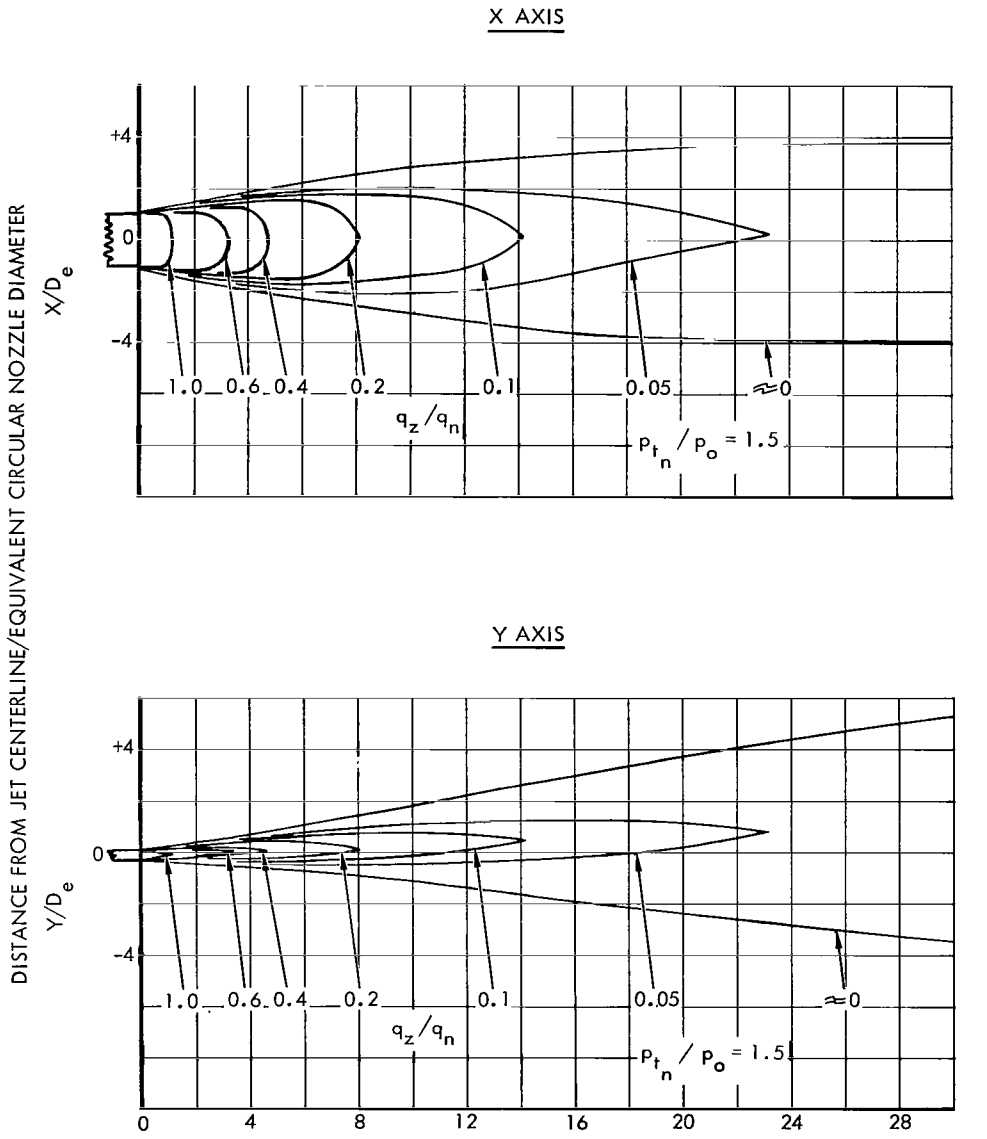

(d) DELTA NOZZLE NO. 8 ($R = 5$, $\beta = 5°$)

Figure 11.- Continued.

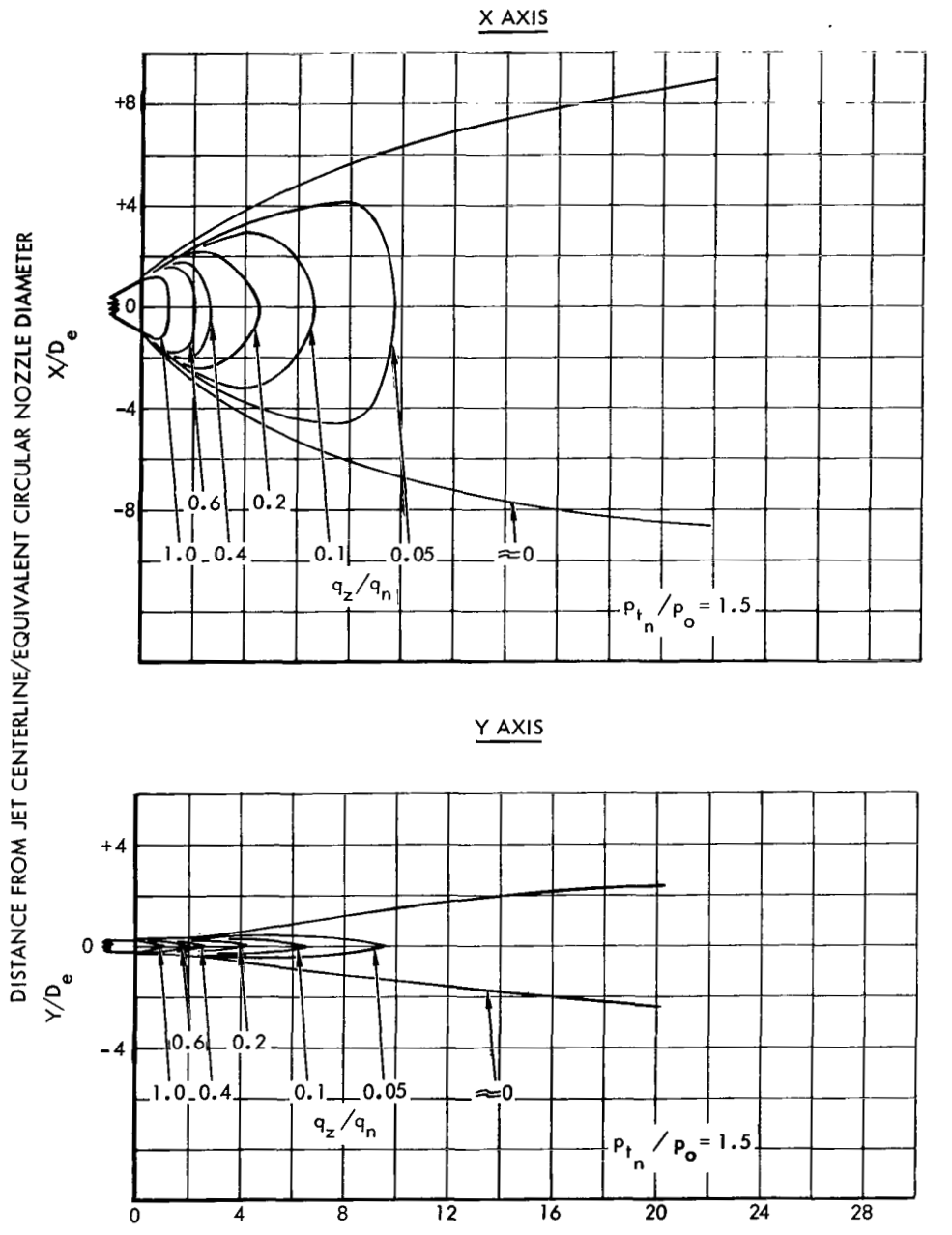

(e) DELTA NOZZLE NO. 9 ($R = 5$, $\beta = 30°$)

Figure 11.- Continued.

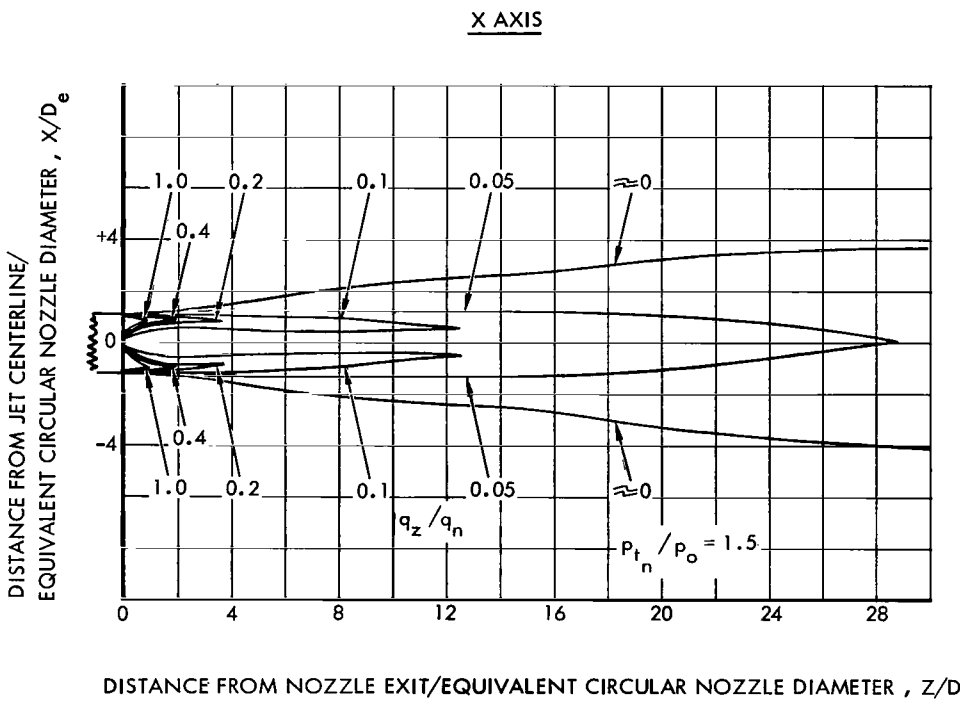

(f) TWELVE SEGMENT NOZZLE NO. 12

Figure 11.- Concluded.

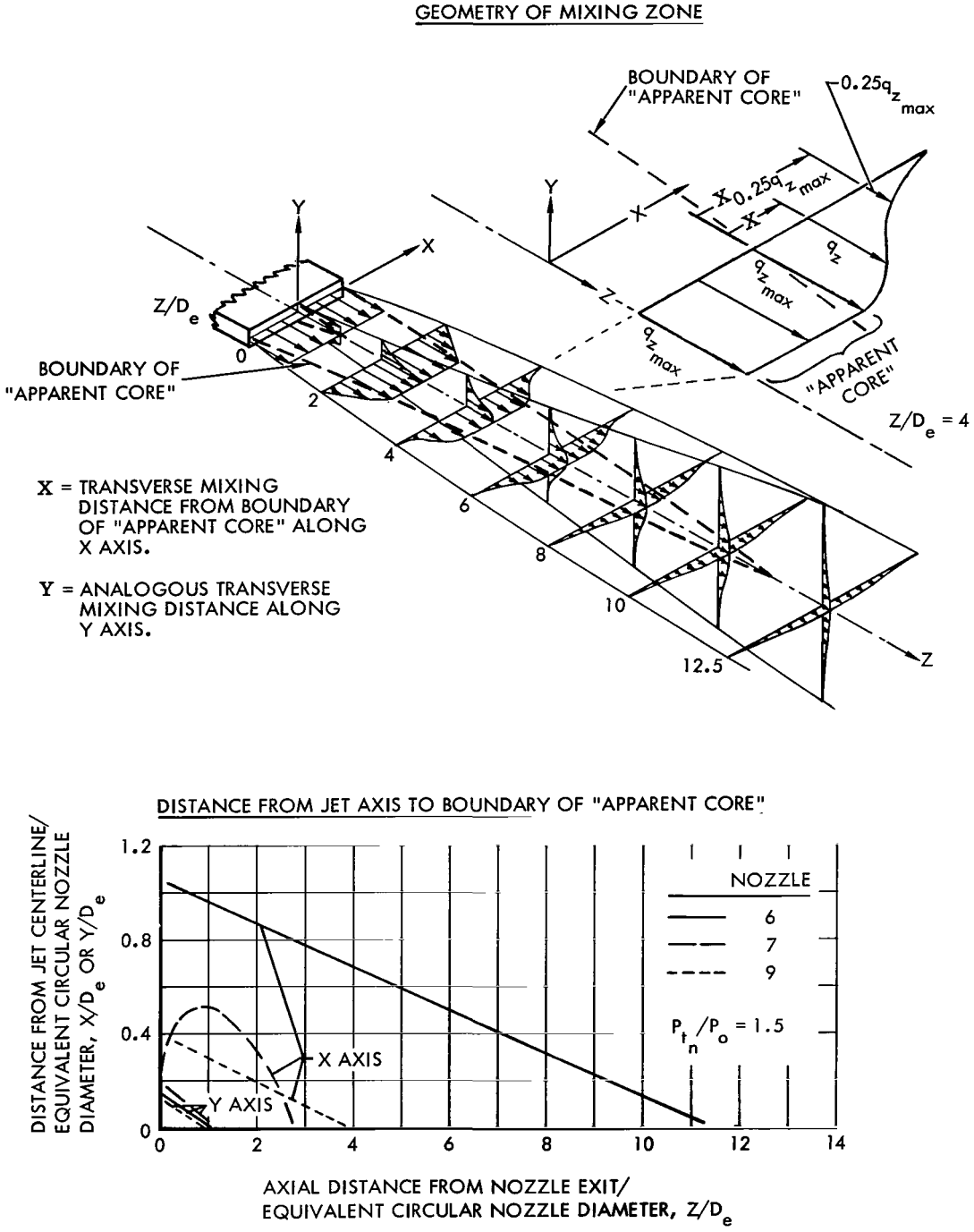

Figure 12.- Definition of mixing zone geometry for similarity analyses.

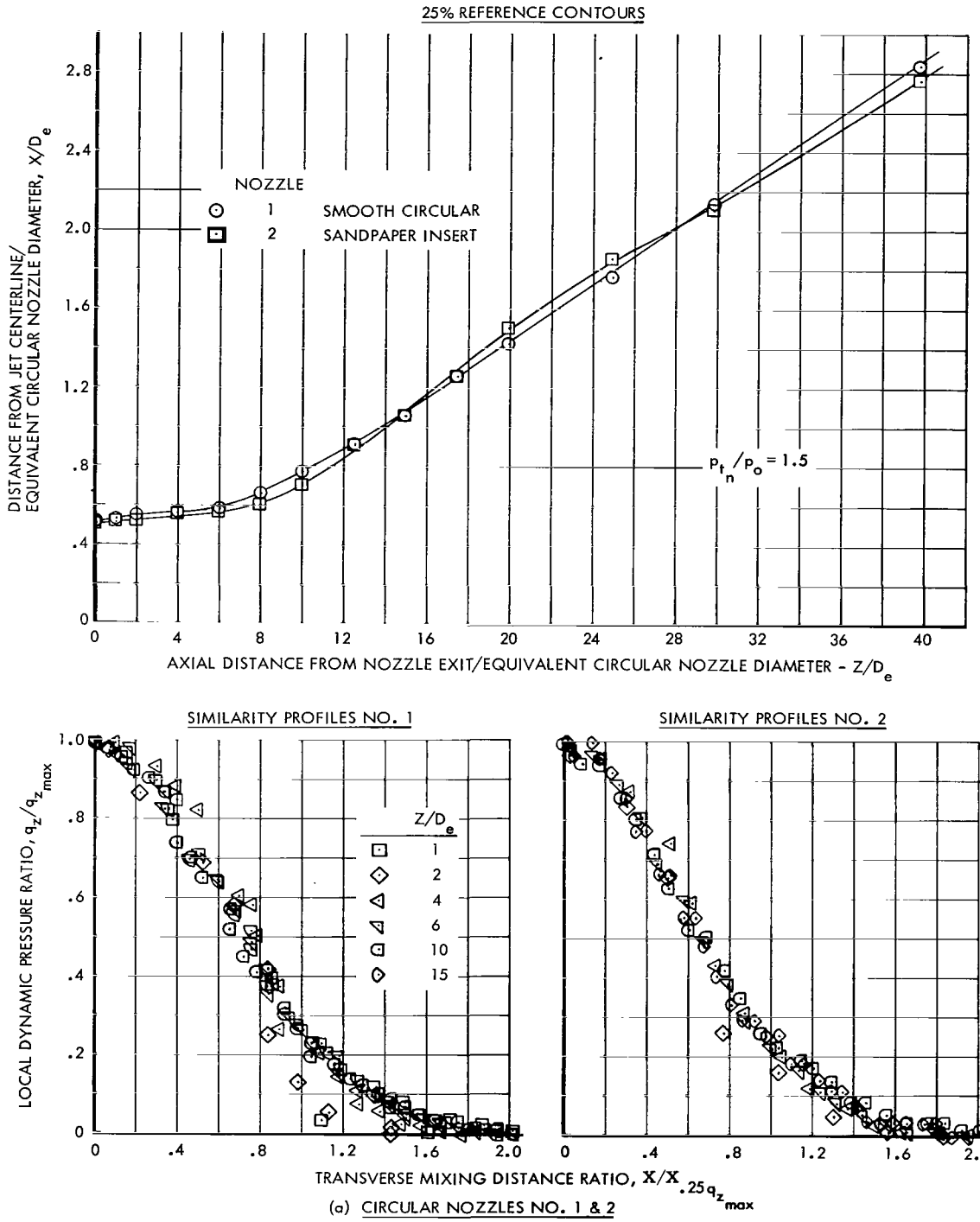

(a) CIRCULAR NOZZLES NO. 1 & 2

Figure 13.- Jet wake 25% reference contours and similarity profiles.

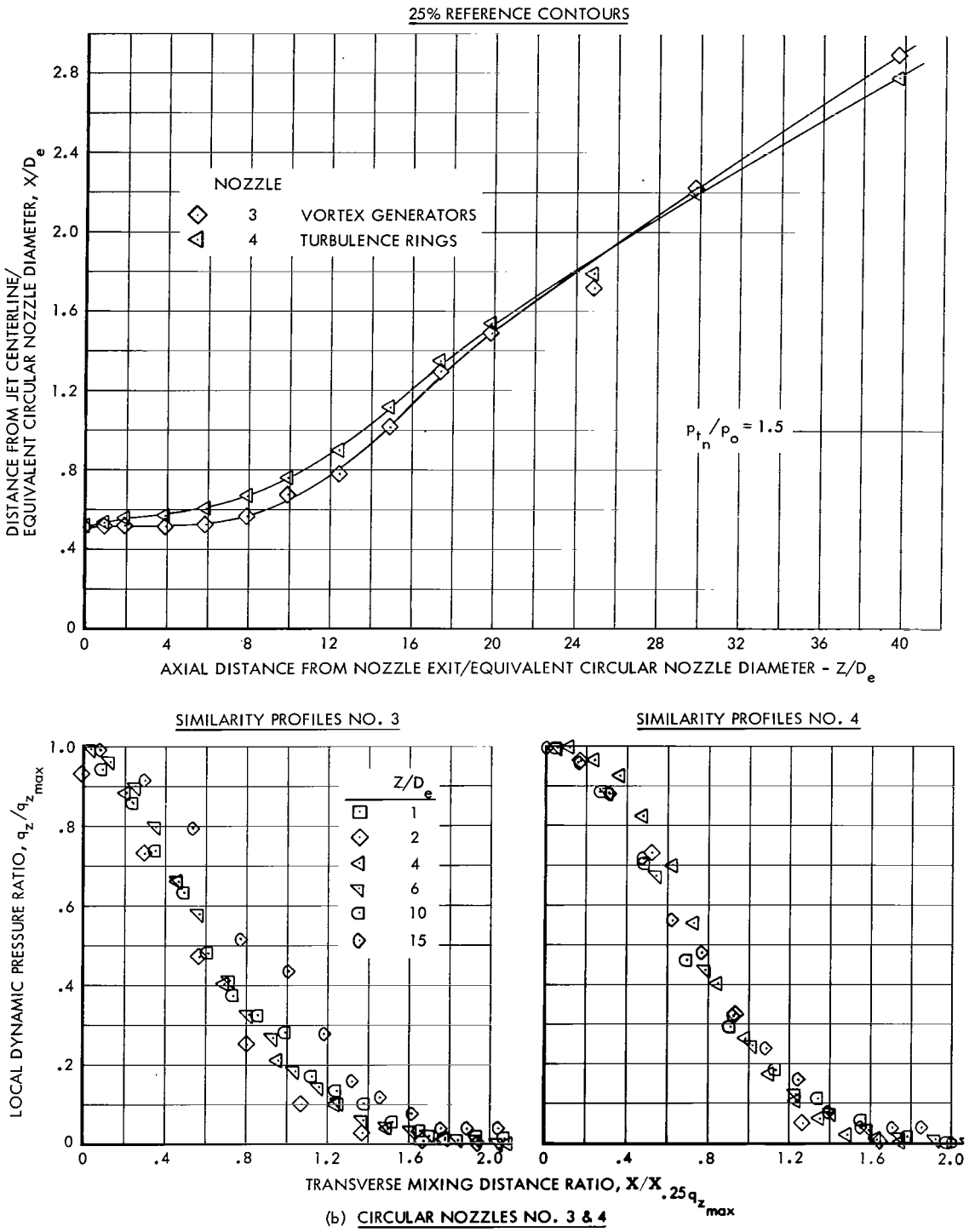

(b) CIRCULAR NOZZLES NO. 3 & 4

Figure 13.- Continued.

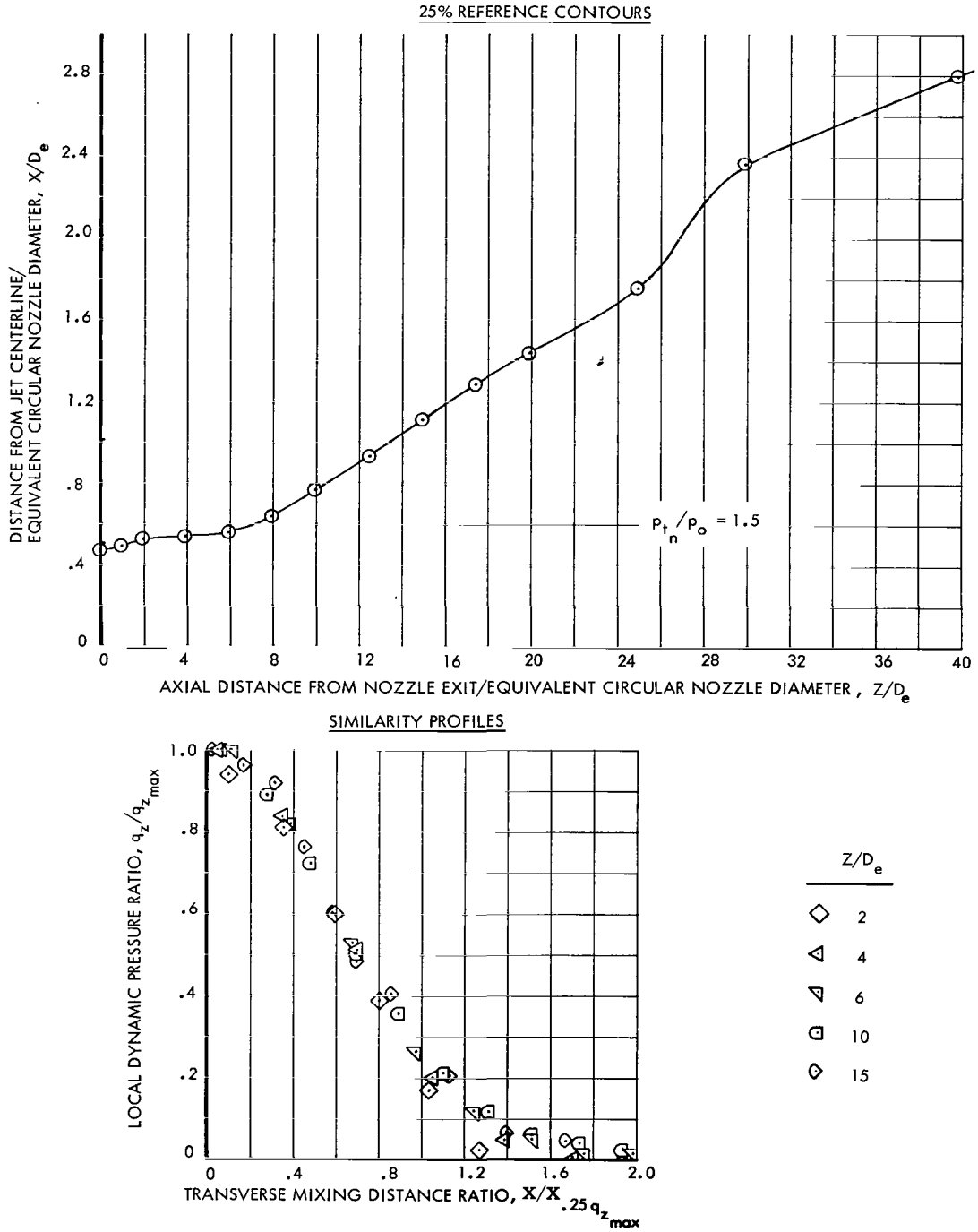

(c) RECTANGULAR NOZZLE NO. 5 ($\mathcal{R}$ = 1)

Figure 13.- Continued.

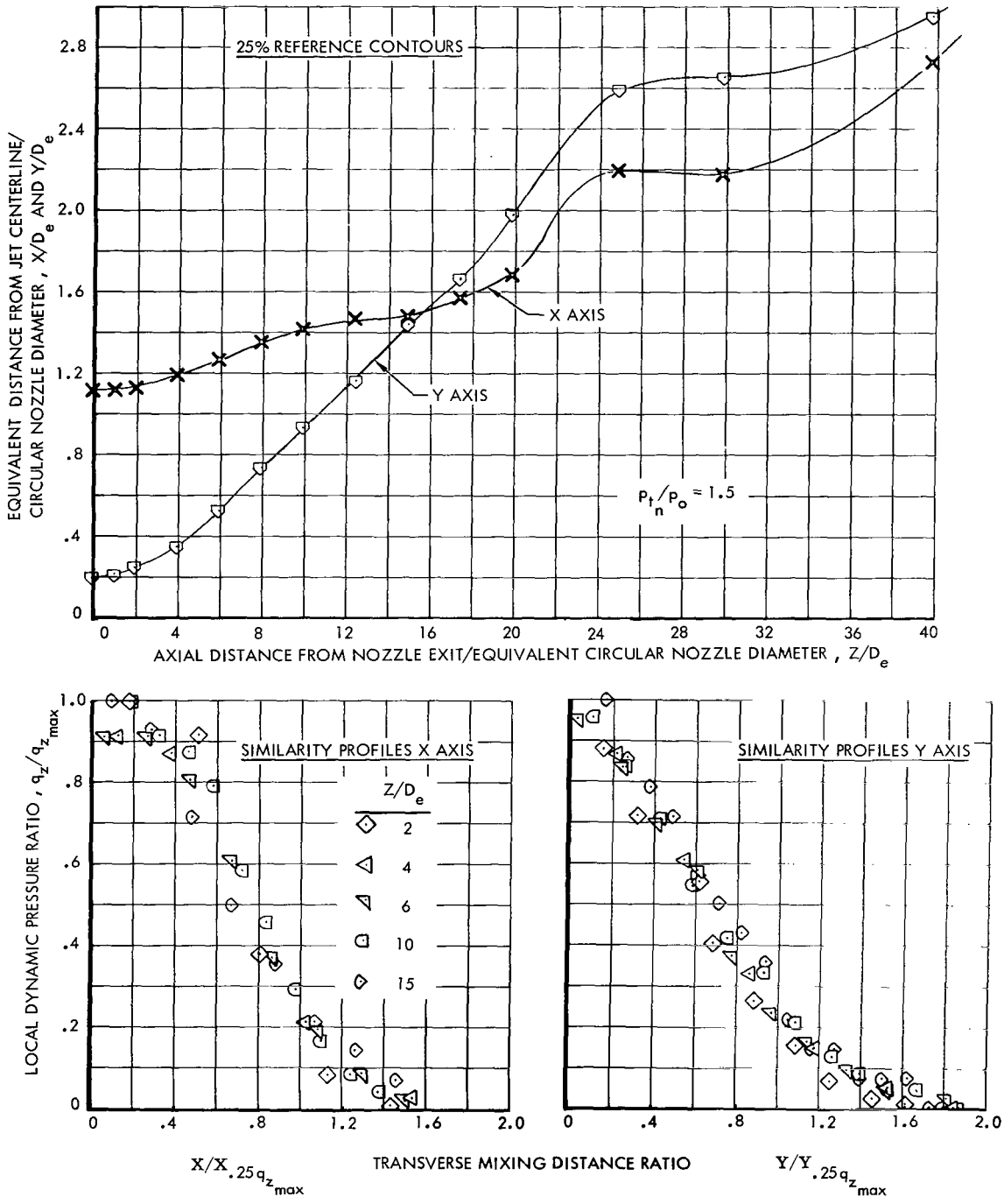

(d) RECTANGULAR NOZZLE NO. 6 (A_R = 6)

Figure 13.- Continued.

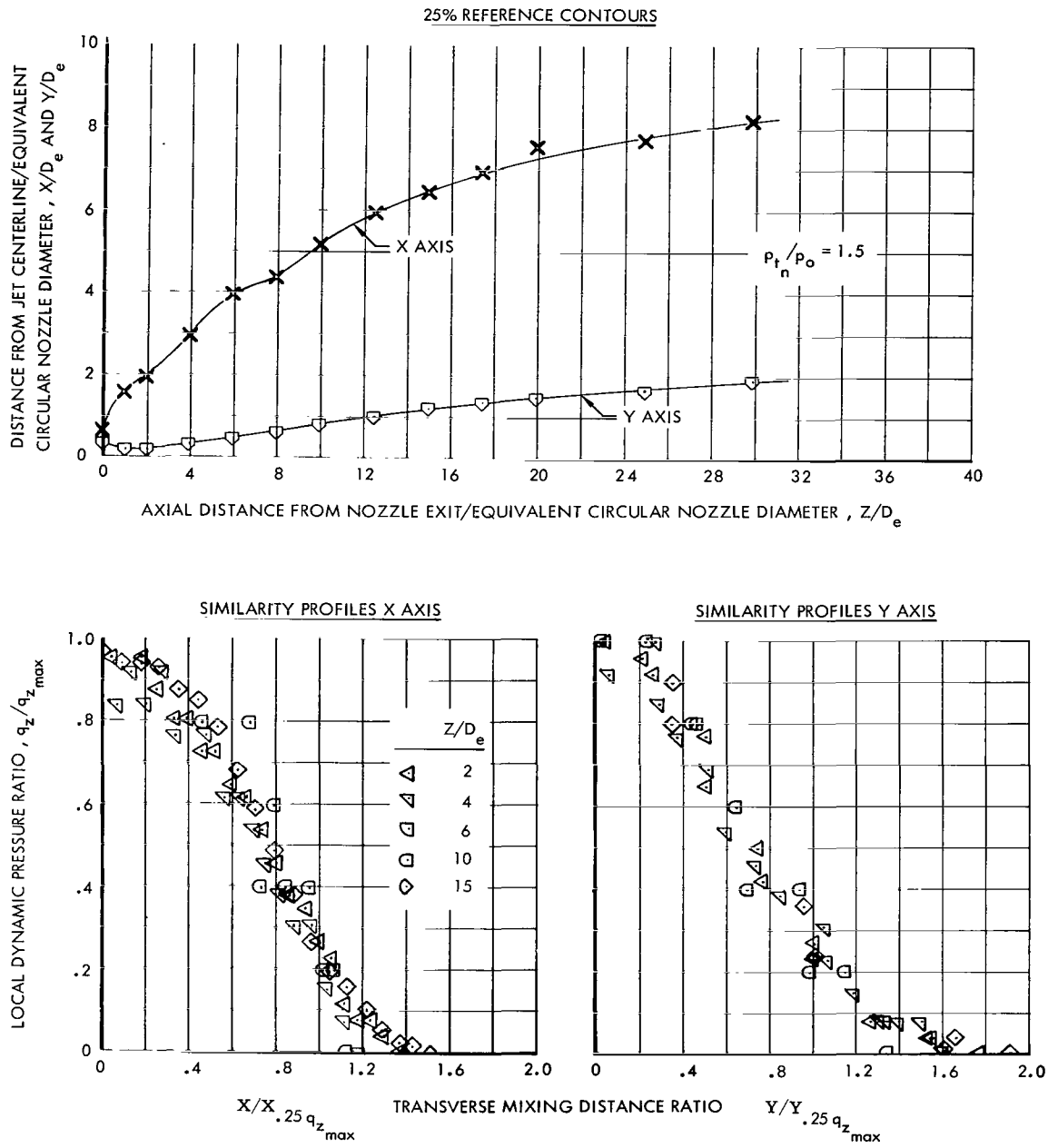

(e) DELTA NOZZLE NO. 7 ($\mathcal{R}$ = 2.0, β = 30°)

Figure 13.- Continued.

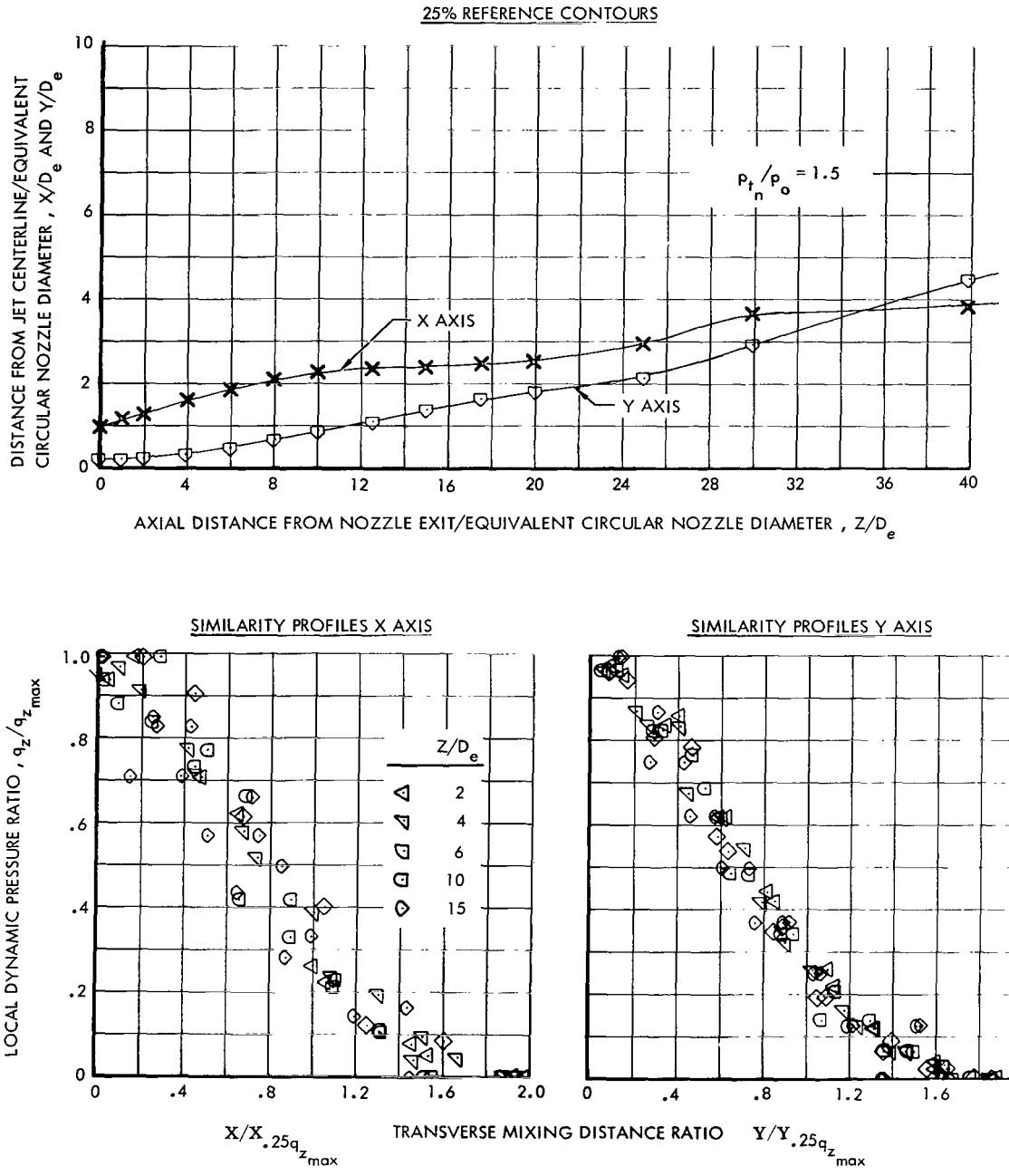

(f) DELTA NOZZLE NO. 8 ($\mathcal{R}$ = 5.0, β = 5°)

Figure 13.- Continued.

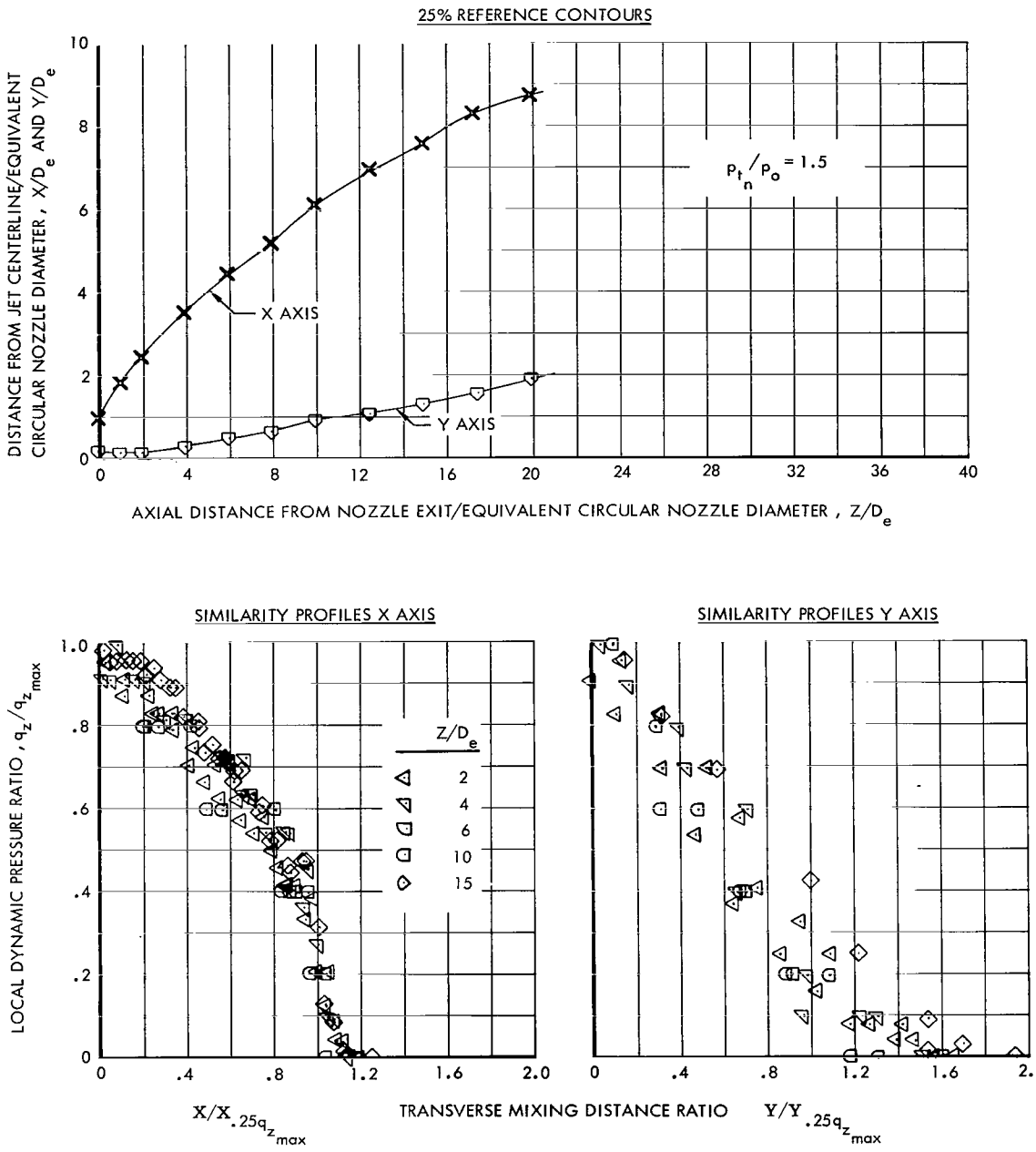

(g) DELTA NOZZLE NO. 9 (R = 5, β = 30°)

Figure 13.- Continued.

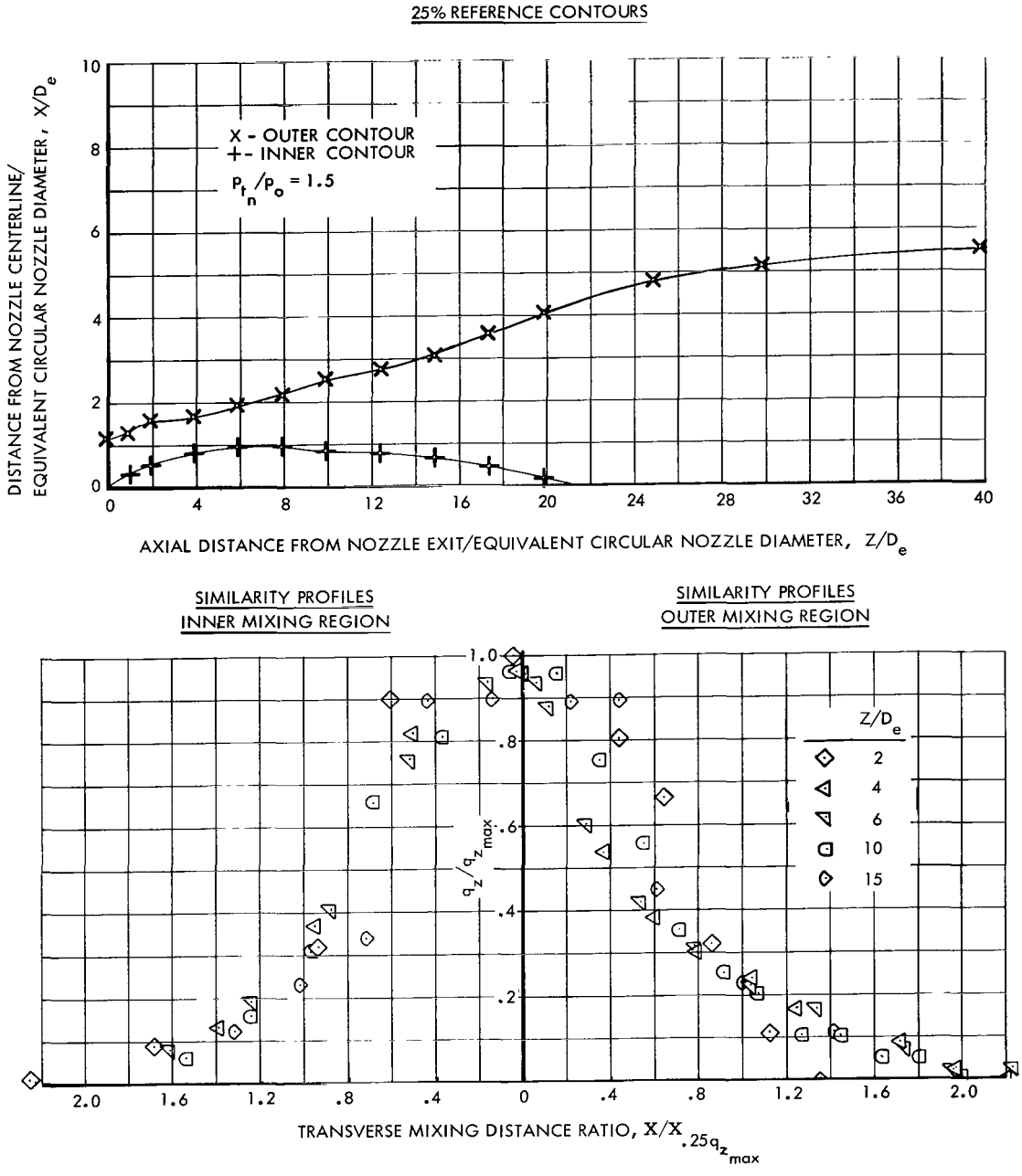

(h) TWO SEGMENT NOZZLE NO. 10

Figure 13.- Continued.

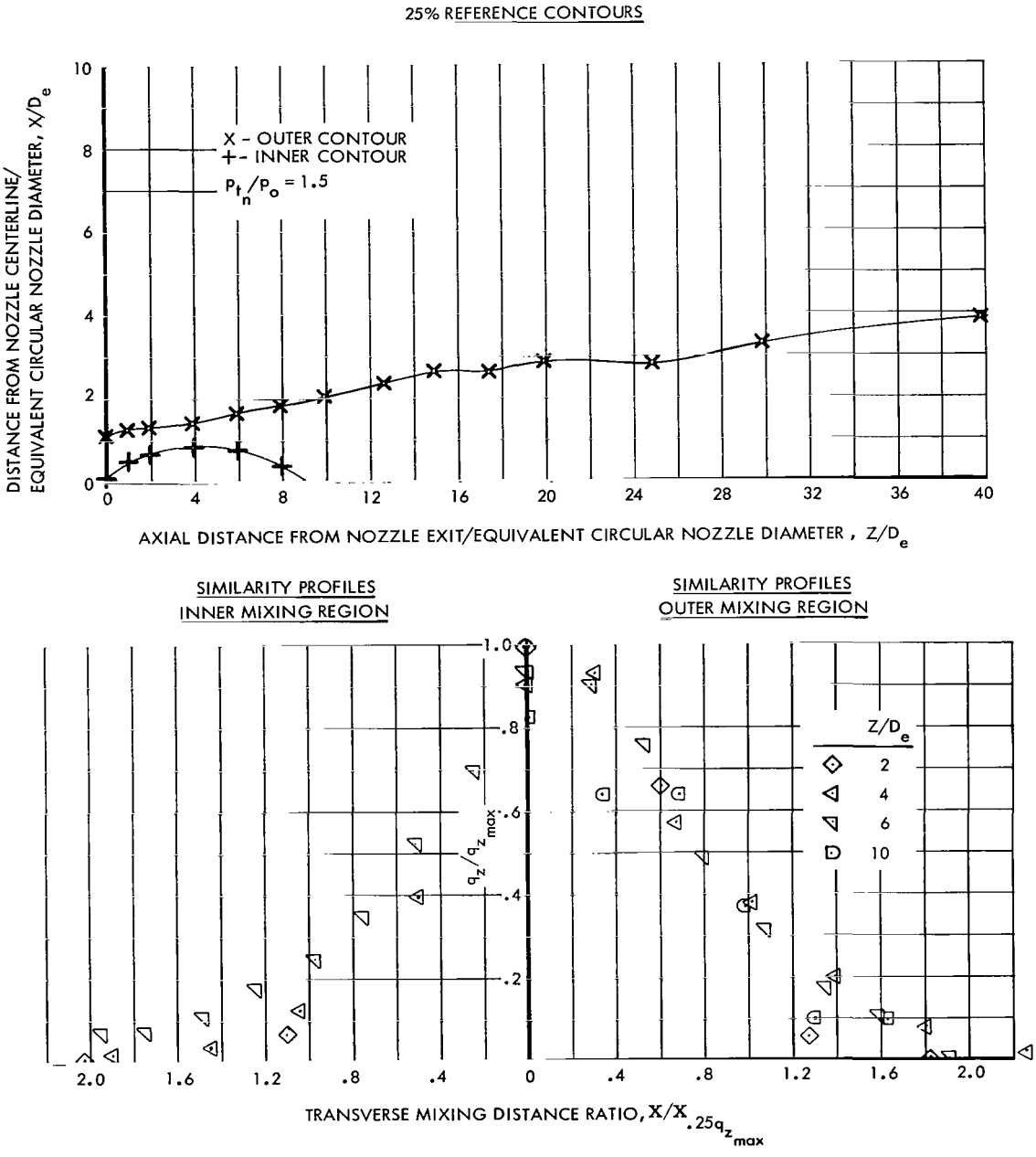

(i) FOUR SEGMENT NOZZLE NO. 11

Figure 13.- Continued.

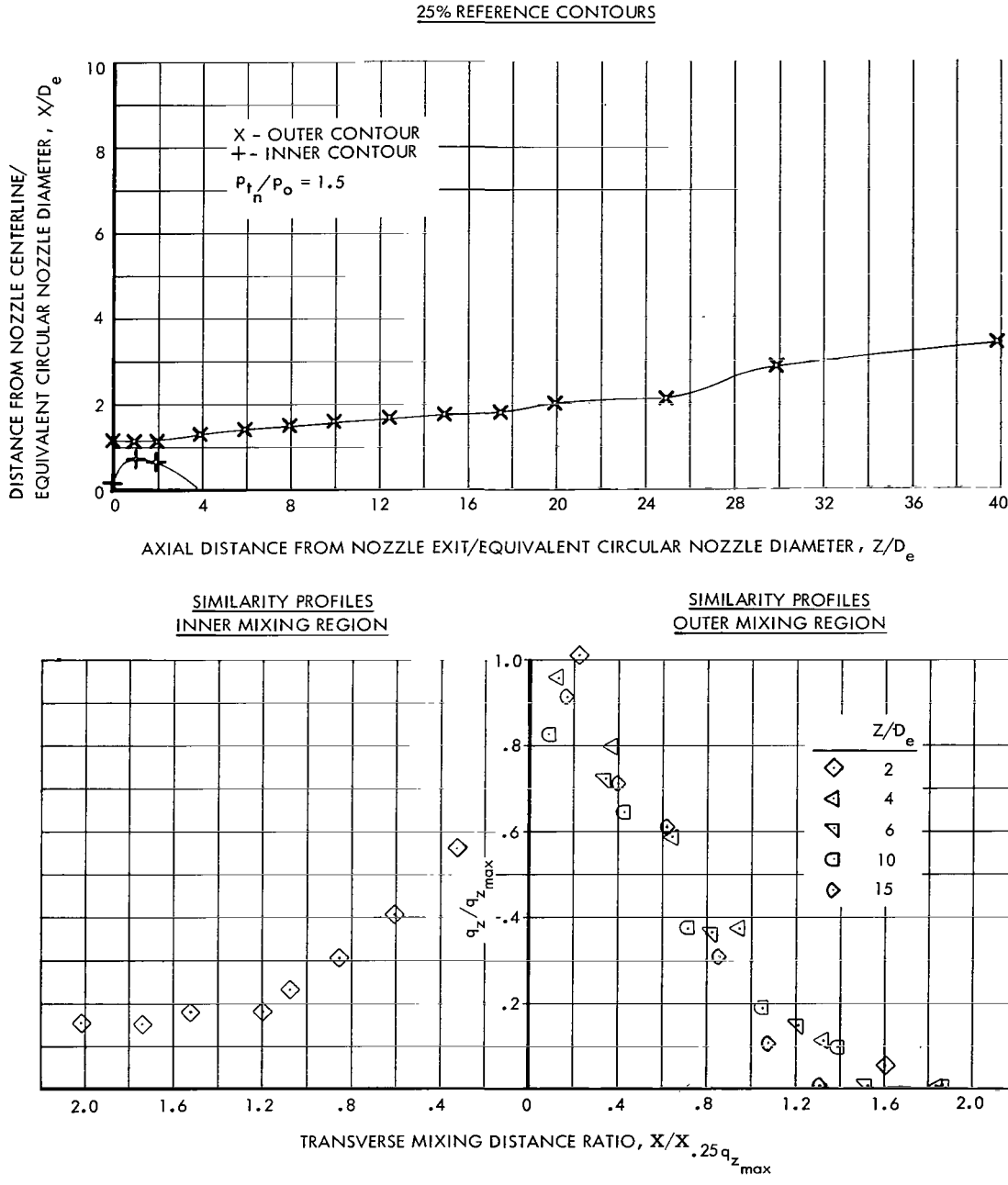

(j) TWELVE SEGMENT NOZZLE NO. 12

Figure 13.- Concluded.

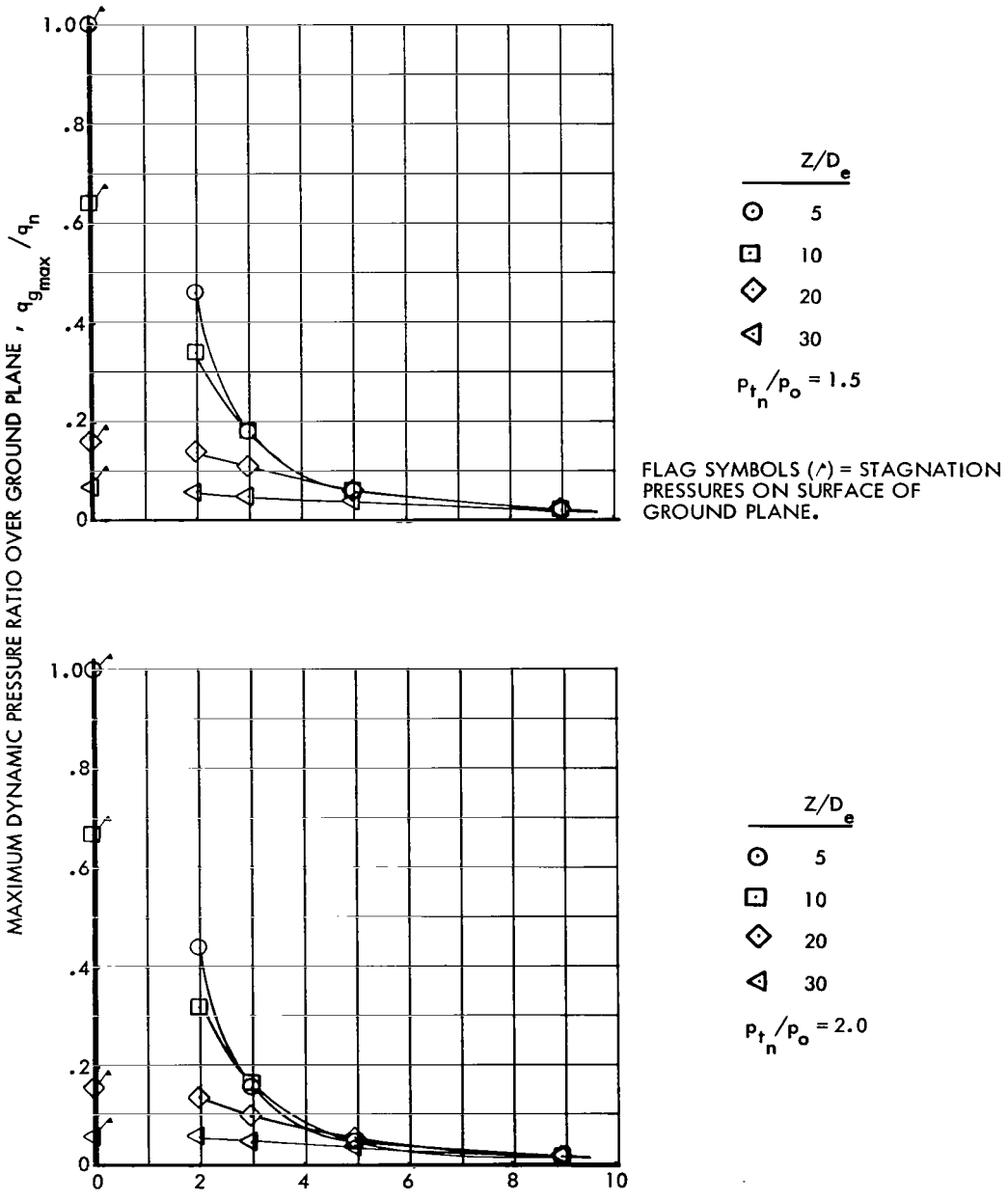

(a) CIRCULAR NOZZLE NO. 1

Figure 14.- Maximum ground plane dynamic pressure at various distances from the nozzle.

(b) CIRCULAR NOZZLE NO. 2

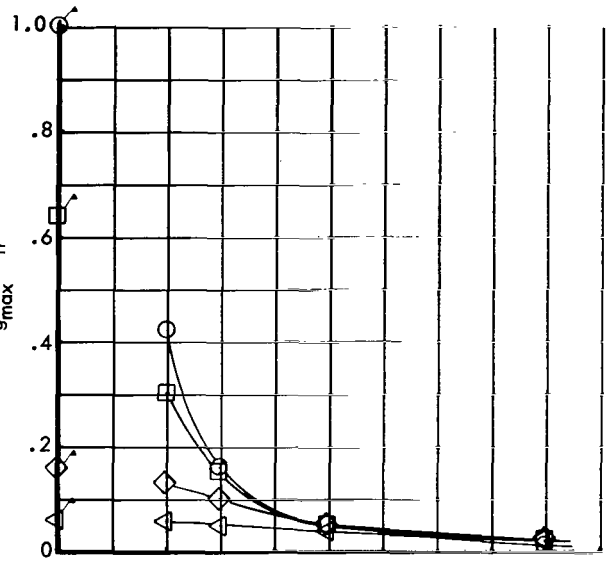

Z/D$_e$

○ 5

□ 10

◇ 20

◁ 30

$P_{t_n}/P_o = 1.5$

FLAG SYMBOLS (↗) = STAGNATION PRESSURES ON SURFACE OF GROUND PLANE.

(c) CIRCULAR NOZZLE NO. 3

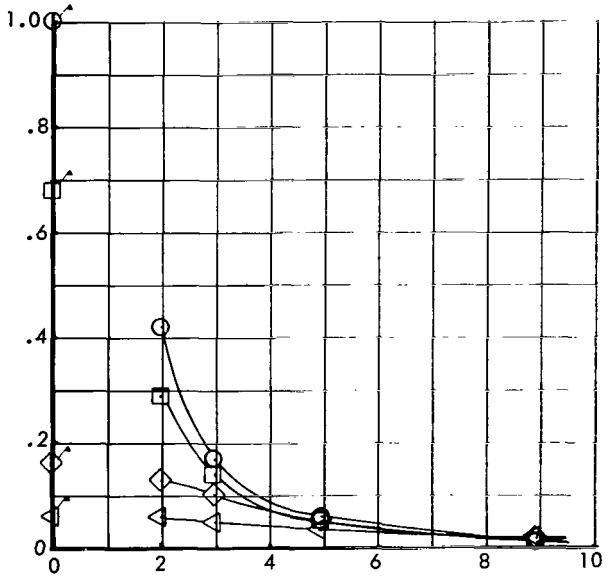

Z/D$_e$

○ 5

□ 10

◇ 20

◁ 30

$P_{t_n}/P_o = 1.5$

MAXIMUM DYNAMIC PRESSURE RATIO OVER GROUND PLANE - $q_{g_{max}}/q_n$

DISTANCE FROM CENTER OF GROUND PLANE/ EQUIVALENT CIRCULAR NOZZLE DIAMETER , R/D$_e$

Figure 14.- Continued.

(d) CIRCULAR NOZZLE NO. 4

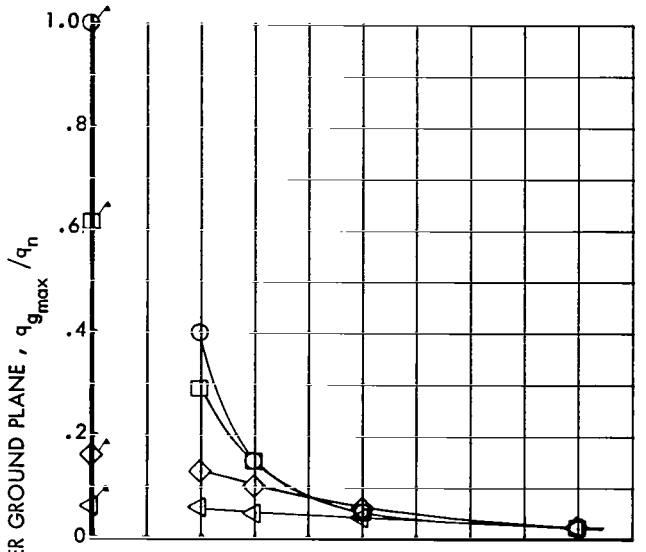

Z/D$_e$

- ⊙ 5
- ⊡ 10
- ◇ 20
- ◁ 30

$p_{t_n}/p_o = 1.5$

FLAG SYMBOLS (⌃) = STAGNATION PRESSURES ON SURFACE OF GROUND PLANE.

(e) RECTANGULAR NOZZLE NO. 5 ($\mathcal{R}$ = 1)

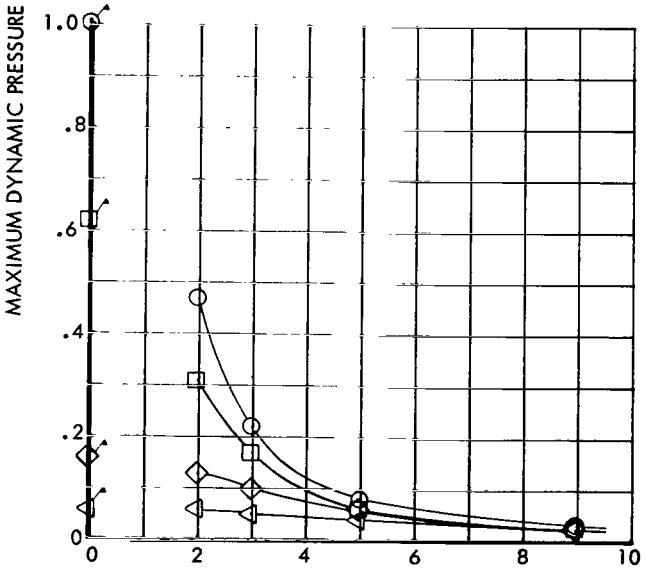

Z/D$_e$

- ⊙ 5
- ⊡ 10
- ◇ 20
- ◁ 30

$p_{t_n}/p_o = 1.5$

MAXIMUM DYNAMIC PRESSURE RATIO OVER GROUND PLANE , $q_{g_{max}}/q_n$

DISTANCE FROM CENTER OF GROUND PLANE/ EQUIVALENT CIRCULAR NOZZLE DIAMETER , R/D$_e$

Figure 14.- Continued.

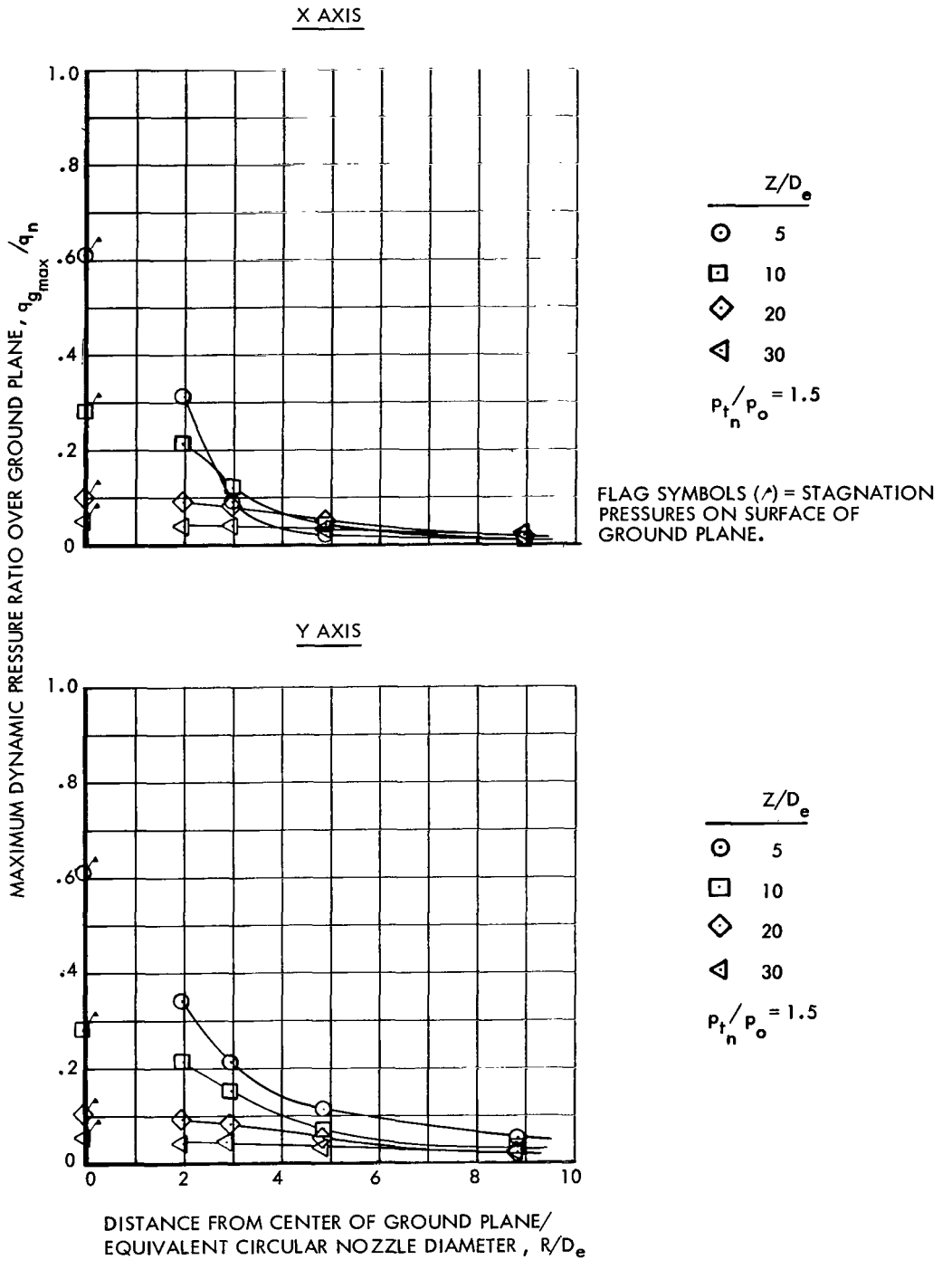

(f) RECTANGULAR NOZZLE NO. 6 (A_R = 6)

Figure 14.- Continued.

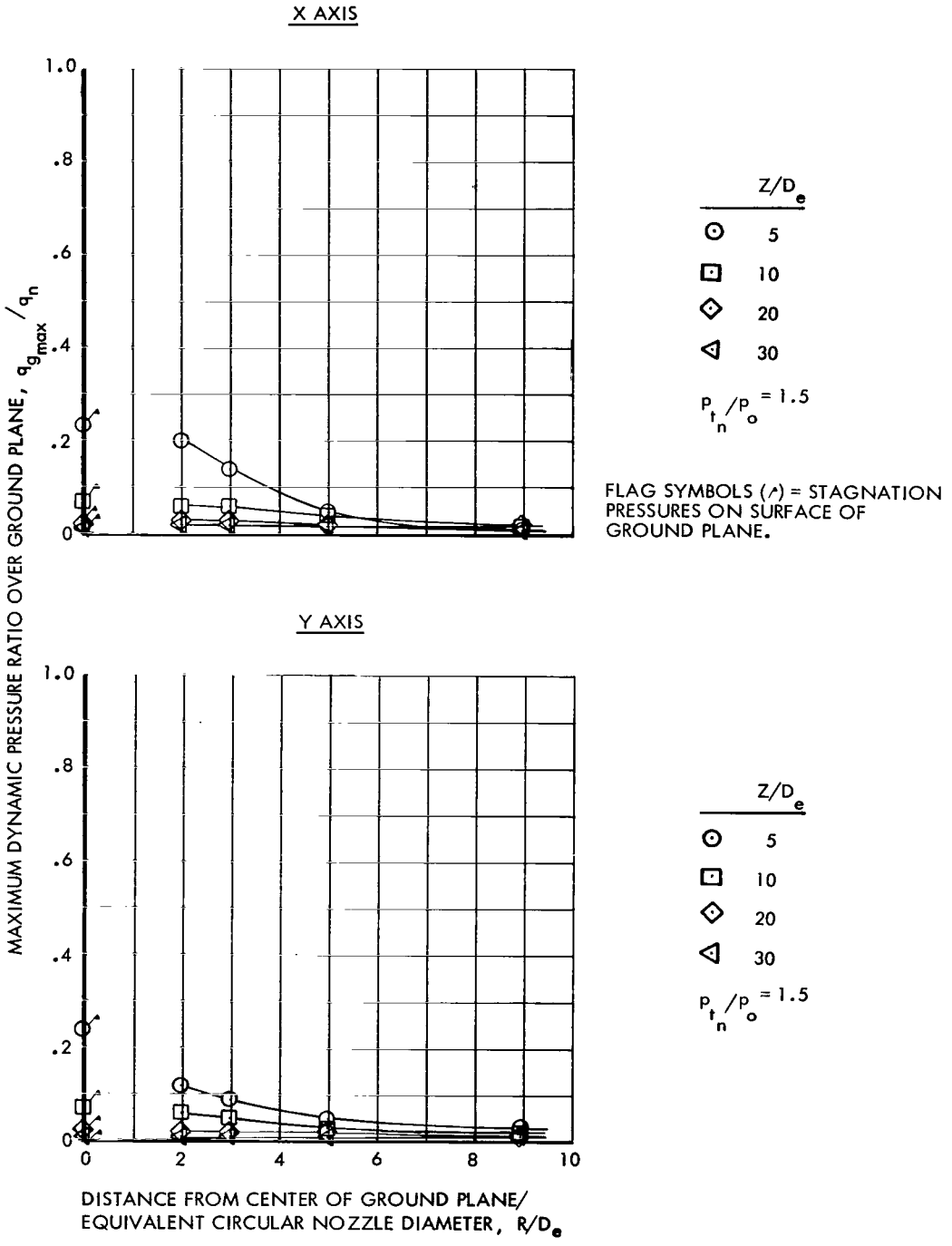

(g) DELTA NOZZLE NO. 7 ($A = 2$, $\beta = 30°$)

Figure 14.- Continued.

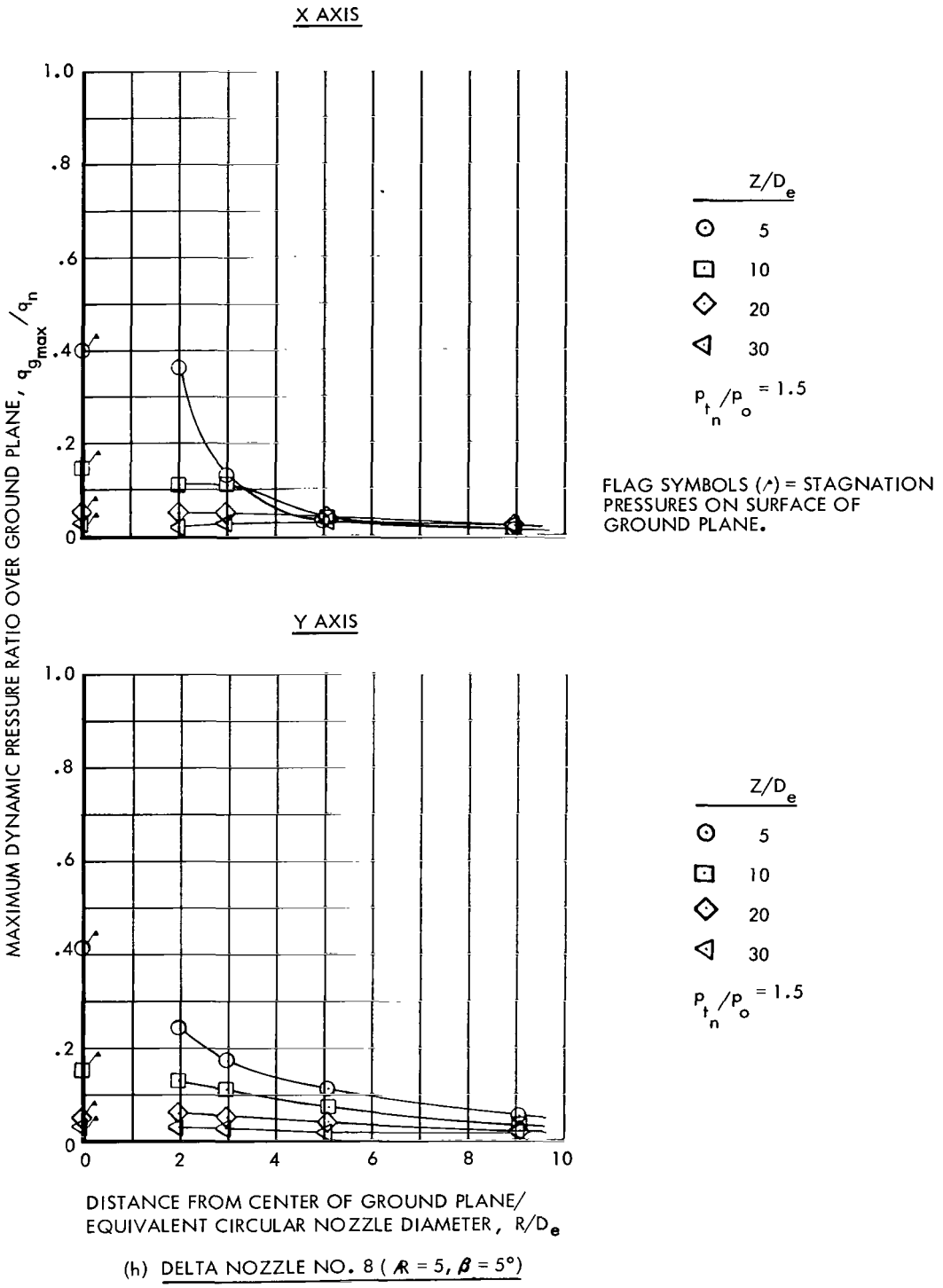

(h) DELTA NOZZLE NO. 8 ($R = 5, \beta = 5°$)

Figure 14.- Continued.

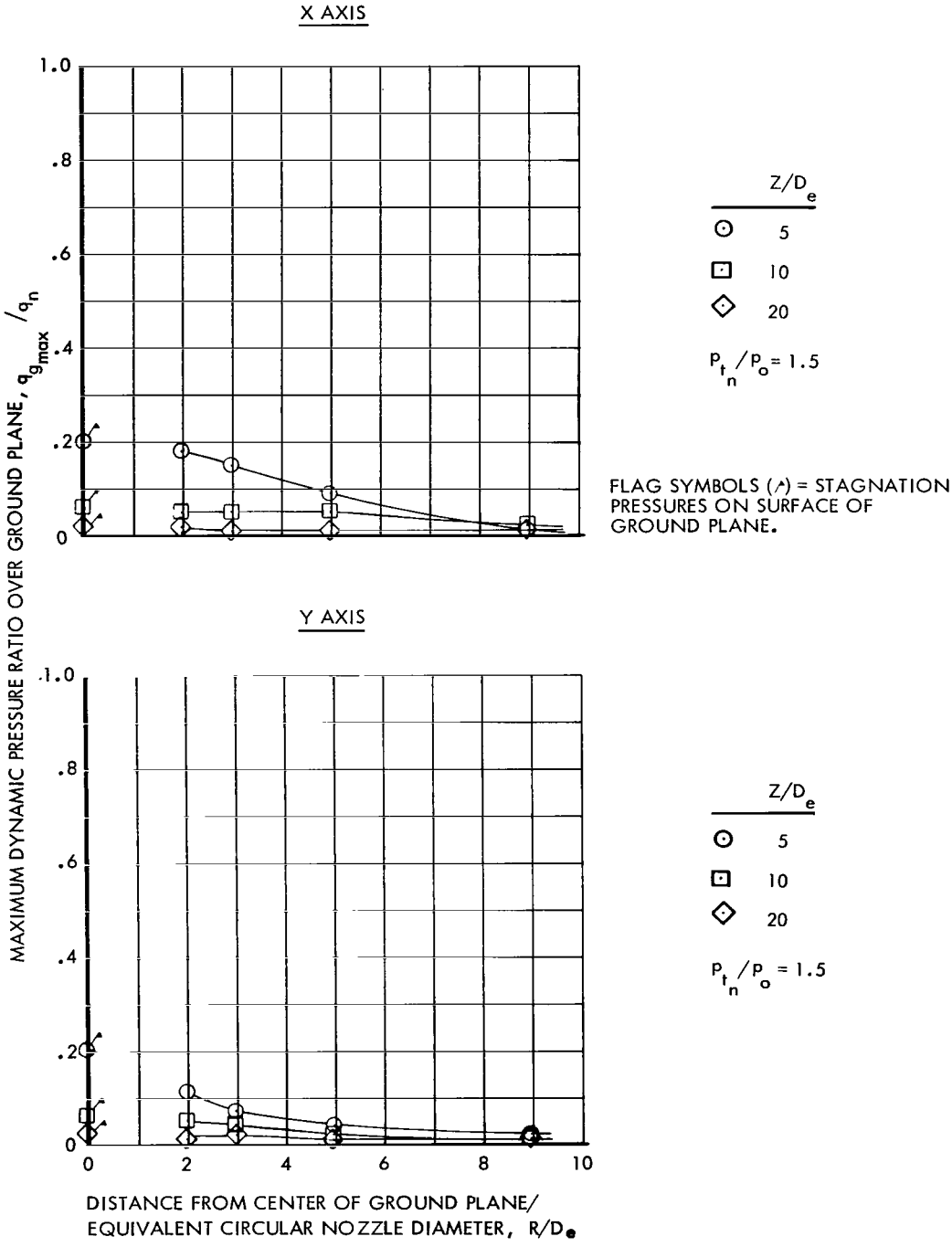

(i) DELTA NOZZLE NO. 9 ($\mathcal{R} = 5$, $\beta = 30°$)

Figure 14.- Continued.

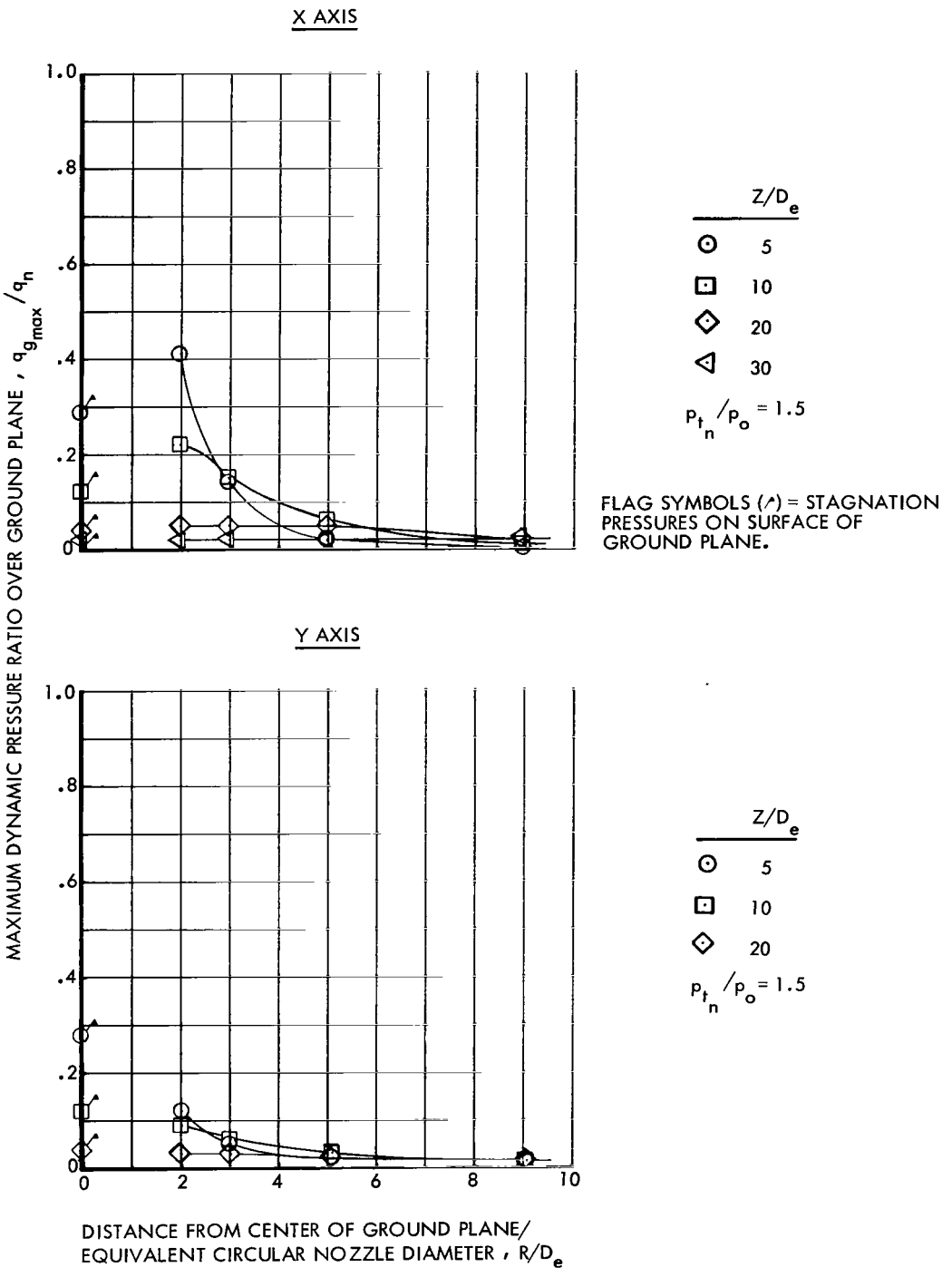

(j) TWO SEGMENT NOZZLE NO. 10

Figure 14.- Continued.

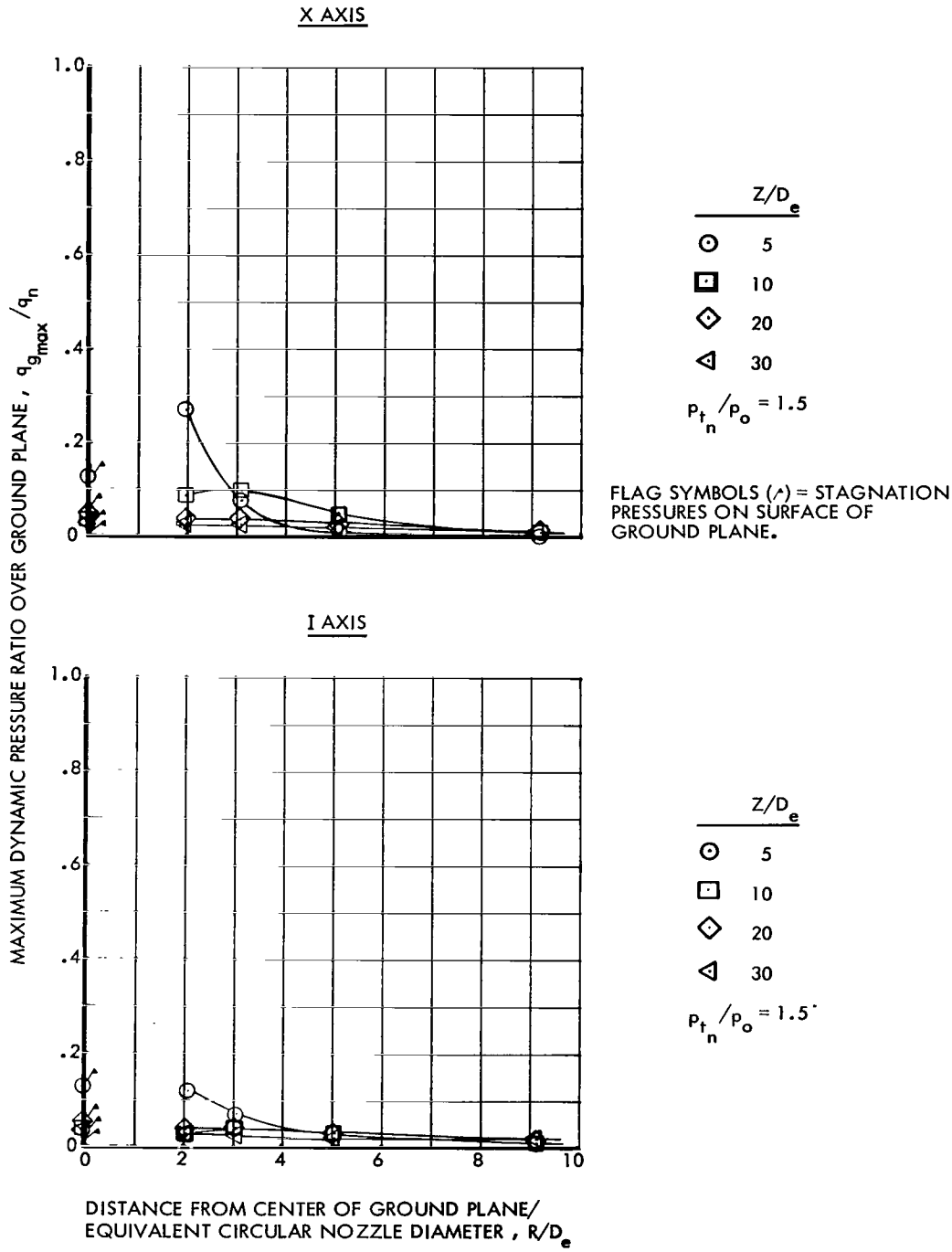

(k) FOUR SEGMENT NOZZLE NO. 11

Figure 14.- Continued.

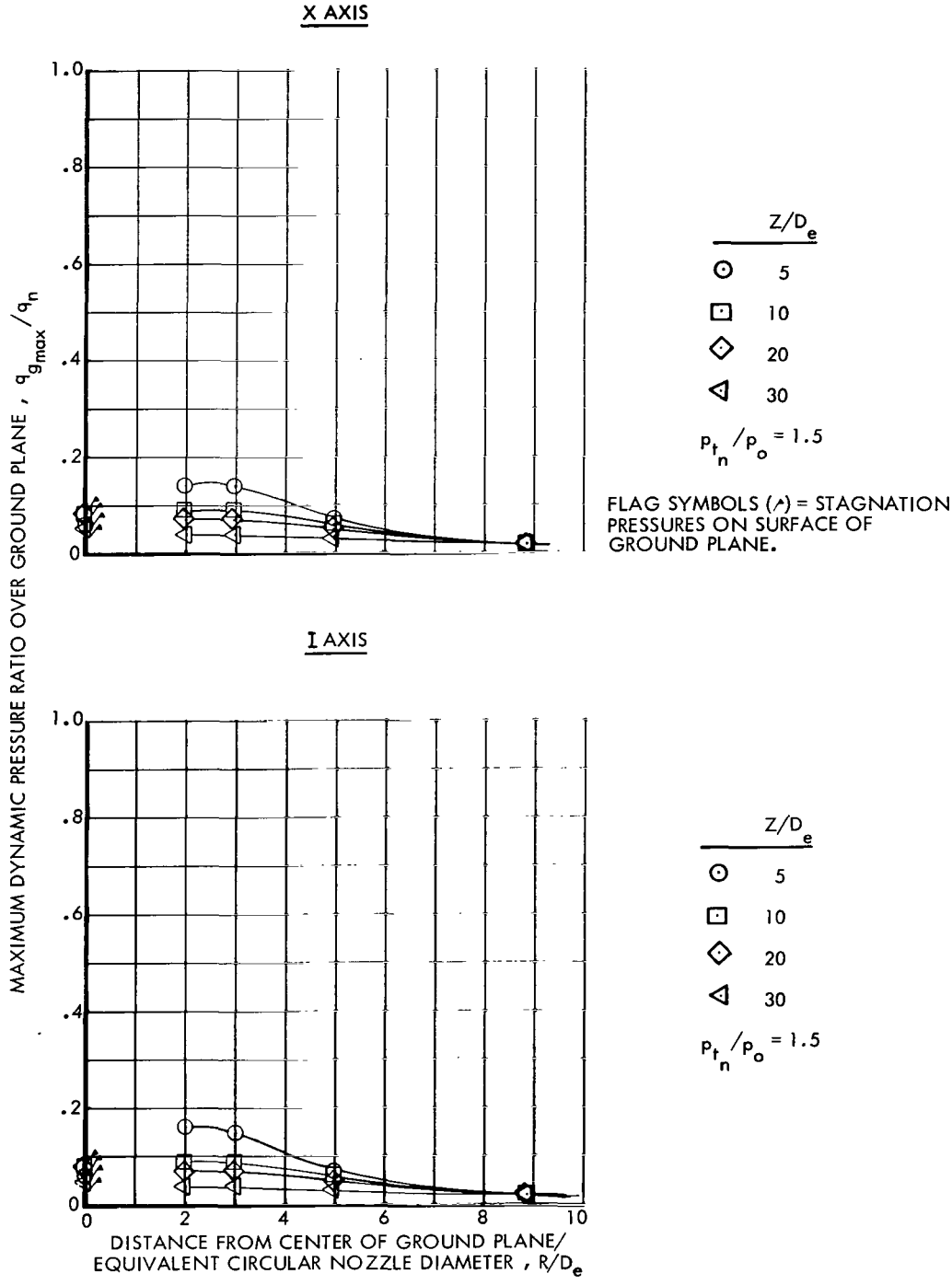

(m) TWELVE SEGMENT NOZZLE NO. 12

Figure 14.- Concluded.

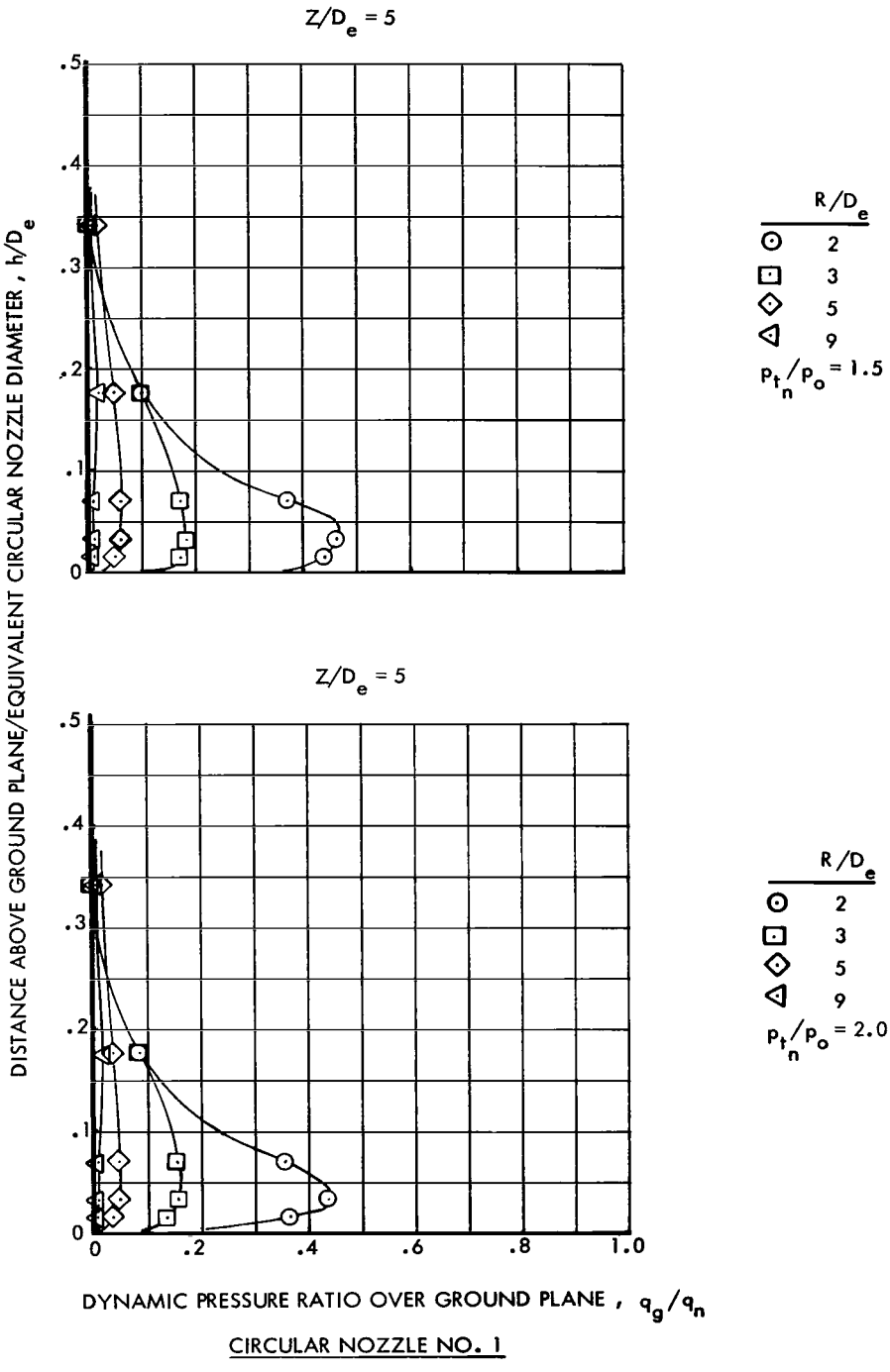

Figure 15.- Effect of nozzle pressure ratio upon dynamic pressure distribution adjacent to ground plane.

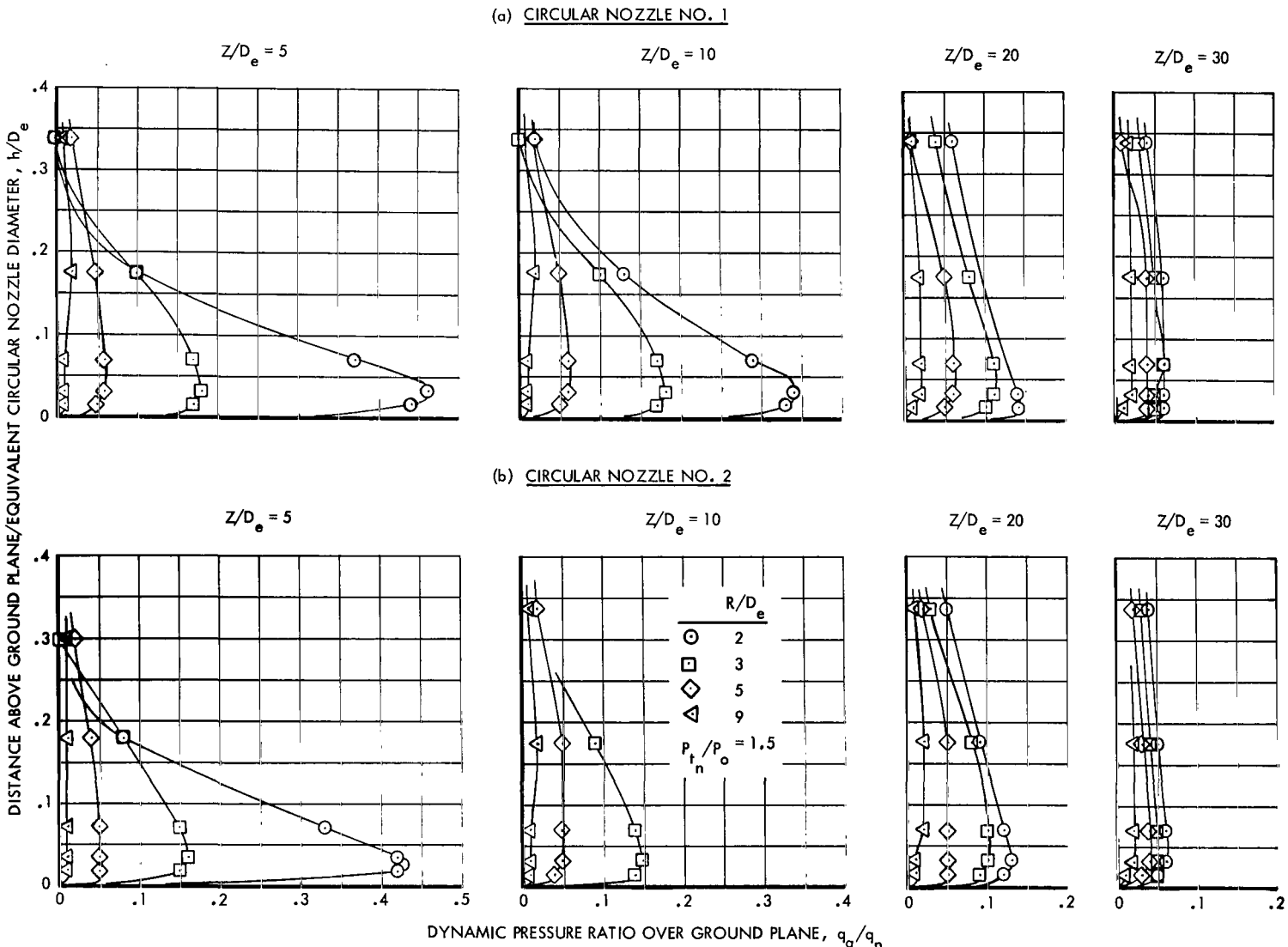

Figure 16.- Dynamic pressure distribution adjacent to ground plane for various nozzles and distances of the ground plane from nozzle exit.

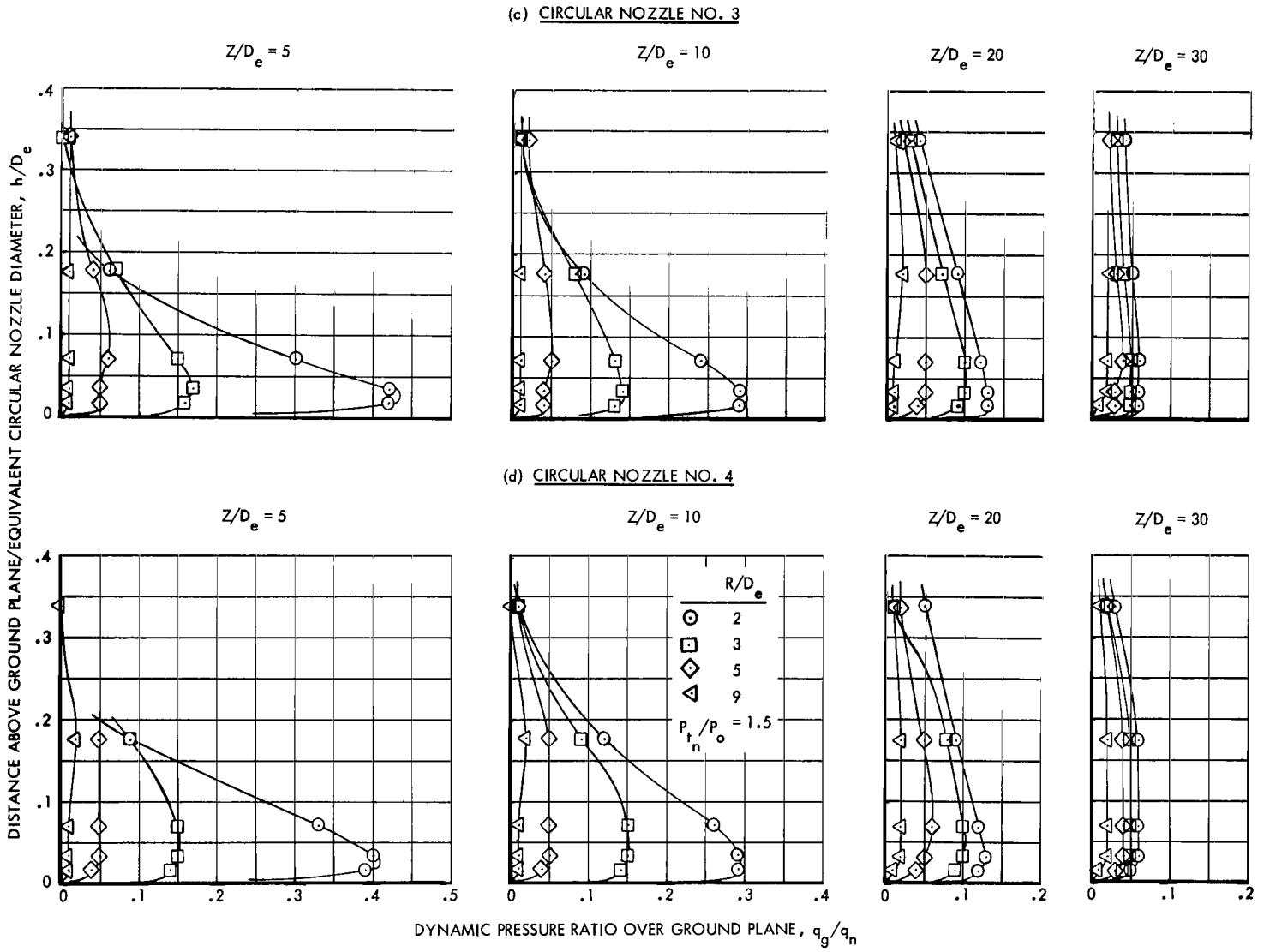

Figure 16.- Continued.

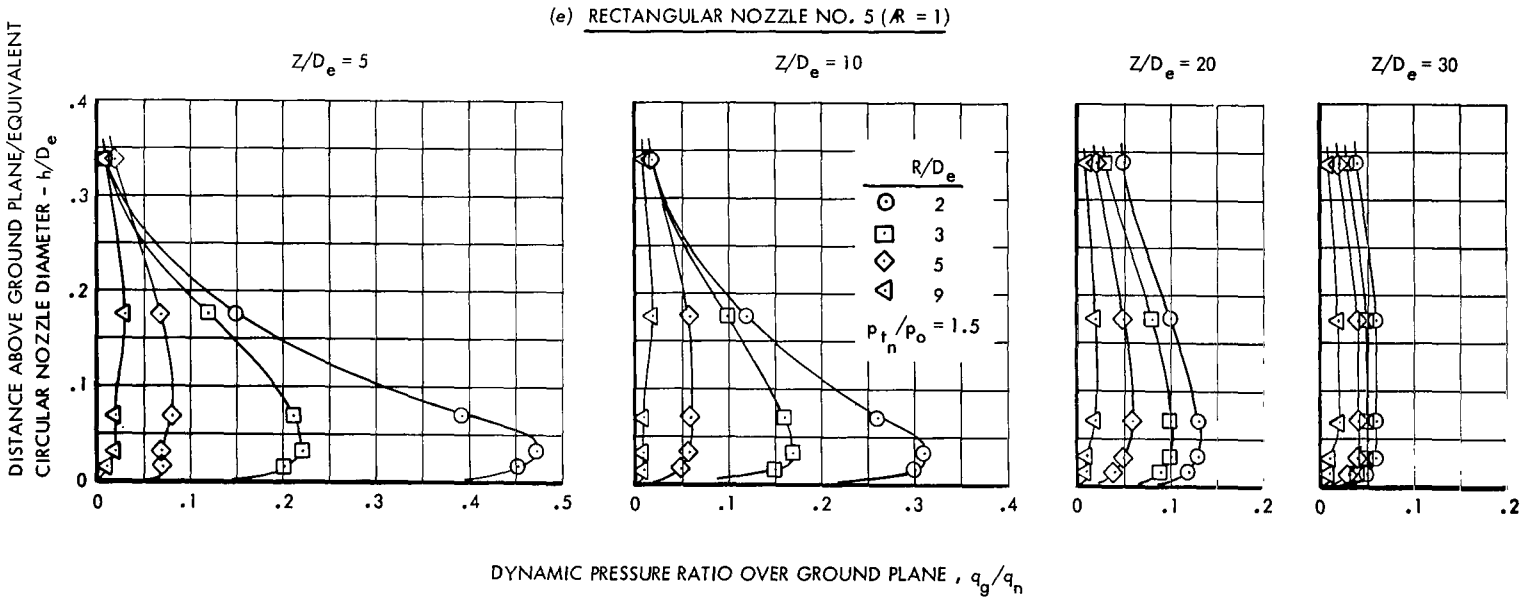

Figure 16.- Continued.

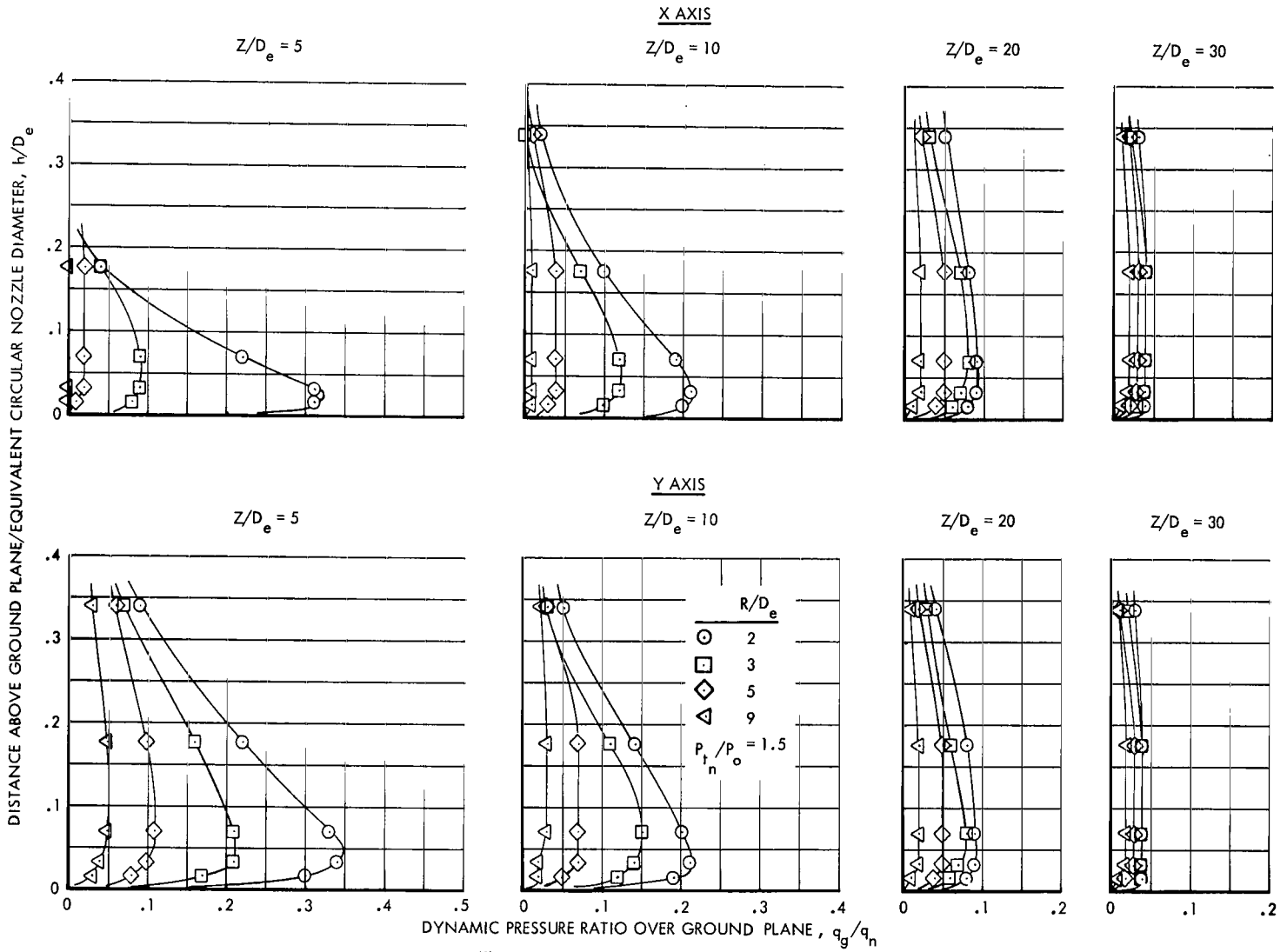

(f) RECTANGULAR NOZZLE NO. 6 ($\mathcal{R}$ = 6)

Figure 16.- Continued.

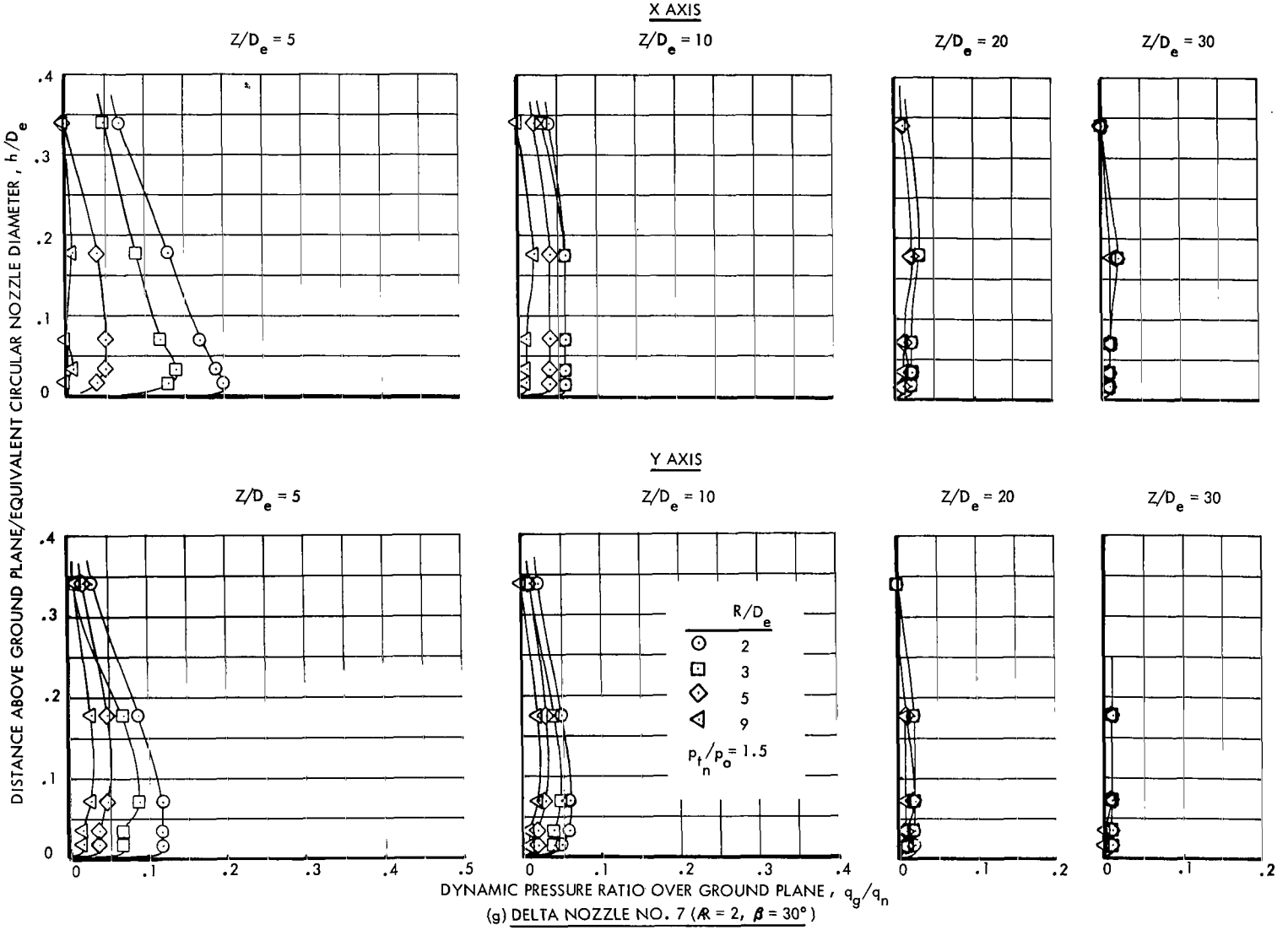

(g) DELTA NOZZLE NO. 7 ($R = 2$, $\beta = 30°$)

Figure 16.- Continued.

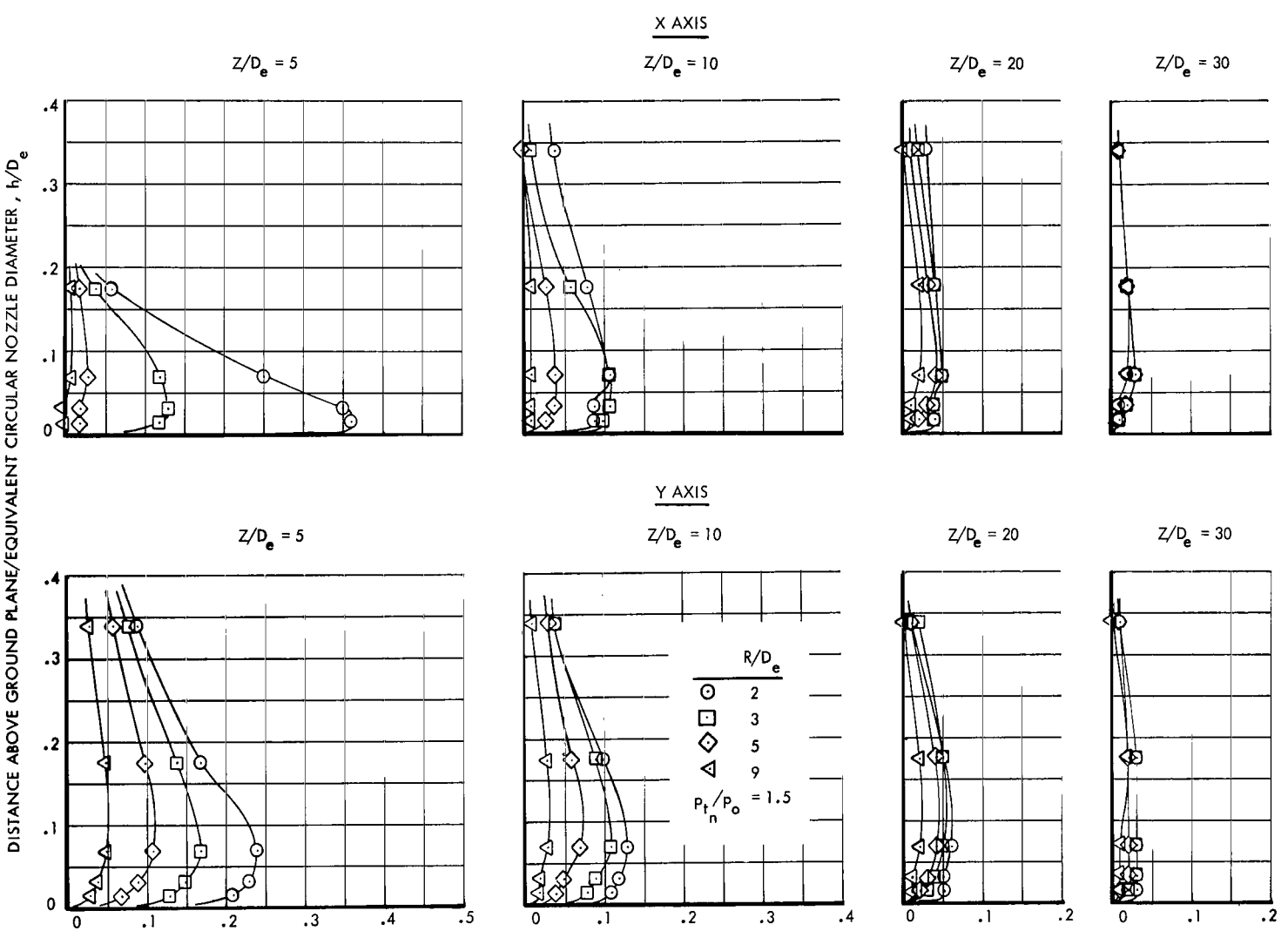

(h) DELTA NOZZLE NO. 8 (A = 5, β = 5°)

Figure 16.- Continued.

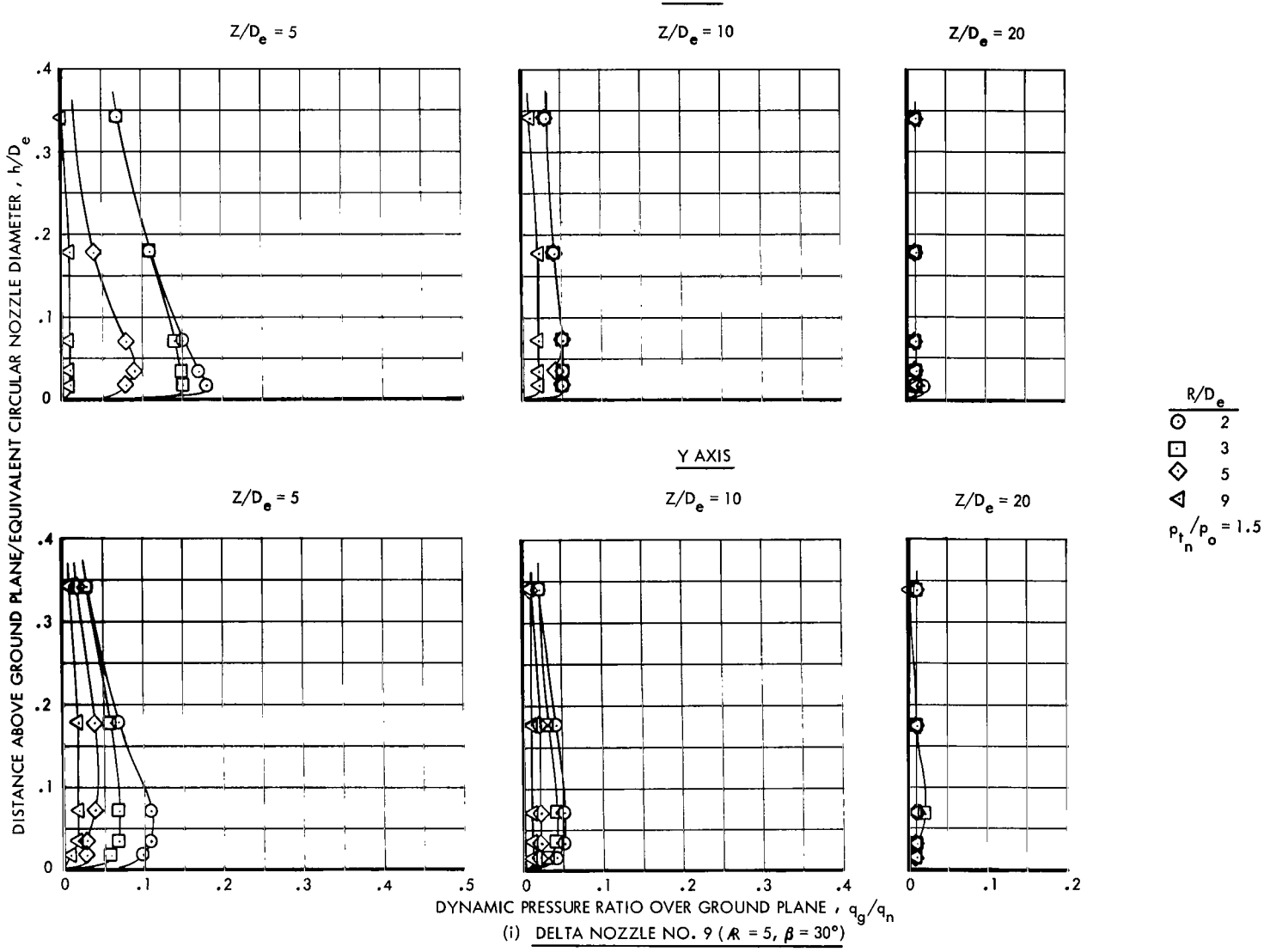

(i) DELTA NOZZLE NO. 9 (A = 5, β = 30°)

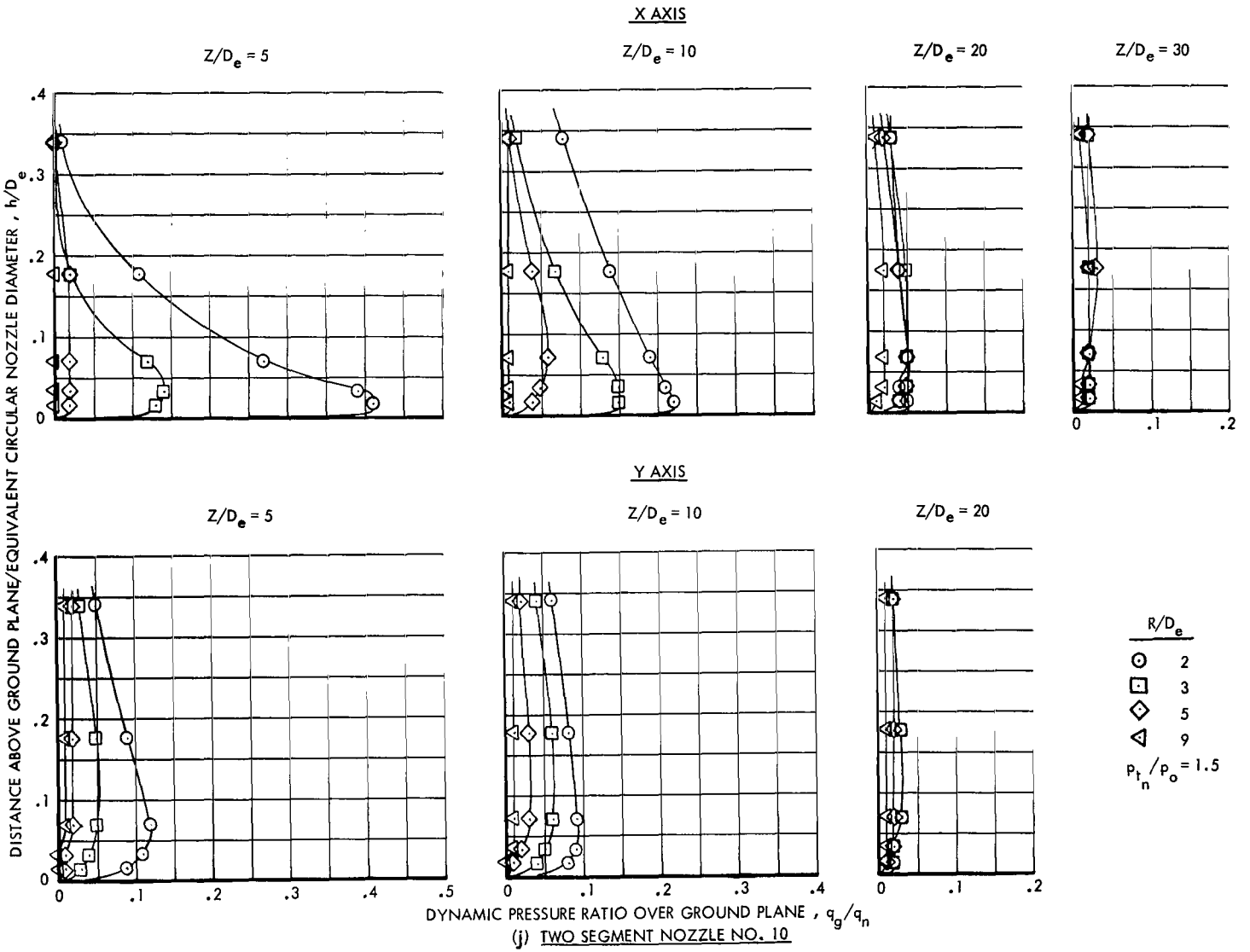

(j) TWO SEGMENT NOZZLE NO. 10

Figure 16.- Continued.

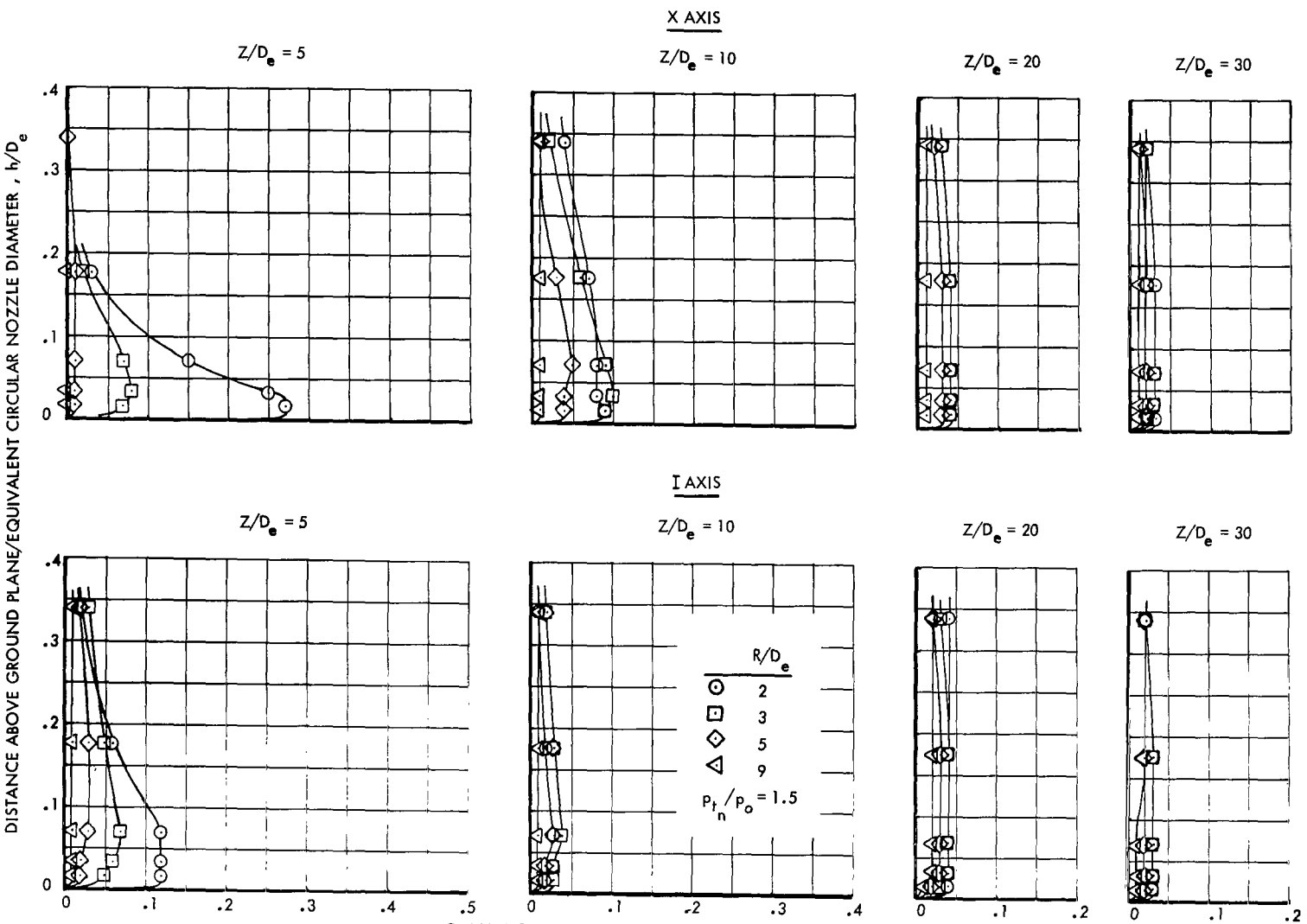

(k) FOUR SEGMENT NOZZLE NO. 11

Figure 16.- Continued.

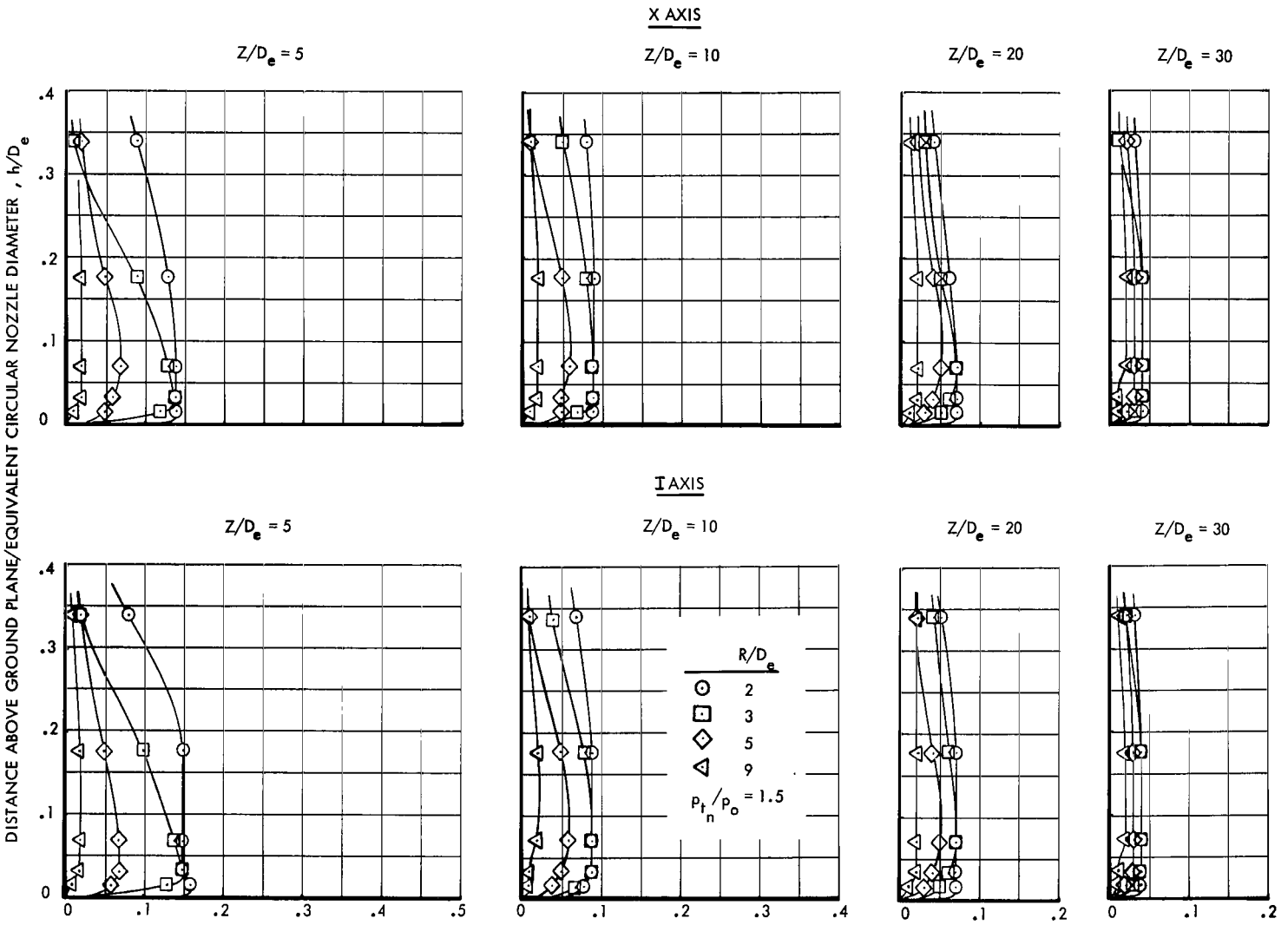

(m) TWELVE SEGMENT NOZZLE NO. 12

Figure 16.- Concluded.

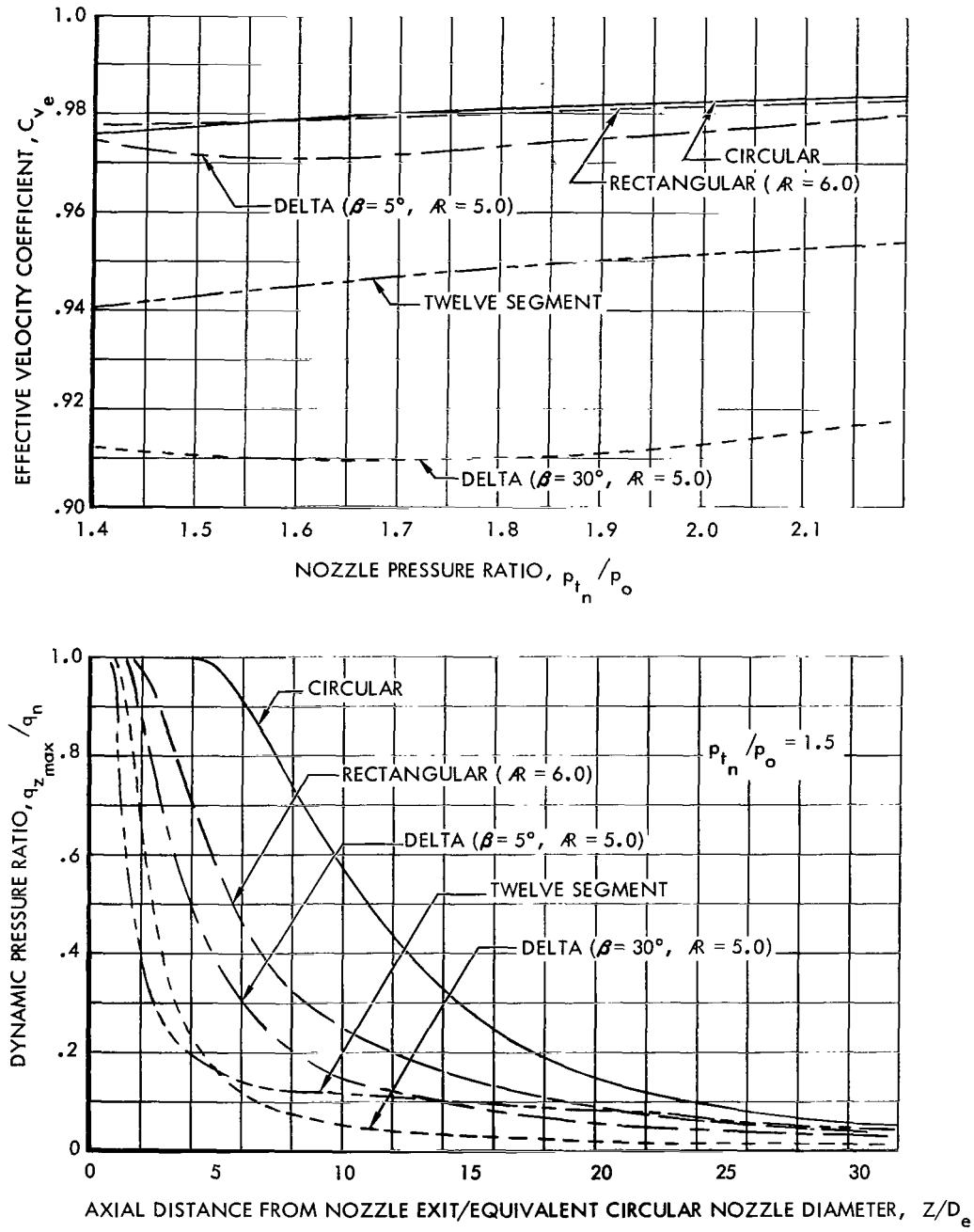

Figure 17.- Comparison of thrust and jet wake degradation characteristics of five nozzles.

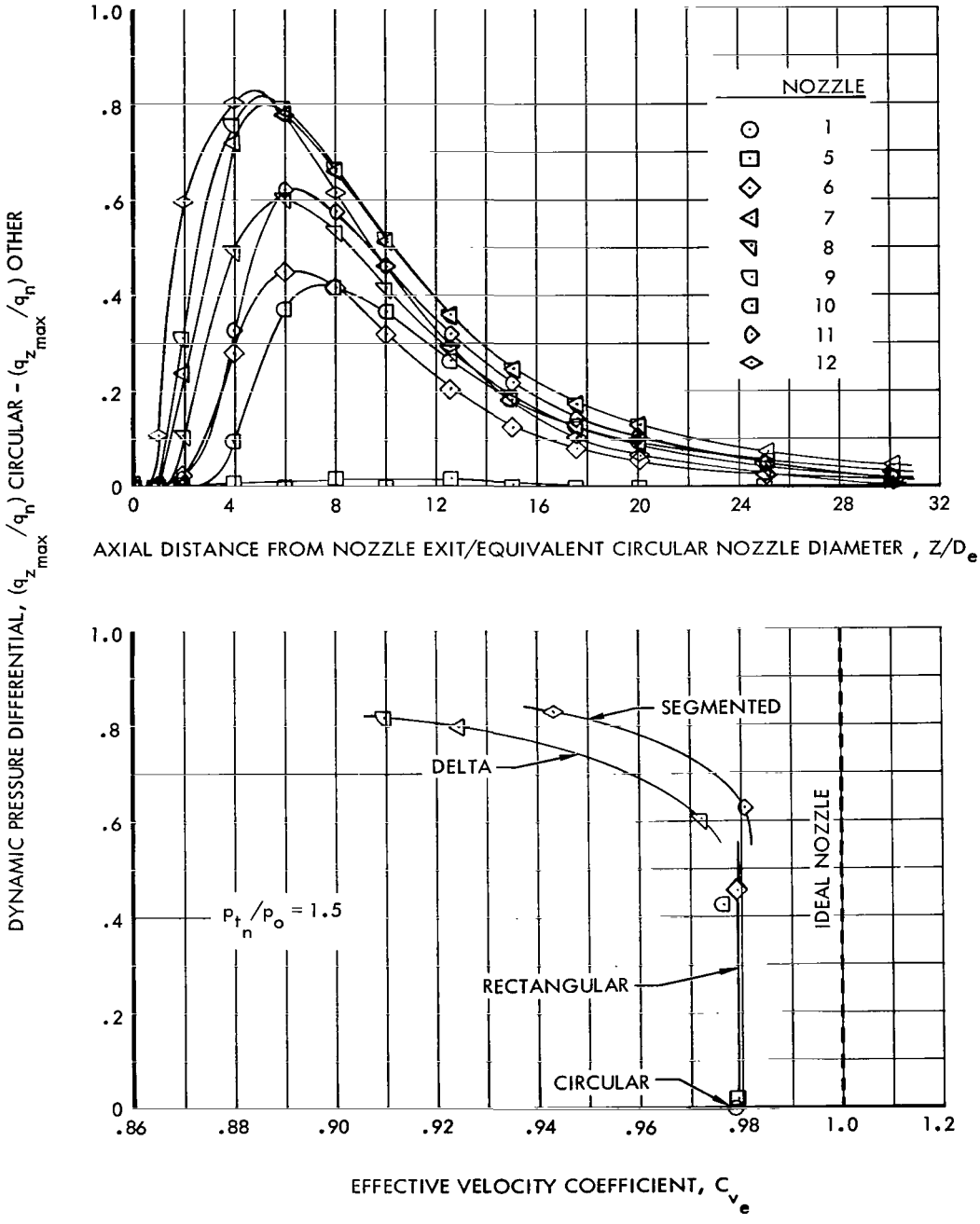

Figure 18.- Variation of maximum dynamic pressure degradation with distance and thrust for various nozzles.

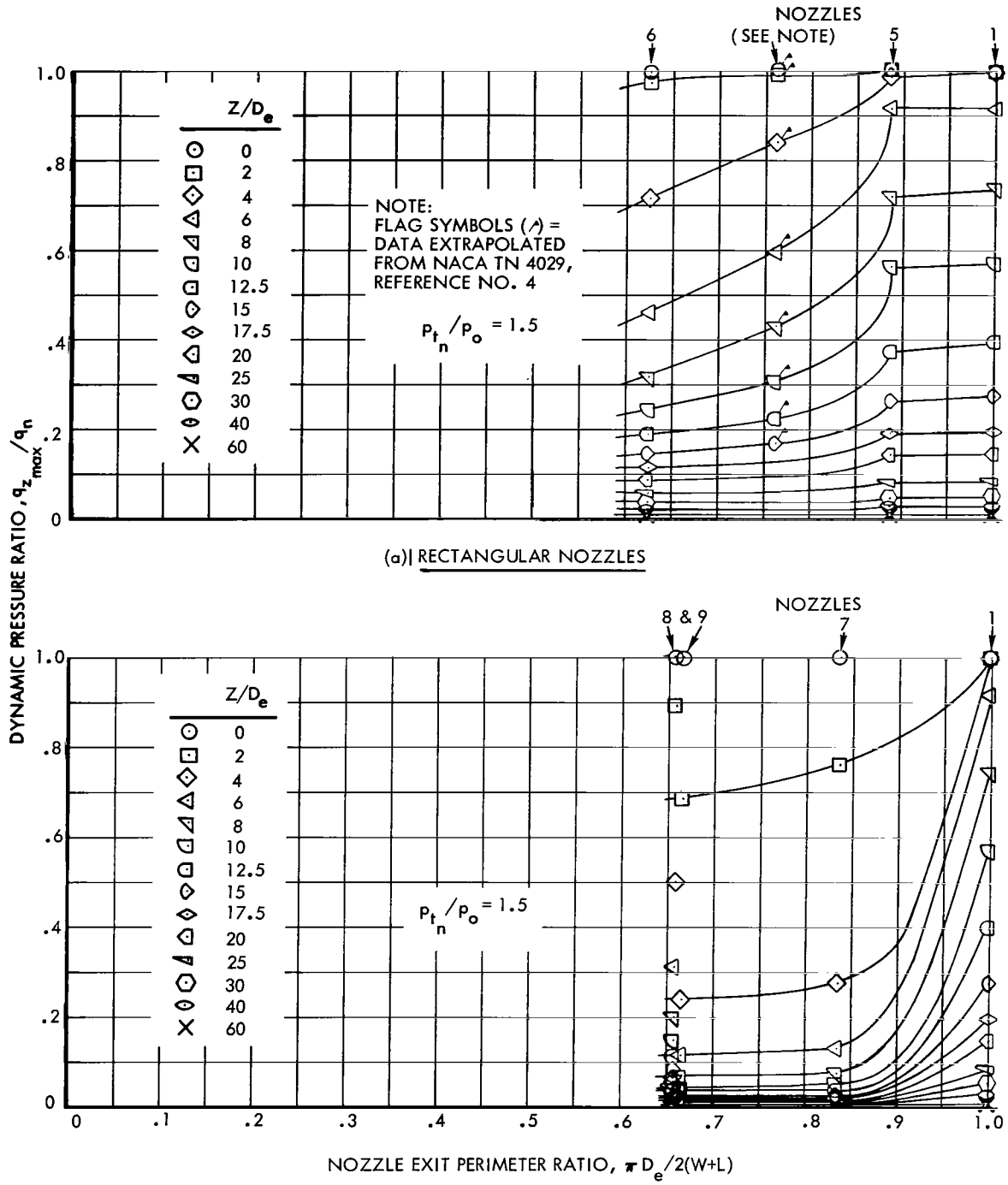

Figure 19.- Variation of dynamic pressure degradation with perimeter for various nozzles.

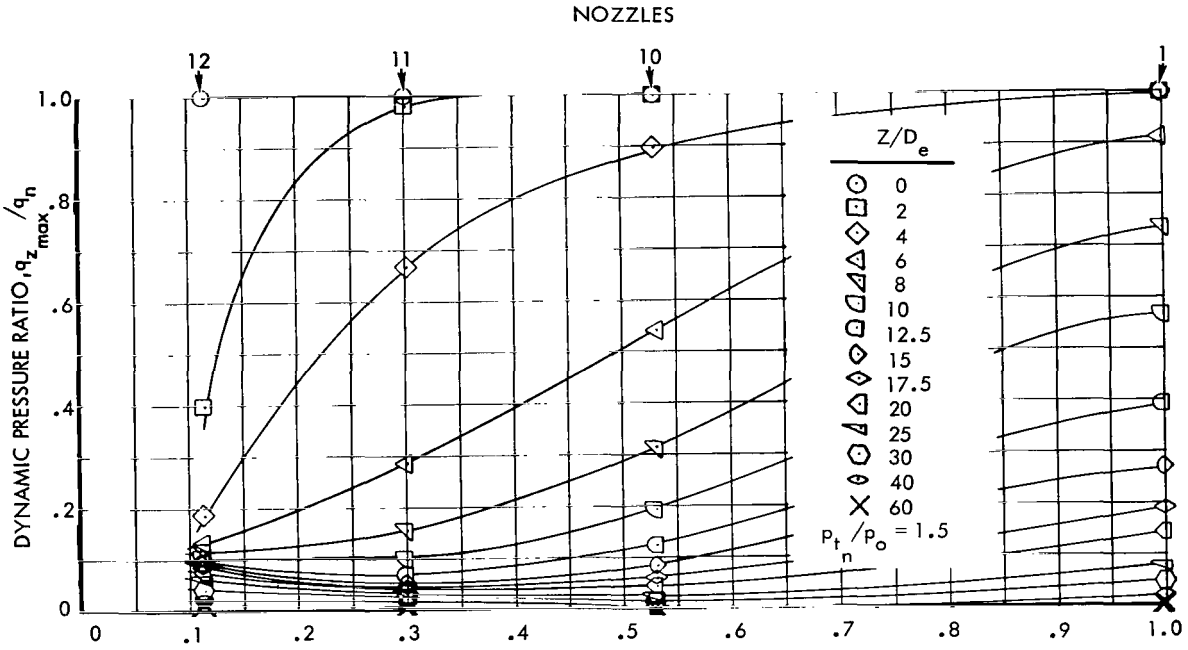

(c) SEGMENTED NOZZLES

Figure 19.- Concluded.

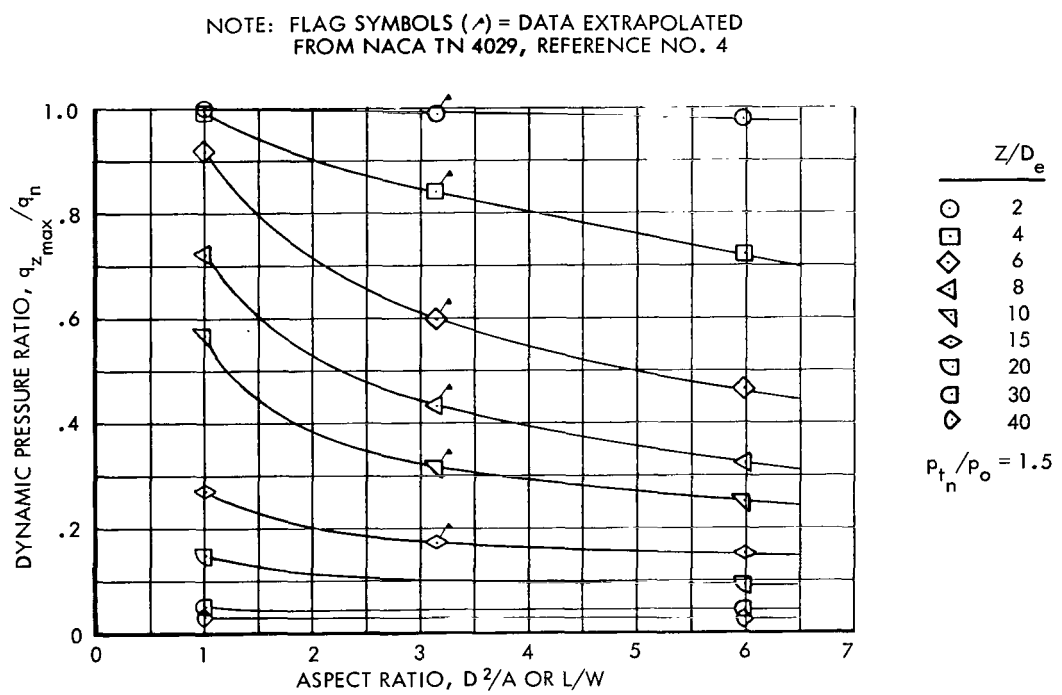

Figure 20.- Effect of aspect ratio upon dynamic pressure degradation for various nozzles.

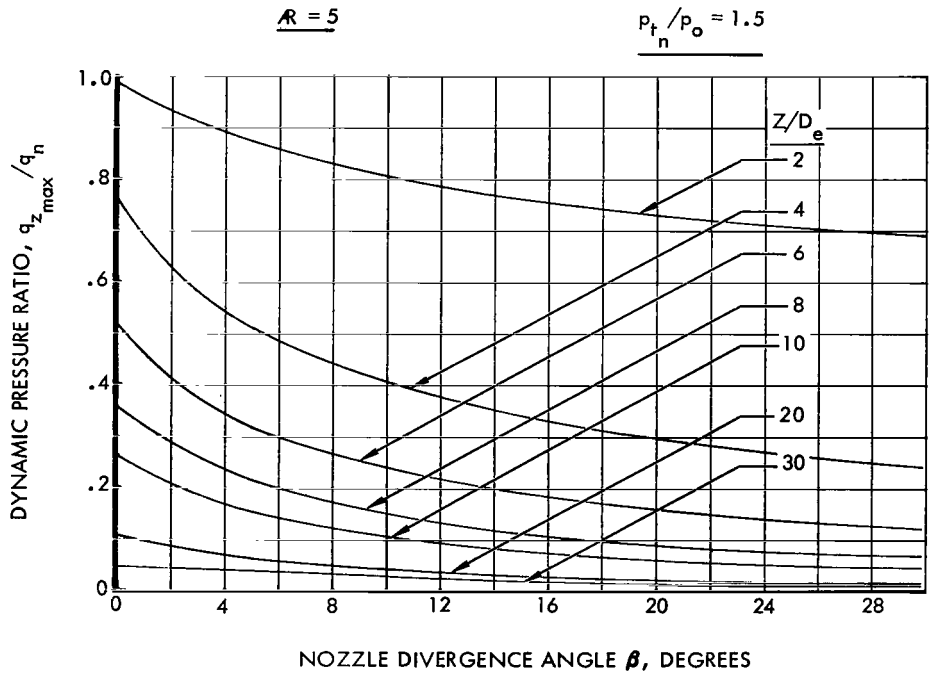

Figure 21.- Effect of delta nozzle divergence angle β upon dynamic pressure degradation.

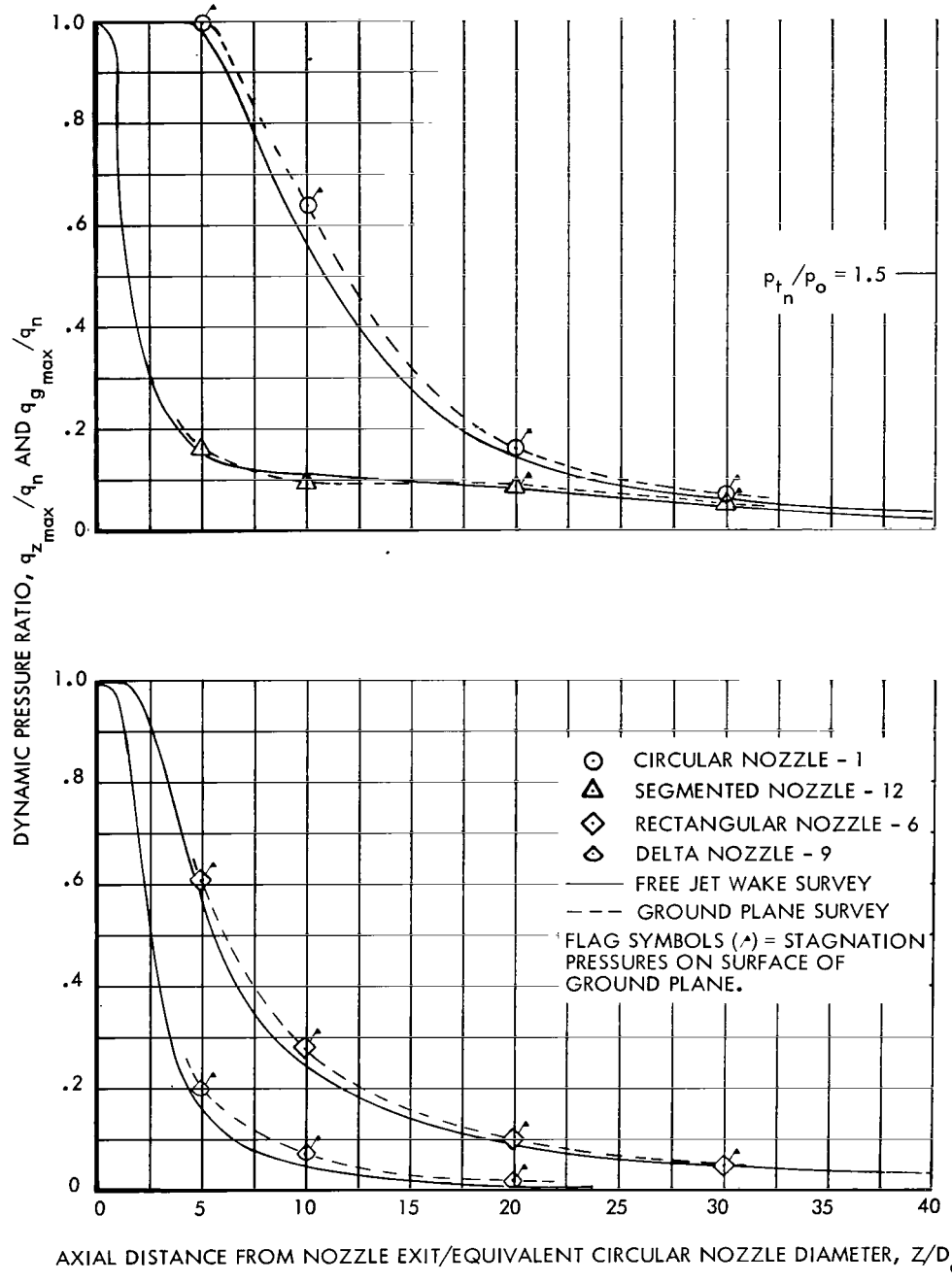

Figure 22.- Comparison of free jet wake surveys with ground plane surveys.

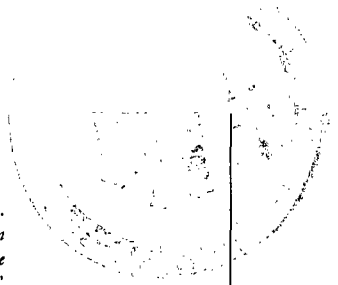

"The National Aeronautics and Space Administration . . . shall . . . provide for the widest practical appropriate dissemination of information concerning its activities and the results thereof . . . objectives being the expansion of human knowledge of phenomena in the atmosphere and space."

—National Aeronautics and Space Act of 1958

NASA SCIENTIFIC AND TECHNICAL PUBLICATIONS

TECHNICAL REPORTS: Scientific and technical information considered important, complete, and a lasting contribution to existing knowledge.

TECHNICAL NOTES: Information less broad in scope but nevertheless of importance as a contribution to existing knowledge.

TECHNICAL MEMORANDUMS: Information receiving limited distribution because of preliminary data, security classification, or other reasons.

CONTRACTOR REPORTS: Technical information generated in connection with a NASA contract or grant and released under NASA auspices.

TECHNICAL TRANSLATIONS: Information published in a foreign language considered to merit NASA distribution in English.

TECHNICAL REPRINTS: Information derived from NASA activities and initially published in the form of journal articles or meeting papers.

SPECIAL PUBLICATIONS: Information derived from or of value to NASA activities but not necessarily reporting the results of individual NASA-programmed scientific efforts. Publications include conference proceedings, monographs, data compilations, handbooks, sourcebooks, and special bibliographies.

Details on the availability of these publications may be obtained from:

SCIENTIFIC AND TECHNICAL INFORMATION DIVISION

NATIONAL AERONAUTICS AND SPACE ADMINISTRATION

Washington, D.C. 20546